

Design, Data Collection, and Driver Behavior Simulation for the Open-
Mode Integrated Transportation System (OMITS)

Liang Wang

Submitted in partial fulfillment of the
requirements for the degree of
Doctor of Philosophy
in the Graduate School of Arts and Sciences

COLUMBIA UNIVERSITY

2016

© 2016

Liang Wang

All Rights Reserved

ABSTRACT

Design, Data Collection, and Driver Behavior Simulation for the Open-Mode Integrated Transportation System (OMITS)

Liang Wang

With the remarkable increase in the population and number of vehicles, traffic has become a severe problem in most metropolitan areas. Traffic congestion has imposed tight constraints on economic growth, national security, and mobility of riders and goods. The open-mode integrated transportation system (OMITS) has been designed to improve the traffic condition of roadways by increasing the ridership of vehicles and optimizing transportation modes through smart services integrating emerging information communication technologies, big data management, social networking, and transportation management. Even a modest reduction in the number of vehicles on roadways will lead to a considerable cost savings in terms of time and money. Additionally the reduction in traffic jams will lead to a significant decrease in both gasoline consumption and greenhouse gas emissions.

As a result, novel transportation management is critical to reduce vehicle mileage in the peak time of the road network. The OMITS was proposed to enhance transportation services in respect to the following three aspects: optimization of the transportation modes by multimodal traveling assignment, dynamic routing and ridesharing service with advanced traveler information systems, and interactive user interface for social networking and traveling information. Therefore, the OMITS encompasses a broad range of advanced transportation research topics, say dynamic trip-match, transportation-mode optimization, traffic prediction, dynamic routing, and social network-based carpooling.

This dissertation will focus on a kernel part of the OMITS, namely traffic simulation and prediction based on data containing the distribution of vehicles and the road network configuration. A microscopic traffic simulation framework has been developed to take into account various traffic phenomena, such as traffic jams resulting from bottlenecking, incidents, and traffic flow shock waves. Four fundamental contributions of the present study are summarized as follows:

Firstly, an accurate and robust vehicle trajectory data collection method based on image data of unmanned aerial vehicle (UAV) has been presented, which can be used to rapidly and accurately acquire the real-time traffic conditions of the region of interest. Historically, a lack in the availability of trajectory data has posed a significant obstacle to the enhancement of microscopic simulation models. To overcome this obstacle, a UAV based vehicle trajectory data collection algorithm has been developed. This method extracts vehicle trajectory data from the UAV's video at different altitudes with different view scopes. Compared with traditional methods, the present data collection algorithm incorporates many unique features to customize the vehicle and traffic flow, through which vehicle detection and tracking system accuracy can be considerably increased.

Secondly, an open mechanics-based acceleration model has been presented to simulate the longitudinal motion of vehicles, in which five general factors—namely the subject vehicle's speed and acceleration sensitivity, safety consideration, relative speed sensitivity and gap reducing desire—have been identified to describe drivers' preferences and the interactions between vehicles. Inspired by the similarity between vehicle interactions and particle interactions, a mechanical system with force elements has been introduced to quantify the vehicle's acceleration. Accordingly, each of the aforementioned five factors are assumed to function as an individual trigger to alter each vehicle's speed. Based on Newton's second law of motion, the subject vehicle's longitudinal behavior can be simulated by the present open mechanics-based acceleration model. By introducing feeling gap, multilane acceleration behavior is included in the presented model. The simulation results fit realistic conditions for the traffic flow and the road capacity very well, where traffic shockwaves can be observed for a certain range of the traffic density. This model can be extended to more general scenarios if other factors can be recognized and introduced into the modeling framework.

Thirdly, a driver decision-based lane change execution model has been developed to describe a vehicle's lane change execution process, which includes two steps, i.e. driver's lane selection and lane change execution. Currently, most lane change models focus on the driver's lane selection, and overlook the driver's behavior during a process of lane change execution which plays a significant role in the simulation of traffic flow characteristics. In this model, a lane change execution is analyzed as a driver's decision-making process, which consists of desire point setting, priority decision-making, corresponding actions and achievement of consensus analysis.

Compared with the traditional lane change execution models, the present model describes a realistic lane change process, and it provides more accurate and detailed simulation results in the microscopic traffic simulation.

Based on the presented open mechanics-based acceleration model and the driver decision-based lane change execution model, a reverse lane change model has further been developed to simulate some complex traffic situations such as reverse lane change process at a two-way-two-lane road section where one lane is blocked by a traffic incident. Based on this reverse lane change model, information on the average waiting time and road capability can be obtained. The simulation results show that the present model is able to reflect real driver behavior and the corresponding traffic phenomenon during a reverse lane change process

Through a homogenization process of the microscopic vehicle motion, we can obtain the macroscopic traffic flow of the roadway network within certain time and spatial ranges, which will be integrated into the OMITS system for traffic prediction. The validation of the models through future OMITS operations will also enable them to be high fidelity models in future driverless technologies and autonomous vehicles.

Contents

List of Figures	v
List of Tables	x
Acknowledgements.....	xii
Chapter 1 Introduction.....	1
1.1 Background	1
1.2 Literature Review	4
1.2.1 Transportation information system and corresponding service	4
1.2.2 Microscopic traffic simulations.....	5
1.3 PhD research objectives	13
1.4 Dissertation outline.....	15
Chapter 2 Open-Mode Integrated Transportation System.....	17
2.1 Design of the OMITS	17
2.1.1 Design philosophy.....	17
2.1.2 Architecture of the OMITS system	21
2.1.3 GIS data structure for routing and networking in the OMITS system	23
2.2 OMITS application for Carpooling.....	27
2.2.1 Background of carpooling	27
2.2.2 OMITS App and web interface	29
2.2.3 Data structure and working mechanism of the OMITS system	29
2.3 Social network.....	31

2.4	Conclusions	33
Chapter 3	Vehicle trajectory data collection by UAV	35
3.1	Introduction	35
3.2	Experiments.....	38
3.3	Vehicle detection and tracking methodology	40
3.3.1	Image registration.....	41
3.3.2	Image feature extraction	45
3.3.3	Vehicle shape detection.....	51
3.3.4	Vehicle tracking	53
3.4	Results and discussions	57
3.4.1	Vehicle detection results	58
3.4.2	Conclusions and discussions	61
Chapter 4	An open mechanics-based acceleration model	64
4.1	Introduction	64
4.2	Open mechanics-based acceleration model.....	66
4.2.1	Vehicle acceleration factors	67
4.2.2	Feeling gap in multilane acceleration behavior.....	72
4.2.3	Governing equation in the mechanical system.....	74
4.2.4	Parametric analysis.....	75
4.3	Field experiments and parameter calibration	80
4.3.1	Experiment design.....	80
4.3.2	Parameters calibration	82
4.4	Simulation	84
4.4.1	Simulation results at different traffic situation.....	84
4.4.2	Shockwaves in simulation result	85

4.5	Conclusions and Summary	87
Chapter 5	A driver decision-based lane change execution model.....	89
5.1	Introduction	89
5.2	Driver decision-based lane change model.....	90
5.2.1	Desire point setting.....	92
5.2.2	Priority decision-making	95
5.2.3	Vehicle corresponding actions based on priority decision	97
5.2.4	Achievement of consensus	100
5.3	Parameter determinations	101
5.3.1	Determination of SELR.....	101
5.3.2	Approximation of other factors	104
5.4	Simulation	106
5.4.1	Simulation structure	106
5.4.2	Simulation results	109
5.5	Conclusions	117
Chapter 6	Reverse lane change simulation.....	118
6.1	Introduction	119
6.2	System specification.....	122
6.3	Region analysis for Vehicle S and L.....	123
6.3.1	Regions for vehicle S	123
6.3.2	Regions for vehicle L	126
6.4	Driver decision-based execution model for a reverse lane change	126
6.4.1	Desire point setting.....	127
6.4.2	Priority decision with different passing section directions	129
6.4.3	Corresponding actions.....	131

6.4.4	Achievement of consensus	133
6.5	Parameter selection and data collection	134
6.5.1	Parameter selection and approximate approach	134
6.5.2	Data collection method.....	136
6.6	Simulation results	141
6.6.1	Simulation result with different r_1 and r_2	143
6.6.2	Simulation result with different generation gaps	144
6.7	Conclusions	146
Chapter 7	Conclusions and Future Work	147
7.1	Research summary	147
7.2	Conclusions	148
7.3	Future work	150
Bibliography	152
Publications during Ph.D. study.....		175

List of Figures

Fig. 1-1 Classification of lane change model.....	10
Fig. 1-2 Structure of microscopic simulation research	16
Fig. 2-1 The information communication framework of the OMITS.....	21
Fig. 2-2 Three modules of the OMITS system for transportation operation and management [5].	22
Fig. 2-3 GIS data in OMITS	24
Fig. 2-4 Simple road network with the shortest travel time for each road section	25
Fig. 2-5 Entity-relationship diagram of the OMITS	30
Fig. 2-6 Interface of the OMITS App on smart phones (a) member management, (b) new service request, (c) service information, (d) rider information for carpooling, and (e) dynamic route direction and pick-up sites	31
Fig. 2-7 Social relationship network sample.....	33
Fig. 3-1 The UAV traffic monitoring system used in this experiment: (a) the whole set-up and (b) the camera mount and camera.....	38
Fig. 3-2 Image capture and transfer system: (a) image taken during the experiment and (b) the remote controller of quadrocopter and video monitor	40
Fig. 3-3 Workflow chart for vehicle detection and tracking in a UAV system	41
Fig. 3-4 Two frames in a UAV experiments: (a) the 120 st frame, (b) the 1530 th frame	42
Fig. 3-5 The camera mount isolate of the quadrocopter	43
Fig. 3-6 Traffic flow in UVA’s frame: (a) the original UVA’s frame and (b) the BW figure by setting the threshold of $V=0.35$	45
Fig. 3-7 Edge feature in the lateral direction of the road	47
Fig. 3-8 Optical flow in the longitudinal direction of the road. (a) The original grayscale frame; (b) The optical flow result.	49
Fig. 3-9 Different relevant angles between vehicle and UAV	50

Fig. 3-10 The result of vehicle shape detection	52
Fig. 3-11(a) The original figure; (b) the optical flow result; (c) the edge feature result; (d) the final detection result.	53
Fig. 3-12 Workflow of vehicle tracking	55
Fig. 3-13 (a) The demonstration of vehicle tracking based on matched local feature points. (b) one example to track vehicle with matched local feature points.	55
Fig. 3-14 The location of the field test (altitude is 150m)	57
Fig. 3-15 A typical vehicle trajectory data; (a) vehicle position trajectory data;(b) vehicle speed trajectory data.....	61
Fig.4-1 Structure of the present acceleration model	67
Fig. 4-2 The Lennard-Jones potential and force. (a) Potential, (b) Force.....	69
Fig. 4-3 The force elements to simulate the 5 factors in the open mechanics-based acceleration model.....	72
Fig. 4-4 Multilane acceleration behavior in a lane change scenario. (a) The original multilane acceleration situation, (b) The equivalent scenario of the multilane acceleration situation for driver S	73
Fig. 4-5 The impact of parameter α in free-flow scenario	75
Fig. 4-6 The impact of parameter δ in a gap increase scenario. (a) Subject vehicle speed; and (b) Gap length.....	76
Fig. 4-7 The impact of parameter ε in a gap increase scenario: (a) Subject vehicle speed; and (b) Gap length.....	77
Fig. 4-8 The impact of parameter γ in a gap decrease scenario. (a) Subject vehicle speed; and (b) Gap length.....	78
Fig. 4-9 The impact of parameter β in a gap decrease scenario. (a) Subject vehicle speed; and (b) Gap length.....	78
Fig. 4-10 Lane change scenario	79
Fig. 4-11 The impact of parameter ζ in a lane change scenario	79

Fig. 4-12 Data collection system. (a) Handhold LIDAR rangefinder, (b) Video camera, (c) Testing vehicle, (d) CAN bus and (e) ECU data collecting system.....	81
Fig. 4-13 Simulation and measured data in free-flow scenario	82
Fig. 4-14 Simulation and measured data in gap increases scenario.....	83
Fig. 4-15 Simulation and measured data in gap decreases scenario	84
Fig. 4-16 A screen shot of simulation result.....	85
Fig. 4-17 Loop road car-following simulation results at different traffic flow densities	87
Fig. 5-1 Notations of the lead, lag and subject vehicles during a lane change	91
Fig. 5-2 Structure of driver decision-based lane change execution model.....	92
Fig. 5-3 Interpretation of lane change.....	92
Fig. 5-4 The most dangerous situation considered in desire point setting.....	94
Fig. 5-5 vehicle S's corresponding behaviors. (a) Vehicle S has priority. (b) Vehicle S doesn't has priority.....	98
Fig. 5-6 vehicle L's corresponding behaviors. (a) Vehicle L has priority. (b) Vehicle L doesn't has priority.....	99
Fig. 5-7 The lag gap and lead gap in a lane change scenario.....	102
Fig. 5-8 Timelines at real situation and simulation model.....	105
Fig. 5-9 Lane change model structure.....	107
Fig. 5-10 A screen shot of simulation result	109
Fig. 5-11 The screen shot of user control interface	109
Fig. 5-12 Lane change number per vehicle simulation and field test results at different traffic situation.....	111
Fig. 5-13 The experiment location (altitude is 150 m)	111
Fig. 5-14 Vehicle L longitudinal speed changes in a dynamical lane change process. (a) field test data, (b) simulation data.....	113
Fig. 5-15 Vehicle S lateral position changes in a dynamical lane change process. (a) field test data, (b) simulation data	113

Fig. 5-16 Lane mark recognition experiment. (a) The camera position on the test vehicle, and (b) the results of lane mark recognition of a frame	115
Fig. 5-17 Lane mark recognition results. (a)Distance between lane mark and front tire, and (b) distance between lane mark and rare tire	115
Fig. 5-18 The vehicles required to be observed by driver S	116
Fig. 6-1 Two types of traffic incident scenarios; (a) an incident happened on a multiple-lanes road, and (b) an incident happened on a two-lane-two-way road.....	121
Fig. 6-2 Notations of the vehicles during a reverse lane change	122
Fig. 6-3 Excluded scenarios in this study. (a) Two vehicles at the “passing section”; and (b) Vehicle order change during a reverse lane change.....	123
Fig. 6-4 Region analysis for vehicle S	123
Fig. 6-5 View scope difference between wide-view and competition regions	125
Fig. 6-6 Region analysis for vehicle L.....	126
Fig. 6-7 Structure of driver decision-based lane change execution model	127
Fig. 6-8 Desire points in a reverse lane change scenario.....	128
Fig. 6-9 Two situations based on the passing section’s direction.....	130
Fig. 6-10 Vehicle S’s corresponding behaviors.(a) Vehicle S has priority, (b) Vehicle S doesn’t has priority	132
Fig. 6-11 Vehicle L’s corresponding behaviors. (a) Vehicle L has priority, (b) Vehicle L doesn’t has priority	133
Fig. 6-12 Important parameter in reverse lane change	134
Fig. 6-13. The difference between real position and observable position of dcS	135
Fig. 6-14 Cameras on a top of a vehicle. (a) Testing vehicle, (b) Forward camera image, and (c) Backward camera image	136
Fig. 6-15 IPM coordinates, Left: the coordinate axes (world, camera, and image frames) right: definition of pitch α and yaw β angles. [228].....	137
Fig. 6-16 A frame in camera on the top of a building.....	139
Fig. 6-17 Camera on UAV.....	140

Fig. 6-18 Reverse lane change model structure 142

Fig. 6-19 A screen shot of simulation..... 142

List of Tables

Table 2-1 The dynamic travel time for each road section at a specific start time.	26
Table 2-2 Weights of Social relationship network at different relationship.....	33
Table 3-1 Parameters of quadcopter in the experiments	38
Table 3-2 Camera parameters in experiments	39
Table 3-3 Transformation models in the image registration.....	44
Table 3-4 The summary of three types of image features	50
Table 3-5 Framework of the Vehicle shape detection with optical flow and edge.....	53
Table 3-6 The rule of vehicle tracking based on optical flow	56
Table 3-7 The main image feature extraction method applied in the code.....	58
Table 3-8 Vehicle detection results.....	59
Table 3-9 Vehicle tracking results	60
Table 4-1 Simulation results at different traffic conditions	85
Table 5-1 Driver’s characteristics based on $SELR^S$ and $SELR^L$	97
Table 5-2 Consensus and conflicts based on priority decision of vehicle S and L.....	100
Table 5-3 Parameters of gap acceptance models	102
Table 5-4 Parameters selection based on the gap acceptance.....	104
Table 5-5 Each vehicle’s static parameters.....	107
Table 5-6 Lane change simulation results at different generation gaps.....	110
Table 5-7 Lane change data from UAV.....	112
Table 5-8 Lane change success rate on MLC and DLC	116
Table 5-9 Traffic crash rate with and without BSAS	117
Table 6-1 Consentaneous and conflicting situations based on priority decision of vehicle S and L	133
Table 6-2 Pros and Cons of the three data collection methods.....	140

Table 6-3 Parameters based on field tests.....	141
Table 6-4 Each vehicle's static parameters.....	143
Table 6-5 Simulation result for different r1 and r2.....	144
Table 6-6 Traffic flow at different traffic situation	145
Table 6-7 Passing section's direction at different traffic situation	145
Table 6-8 Average traveling time at different traffic situation	145

Acknowledgements

I would like to express my deepest gratitude to my doctoral supervisor Professor Huiming Yin for his continuous guidance and encouragement throughout my graduate study. Besides his wealth of knowledge in the field of multiscale science and engineering, his energetic, creative and open mind to problem-solving have been motivational for me. His logical thoughts and expression with unique clarity make the courses and discussions more accessible and interesting, from which I benefited significantly.

During the last two years at Columbia University, I enjoyed tremendous support from Dr. Fangliang Chen, who has dedicated time and expertise, unreservedly mentored me step-by-step. He has taught me many valuable lessons, offered me plentiful advice and guidance in pursuing higher quality of work and independent thinking. I greatly appreciate the help and support he has given me. I treat it as my fortune to work with him.

I wish to extend my gratitude to my Ph.D. defense committee, Professor George Deodatis, Professor Andrew W. Smyth, Professor David A. King of Columbia University, and Professor M. Anil Yazici of Stony Brook University, for their valuable comments, remarks and suggestions in completion of my dissertation.

I'm also indebted to many of my exceptional colleagues at Columbia University. I'm thankful to Dr. Pohua Lee, Ms. Fangrui Guo, Ms. Gisele Guimaraes Ribeiro, Mr. Xin He, Mr. Gan Song, Mr. Qiliang Lin, Mr. Zhenyu Shou, Dr. Dan Hochstein, Mr. Paul Maurin, Mr. Blanche Luis, and Mr. Rodolfo Felipe Kusma. Without their collaborative efforts, much of my work would not have been possible.

Finally, my sincere thanks are given to my parents, Shufang Wang and Peiru Li, who always love and encourage me. Without their support, I could not accomplish my Ph.D studies.

To my parents
who love, encourage and support me all the time

Introduction

This chapter introduces the background of my PhD studies, the literature review of the relevant work, and the outline of this dissertation.

Background

With the remarkable increase in the population and number vehicles, traffic has become a severe problem in most metropolitan areas. Traffic congestion has imposed tight constraints on economic growth, national security, and the mobility of riders and goods. Policy makers, transport planners, traffic engineers, and those in the private sector engaged in developing new transport technologies are constantly looking for solutions to lessen the energy consumption, land usage, congestion, casualties, and money required to build new transportation infrastructures. As a result, developed countries have shifted their priority from infrastructure and capital intensive transportation strategies to more balanced and sustainable transportation solutions [1]. In general, an effective and friendly transportation service system should include three factors: multimodal travel systems, an advanced traveler information system and an interactive user interface for communication.

Multimodal travel systems are an effective method for significantly raising the quality of traveling services and increasing the operational efficiency in current transportation solutions [2]. Through the combination of different traveler modes and transportation operation systems, a traveler is able to use either public (bus, taxi, metro, railway, carpool, and ferry) or private (car, motorbike, bicycle, and walking) modes [3] to achieve the transportation needs and optimize the transportation services.

An advanced traveler information system (ATIS) is a type of intelligent transportation system application that integrates emerging computer, communication, and information technologies to provide vital information to the users of a system regarding traffic regulation, route and location

Introduction

guidance, hazardous situations and safety advisory, and warning messages [1]. ATIS requires a large amount of data for processing, analysis, and storage for the effective dissemination of traveler information to users. A geographical information system (GIS) allows large amounts of data to be effectively processed, stored, analyzed, logically associated, and graphical displayed. Thus, GIS-based ATIS provides a convenient and powerful tool for the storage and graphical representation of the massive amount of information. Further, by availing the powerful GIS functionalities, a user can submit a request and allow the appropriate software to assist her or him in the decision-making process regarding optimum route selection and trip planning [4].

With the development of smart phones, different types of sensors and probes, global positioning system (GPS), and Wi-Fi connectivity to the Internet, many new transportation services have emerged in traffic control and monitoring, such as traffic routing, vehicle-infrastructure communication, vehicle-vehicle connection, and accident reporting [5]. As an interactive user interface for communication, smart phones are showing great potential and are playing a significant role in an advanced transportation service system.

On the other hand, since traffic phenomena are the accumulation of the relevant behavior of individual vehicles, microscopic simulation becomes a powerful approach to take into account explicit and detailed behaviors of an individual driver and predict the traffic evolution under certain time-spatial boundary conditions. Theoretically, any traffic phenomenon can be simulated and explained by microscopic traffic simulation [6]. As a result, microscopic traffic simulation has been widely used as a powerful tool in transportation for both researchers and practitioners. Through a homogenization of the microscopic traffic information, macroscopic traffic flow can be obtained and analyzed. Many methods, algorithms and plans proposed at the macroscopic level can be calibrated and tested through such a cross-scale approach, especially when direct validation by field tests is not feasible due to high costs as well as the issues of public acceptance and safety considerations [7].

In addition, microscopic traffic simulation is able to predict a traffic situation based on real-time traffic information [8]. For example, when a traffic incident happens on a highway, by introducing the traffic flow information from its upstream sensors, the traffic situation at the incident location can be predicted by simulations. Such a short period of prediction is important for urban traffic management [9] and an advanced traveler information system [1]. As a result, the

Introduction

microscopic traffic simulation has attracted significant attention as a fundamental research area in the traffic research field and has been widely used in transportation management and information systems.

There are two important topics in microscopic traffic simulation, namely driver behavior modeling and trajectory data collection. Driver behavior modeling describes drivers' decisions and actions under different traffic conditions, which directly affect the simulation results. Trajectory data collection, however, is able to test behavior models, and calibrate the model's parameters through a homogenization process. Due to the high demand for rigorously validated traffic flow models and the limited availability of detailed trajectory data [7,10,11], vehicle trajectory data collection becomes a requisite for transportation analysis, especially for driver behavior models. However, existing data collection methods are not very useful for vehicle trajectory data collection. For example, most current traffic data collection sensors, such as inductive-loop traffic detectors, were designed to collect traffic information on fixed cross-road sections in certain limited road areas. Though it may be convenient to obtain traffic data at the lane's level such as each lane's average traffic speed, density and flow, it is hard to obtain traffic data at vehicle's level based on these discretely distributed sensors.

As a useful and powerful aerial robot, unmanned aerial vehicles (UAV) play an important role in data and image acquisition. For example, they have been widely used in the research fields of agriculture, geology, hydrology, cinematography, etc. [12–17]. Compared with traditional transportation sensors located on the ground or low angle cameras, UAV exhibits many advantages, such as low cost, easiness to deploy, high mobility, large view scope, uniform scale, etc. UAV is able to record different lengths of the road by adjusting its flying altitude to fulfill different research requirements. Compared with low angle cameras, UAV is able to measure a vehicle's position more accurately from the top view [18]. However, UAV has been rarely applied in transportation monitoring. One of the main reasons is the lacking of effective and robust methods to detect and track vehicles in UAV's image data. Hence, there is an urgent need to develop an accurate and robust vehicle trajectory data collection method based on a UAV's video.

As an important component in microscopic traffic simulation, the modeling of a driver's behavior describes a driver's decisions and corresponding actions under different traffic conditions, which in general traces back to a driver's acceleration and lane change behaviors. The acceleration

Introduction

model describes the movement of the vehicle in the longitudinal direction, and the lane-change model describes drivers' behaviors in the lateral direction. Generally, lane change behavior models can be further classified into lane change selection models and lane change execution models [19]. A lane change selection model simulates a driver's thoughts and decision before a lane change, which consists of the lane change request, target lane selection, and gap selection. The lane change execution model simulates the lane change operational process, which includes speed change, safety considerations and lateral movements. However, it is always challenging for a single driver behavior model to accurately describe a driver's complex behavior in different traffic situations [20–22]. Hence, there exists a strong need to develop more realistic driving behavior models that is able to reflect the complexity of human decision-making processes.

Literature Review

Transportation information system and corresponding service

Generally, the development of traveler information systems can be classified into three different generations [23]. The first generation traveler information systems arose in connection with the emergence of computer technology in the late 1960s and early 1970s [24]. Traffic information was provided separately for motorists and for public transportation travelers by one-way communication [25]. It was possible to improve traffic flow on congested roads and also to make road users aware of the disturbances and traffic incidents through dynamic message signs and highway advisory radios [23]. At the end of 1980s the timetable for public transport in Stockholm was computerized and made available through interactive voice response via phone for travelers [25].

The second generation systems aimed at vehicle driver and were developed during the 1990s, which became advanced traveler information systems with dynamic route guidance and real-time traffic conditions by using two-way communication through an interactive user interface [25]. They were originally designed to provide personalized trip advice, where navigation systems for route guidance were primarily embedded within in-vehicle systems or handheld navigation devices. Individualized path search and dynamic route guidance is available, but not very popular due to the high cost [26].

Introduction

The third generation of traveler information systems for motorists were the result of a combination of the second generation transportation information system and artificial intelligence to create intelligent traveler information systems [27]. This type of system can store different travel patterns and route choices from previous sessions for each driver, so that machine learning can be conducted with the big data accumulated in the system. The system is able to evaluate the accessibility of roads, dialogue with drivers on the roads and provide personalized route guidance for specific traffic conditions. However, today's navigation systems usually do not have information about other modes of transport [28]. The third generation systems for public transportation are now starting to utilize smart phones, mobile broadband, and GPS functionalities, among other information technologies. As a consequence, a series of user-generated content and open application programming interfaces are emerging, which enables the system or system components to communicate with each other to exchange data or functionality.

Microscopic traffic simulations

Microscopic traffic simulation is a fundamental tool for dynamic traffic management and in a transportation information system. In this part, a literature review is conducted of vehicle trajectory data collection based on UAV system, the acceleration model and lane changing model are introduced, and their limitations are summarized at the end of each section.

Vehicle trajectory data collected by UAV

As a useful and powerful aerial robot, UAV plays an important role in data and image acquisition. However, it is limited by the lacking of an effective and robust method to detect and track vehicles in UAV's image data. As a result UAVs are rarely applied in the transportation monitoring.

Some approaches to vehicle detecting and tracking based on UAV systems have been proposed in the literature [29]. Based on the recognition methods discussed on the literature, the vehicle recognition method can be categorized into the optical flow and feature extraction-matching methods. The optical flow method has many advantages in tracking and detecting moving objects in consecutive frames, such as autonomous robot navigation and surveillance of large facilities. Optical flow can capture the moving objects in a video, but the movement is the sum of motion of both the camera and the vehicles. It is essential to identify and separate the

Introduction

camera's motion from the vehicle's motion. Rodríguez-Canosa, et al. [16] developed a real-time method to detect and track moving objects from UAVs' videos. In this method, an artificial optical flow is introduced by estimating the camera's motion, comparing it with the real optical flow directly calculated from the video, and then calculating the actual motion of the objects. Xu et al. [30] introduced a vehicle detecting and tracking method for the low angle camera video. The Cellular Neural Network was used to subtract the background and to refine the detection results with optical flow. Frarnebäck and Nordberg [31] constructed a polynomial expansion to approximate the movement between two consecutive frames at the pixel level. Based on the constructed optical flow field, the vehicle's motion could be calculated.

The feature extraction-matching method has been widely used in photogrammetry and computer vision. The working process consists of extracting features of interest from two or more images of the same object and matching these features in adjacent images [32]. Photo-based methods generally search for vehicle-like features in one or two photos, and then refine the detection results through classification and representation based on a predefined database. The vehicle-like features include the vehicle's edges, shapes, feature points, colors, gradients, etc. Zhao and Nevatia [33] figured out some important car features based on human experience in psychological tests, and then used the boundary of the car, front windshield and the shadow as car features in car recognition from a photo. Kanihche et al. [34] presented a vision system for traffic surveillance with a fixed-wing UAV. The method analyzed the corner and edge information in a frame, and the Dempster-Shafer theory was used in the process of verification to increase the accuracy of vehicle detection. Kim and Malik [35] introduced a new vehicle detection method, which combines photos of multiple cameras and generates a 3D-model of vehicles. This vehicle detection and description algorithm was based on a probabilistic line feature grouping, and it could increase the computing speed and reliability. Gleason et al. [36], introduced a multiple features extraction and classification method for vehicle detection. The vehicle features, such as histogram of oriented gradients, edge orientation, and color are considered to increase the detecting accuracy. Leifloff [37] presented an approach for vehicle detection from optical satellite images, where an improved Haar-like feature was used in the method. Vehicle queues were detected using a line features extraction technique in the analysis. Tuermeret al. [38] applied the features of histogram of oriented gradients, Haar-like features and local binary patterns in the vehicle detection. And a

Introduction

sophisticated blob detector was used in another work for vehicle detection. Leitloff et al. [39] developed a vehicle detection method that relies on an extended set of Haar-like feature operators. The support vector machine was used in the process of classification and refine vehicle detection results.

In general, because of the limited information available in one photo, the photo-based vehicle recognition method can only obtain the vehicle's static information, like position or gap between vehicles, but it is impossible to get the dynamic information, such as the speed and acceleration of vehicles. However, the video based feature extraction-matching method focus on the relationship and connection among matched feature points, rather than their characteristics. Therefore, the method exhibits many advantages for research of vehicle tracking. Cao et al. [40] introduced a new framework of multi-motion layer analysis to detect and track moving vehicles in UAV's videos. The Kanade–Lucas–Tomasi (KLT) feature was selected in the vehicle motion and background motion layers. The new method is more effective and robust in the application. Cao et al. [41] applied Histogram Orientation Gradients (HOG) feature on vehicle detection. All HOG features are combined to establish the final feature vector to train a linear Support Vector Machine (SVM) classifier for vehicle classification. Lingua, et al. [32] analyzed the advantages of using the scale invariant feature transform (SIFT) operator for the feature extraction-matching method in UAV systems, and developed an auto-adaptive version of the SIFT operator used in the UAV's photogrammetry field. Many researchers have used the feature extraction-matching method for vehicle tracking. Some studies used the vehicle image as a feature [39,42] or the matched feature points [43–45] to track vehicle's motion on the road.

Overall, detecting and tracking vehicles in traffic using UAV videos and photos has been attracting increasing attention among those in the transportation research community. However, to the best knowledge of the author, a well-developed vehicle detecting and tracking method for actual transportation applications has not been developed yet. There are two challenges in the current practice:

- Firstly, the accuracy of vehicle recognition is low. Normally, the detecting accuracy rate is lower than 90% based on the current technology[36,38,39,46], and the driver's detailed data is not available [47,48].

Introduction

- Secondly, there is no customized method for vehicle trajectory data. It is difficult to recognize the traffic features, such as road, traffic flow and driver behavior features from the images or videos [29,43,49].

Acceleration models

An acceleration model describes the longitudinal behavior of vehicles on the road [50]. It is an essential component in microscopic traffic simulation and plays an important role in transportation science and engineering, including safety studies and capacity analyses[21,22,51–54]. Over the past decades, as a fundamental research topic in transportation, a large number of vehicle acceleration models have been developed to describe longitudinal behavior of vehicles in different traffic conditions.

Based on the considered impact factors, the existing vehicle acceleration models can be classified into five categories. The first one is the speed difference model, such as the Gazis-Herman-Rothery (GHR) model [55,56] and the extended GHR models [54,57], which assumes that the car following stimulus is the relative speed between the leading and subject vehicles. The second one is the spacing model [58,59], which assumes that a driver reacts to the gap rather than the relative speed. For example, the Newell model [60] has been widely used in car-following simulation. The third one is the desired measures model, which assumes that each driver has a desired following distance, speed or headway, and that a driver seeks to minimize the difference between the desired measures and the actual states. The Helly's model [61,62] and the intelligent driver model (IDM) [63,64] are very popular in this category. The fourth one is the collision avoidance model, which accounts for safety considerations. The collision avoidance model assumes that the speed is selected by a driver in order that the vehicle can avoid any collision in case the leading vehicle suddenly brakes. For example, the Gipps model [53], which includes the free and following driving modes for different traffic conditions, has been widely used. The fifth category uses a driver's personal features to analyze the vehicle's acceleration behaviors, among which the driver's age [65–67], gender [68,69], state [70–72], temper [20,73,74] and perception [75] are considered. Generally, the relative speed, gap, desired measures, and safety are considered as the dominant factors in above mentioned models that will influence a vehicle's acceleration behavior.

Introduction

It is well known that the vehicle acceleration behavior of a vehicle driving on the way is very complex, which may be affected by various factors. An ideal acceleration model is expected to be able to reflect a driver's behavior in different situations, such as different traffic situations, driver characteristics and even specific behaviors during driving, like distraction, fatigue, talking on the phone. Although a large number of acceleration models have been developed over the past few decades, two limitations are often exhibited in the current models:

- Firstly, many of them were developed in a rigid form by only considering certain factors, while other relevant or emerging factors are not able to be accounted for or integrated. As a result, driver's psychological behaviors [65–73,75] are usually ignored.
- Secondly, most existing acceleration models cannot be adapted to the lane change process very well [10,54,76]. So that, many lane change models have to introduce specific parameters and formulas to describe a vehicle's longitudinal behavior in the lane change process [77,78].

Lane changing models

Lane changing behaviors have fundamental impacts on the microscopic characteristics of traffic flow due to the interference effect that they have on surrounding vehicles [19,79]. It is also an important component of driving behavior to meet driver's tactical and operational maneuvering decision in different traffic situations [6]. A reasonable and adaptable lane change model has significant meaning in the study of driver behaviors, driving safety, capacity analysis and traffic predictions, etc.

Generally, a lane change simulation often consists of two main steps: the target lane and gap selection and lane change execution [19]. The target lane selection mimics a driver's thoughts before lane change execution, which includes lane change request and target lane and gap selection. The lane change execution simulates the lane change operational process, such as speed change and lane change selection. Driver's decisions, safety considerations, lane change priorities and courtesies have been the main research topics in the study of the execution of lane change. In general, the process of lane change selection has been well developed in the literature [21]. Accordingly, different lane change selection theories and models can be applied in different traffic situations and different driver features [80,81]. However, compared with the investigations on lane

Introduction

change selection, the study on lane change execution is limited. This dissertation will focus on the lane change execution model.

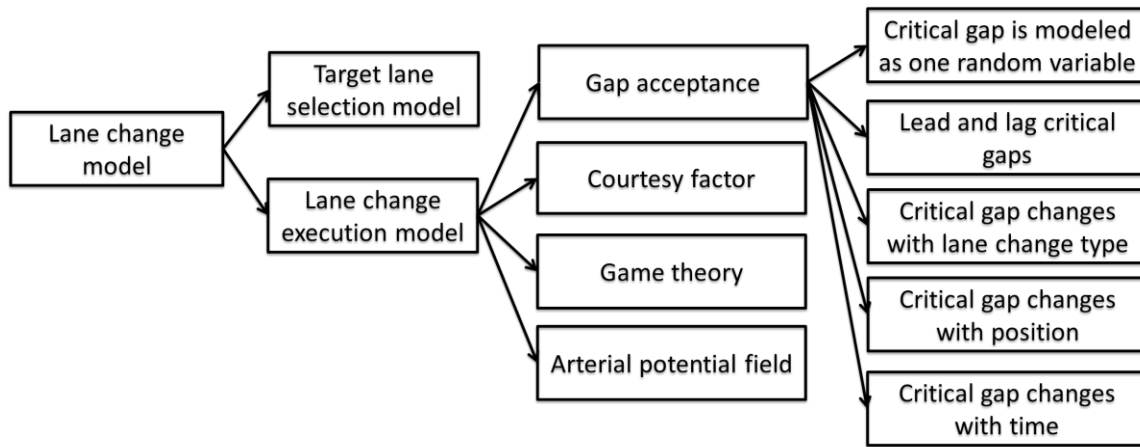


Fig. 0-1 Classification of lane change model

According to the main analysis factors, the lane change execution model can be classified into four categories: The gap acceptance, courtesy factor, game theory, and arterial potential field, which are illustrated in Fig. 0-1.

The gap acceptance model (GAM) is currently the major theory and method in the lane change execution. The GAM was formulated as a binary choice problem: when an available gap on the target lane is longer than the critical gap, the lane change is accepted, otherwise the lane change is rejected [82]. Based on different assumptions of the critical gap, the GAM can be further classified into the following four subcategories.

(1) Critical gap is modeled as a random variable. This type of model was mainly developed during the earlier stages of lane change simulation. Herman and Weiss [83] assumed that the length of the critical gap satisfies an exponential distribution. Miller [84] used the maximum likelihood method to prove that the critical gap is a normal distribution for different drivers. However, most results are qualitative and statistical solutions, which are reasonable only in macroscopic level analyses.

(2) Critical gap is classified into lead and lag critical gaps. In this situation, the lane change is accepted only if the both of lead and lag gaps are longer than the corresponding critical gaps. Ahmed et al. [82] generated a framework for the lane change model based on discrete choice, where lead and lag critical gaps are defined separately and the parameters are set by on-ramp

Introduction

merging data. Toledo et al. [77] introduced an integrated driving behavior model. The probability expressions of lead and lag critical gaps are introduced.

(3) Critical gap changes with lane change type. In this type of model, gap acceptance parameters are estimated jointly with a driver's lane change type, and a critical gap during a Mandatory Lane Change (MLC) is usually shorter than that in a Discretionary Lane Change (DLC). Based on this assumption, Toledo et al [7], Gipps [85], and Salvucci et al. [86] independently developed two sets of parameters for DLC and MLC situations in gap acceptance models.

(4) Critical gap changes with location. Based on the distance between subject the vehicle and the intended turn, the critical gap has different values. In general, when a vehicle is close to the intended turn, the critical gap is short, and vise-versa. Gipps [85] set three different lane change execution criteria based on the distance to the intended turning position. Kesting et al. [87] introduced the Minimizing Overall Braking Induced by Lane Changes (MOBIL) lane change model. A vehicle's relative distance and speed can affect its lane change criteria. Schakel et al. [88] proposed a lane changing model with relaxation and synchronization (LMRS). The vehicle's relative distance and speed can affect its acceleration during a lane change. A gap is accepted if the acceleration of the subject vehicle and the new follower are larger than a safe deceleration threshold.

(5) Critical gap changes with time. In general, when the waiting time increases, a driver usually prefers a short critical gap. Mahmassani and Sheffi [89] assumed that the mean critical gap is a function of an explanatory function, and the critical gap decreases on average, as a driver is waiting for an acceptable gap. Sayed et.al[90] introduced a traffic conflicts computer simulation model, in which the waiting time is an important parameter affecting driver's critical gap. Kaysi, Abbany [91] and Hamed, et al [92] analyzed the driver's behavior in unsignalized intersections, and concluded that the mean critical gap becomes shorter while the waiting time is increased.

In normal traffic conditions, the GAM was developed to properly simulate the lane change process. However, in heavily congested traffic situations, the gap in a target lane may be much smaller than the critical gap, which is becoming more prevalent in traffic nowadays, especially in large cities. In such cases, any lane change in a road section will not be accepted at all based on the GAM. To overcome such limitations of the GAM, the concept of courtesy factor was introduced [81]. This means that the courtesy vehicle will enlargen the gap for the lane change

Introduction

vehicle to help it finish the lane change. In addition, Hidas [93] analyzed the courtesy behavior involved in lane changes and categorized them into force and cooperation lane changes based on the aggressiveness of the subject vehicle in the simulation. The courtesy rate of a vehicle directly affects the simulation results, however, it is hard to quantify the courtesy rate of a vehicle in real traffic flows. Kind and Kesting [94] modeled drivers associated behaviors with a lane change via a "politeness factor" in lane change decisions based on the Minimizing Overall Braking Induced by Lane Changes (MOBIL) model.

The game theory model considers that a lane change execution process is an interaction between the subject and lag vehicles when a traffic conflict arises [10]. During the lane change execution process, the subject and lag vehicles try to influence each other. Kita [95,96] modeled a lane change execution based upon the game theory and specified the game type, the number of players and the repetition of games.

Artificial potential field (APF) was firstly introduced for robot control [97], and it was used to avoid collisions when the robot hand moves to capture objects. In the driver behavior simulation, APF is also applied in the lane change execution. Yang et al. [98] assumed that each vehicle on the road will cause a potential energy field, and a vehicle during a lane change is regarded as a sphere always rolling to the low potential energy area. If the magnitude of the energy field is too high in the target lane, the lane change is rejected, and vice-versa. A vehicle's energy is influenced by its relevant speed with respect to the subject vehicle. The lateral distance between vehicles are also considered in the lane change execution process.

Although, as stated above, a large amount of lane change models have been introduced over the decades, some limitations still exist in those models.

- A lane change execution model is rare. Most lane change models overlook the driver's actual behavior during lane change execution process which plays a significant role in estimating traffic flow characteristics.
- The interaction between the subject and lag vehicles during a lane change is ignored. A lane change execution process is actually a behavior in that the subject vehicle wants to get the lag vehicle's permission to break the original order in the target lane and take the lag vehicle's original position. In this sense, the lane change should be a series of interactions between the

Introduction

subject and lag vehicles. However, most existing models consider the lag vehicles using certain parameters, while ignore the interaction between the subject and lag vehicles.

- Lateral dimensions is not considered in a lane change execution model. A lane change is actually a process to change vehicle lateral position, which will also plays an important role in the whole lane change process. However, most existing models ignore such lateral position effect in a lane change execution model.

PhD research objectives

This work aims to improve the traffic condition of roadways by increasing the ridership of vehicles and optimizing transportation modes through smart services by integrating emerging information communication technologies, big data management, social networking, and transportation management. As the first step to this end, this dissertation presents the design of the OMITS and develops a relevant microscopic simulation framework that includes vehicle trajectory data collection, an acceleration model, and a lane change execution model, for traffic prediction in the OMITS. My PhD studies aim to achieve the following research objectives:

- **OMITS design and application**

By integrating emerging information and communication technologies, such as smart phones, Internet services, GPS/GIS, and data mining and fusion technologies, the goal of the proposed OMITS is to improve ridership of vehicles and optimize the operation of transportation systems by enhancing transportation services in the following three aspects: optimization of the transportation modes by utilizing multimodal traveling assignment, dynamic routing and ridesharing service with advanced traveler information systems, and development of an interactive user interface for social networking and traveling information.

- **Vehicle trajectory data collection**

The camera of a UAV surveillance platform changes frequently because the camera in a UAV may rotate, shift and roll during video recording. In order to accurately detect and track vehicles, the negative effects of such platform changes have to be eliminated or minimized. To this end, a proposed method will be presented to collect more stable and accurate vehicle trajectory data by developing a reliable image registration method for UAV's video. Furthermore, in driver behavior research models, such as car following and lane changing, accurate trajectory data of each vehicle

Introduction

is needed. Lack of vehicle data and tracking error may greatly decrease the accuracy of the model parameters settings. Therefore, the collected trajectory data via the presented method will also benefit future research on car following and lane changing.

- **Acceleration model**

In general, the acceleration behavior of a vehicle driving on the road is very complex, which may be affected by various factors. To reflect a driver's behavior at different situations, such as different traffic situations, driver characteristics (ages, genders, health states, temper and perception) and even specific behaviors during driving, like distraction, fatigue, talking in phone must be considered. An acceleration model will be developed to consider longitudinal motion of vehicles on a road for microscopic traffic simulation. With multiple impacting factors being accounted for, it is expected that the present model will provide a smooth transfer between different following states, such as leading vehicle change, so that it is able to be used in the lane change scenario.

- **Lane change execution model**

A lane change process is a series of interactions between subject and lag vehicles. During this process, many decisions and corresponding actions need to be made by both vehicle drivers. Although a large amount of lane change models have been developed in the literature, most of them have only considered the certain parameters associated with the lag vehicle, but ignored the interactions between subject and lag vehicles. Furthermore, during a lane change process, a vehicle's lateral position will keep changing, which will play an important role in the whole lane change process. However, such lateral position effects were mostly ignored in existing lane change execution models. To overcome these limitations in the current models and to better reflect the communication and interaction among vehicles during a lane changing process, a driver decision-based lane change execution model will be developed, which will be based on a driver's personal perspective to analyze the decision and corresponding behaviors.

- **Simulation of reverse lane change**

The information on incident-induced traffic flow, such as reduced road capability, waiting time, and queue length estimation etc., are important for accurate traffic simulation and prediction. However, very few efforts have been made in the literature to obtain such information by

Introduction

microscopic traffic simulations. Based on the presented open mechanics-based acceleration model and the driver decision-based lane change execution model, a reverse lane change model will be further proposed to simulate some complex traffic situations such as reverse lane change process at a two-way-two-lane road section where one lane is blocked by a traffic incident.

Dissertation outline

To implement the objectives stated above, Chapter 2 will introduce the structure of the proposed OMITS, including the design of the OMITS, a carpool-based OMITS application and the social network design. In Chapter 3, an accurate and robust UAV-based vehicle trajectory data collection method will be established. Chapter 4 to Chapter 6 will focus on the research of driver behavior models in microscopic simulations, where an open mechanics-based acceleration model will be introduced in Chapter 4, followed which the development of a driver decision-based lane change execution model in Chapter 5. Based on the presented acceleration and lane change execution model, a reverse lane change model will be further proposed to simulate some complex traffic situations such as the reverse lane change process at a two-way-two-lane road section where one lane is blocked by a traffic incident. Conclusions and future work will be finally provided in Chapter 7.

The relationship among the vehicle trajectory data and driver behavior models developed in this dissertation can be illustrated in Fig. 1-2, which constitutes a representative microscopic simulation research scope. (1) The presented UAV and its corresponding data collection and vehicle detection algorithm belong to the computer vision, (2) the developed acceleration model is inspired by the interaction mechanics among surrounding vehicles, (3) the proposed driver decision-based lane change execution model is based on the psychology and decision-making of each driver during the lane change process, and (4) the reverse lane change model is an application of the developed acceleration and lane change execution models. It will show unique capabilities that are lacking in existing models, such as simulating certain complex traffic situations. For example, the reverse lane change process at a two-way-two-lane road section where one lane is blocked by a traffic incident.

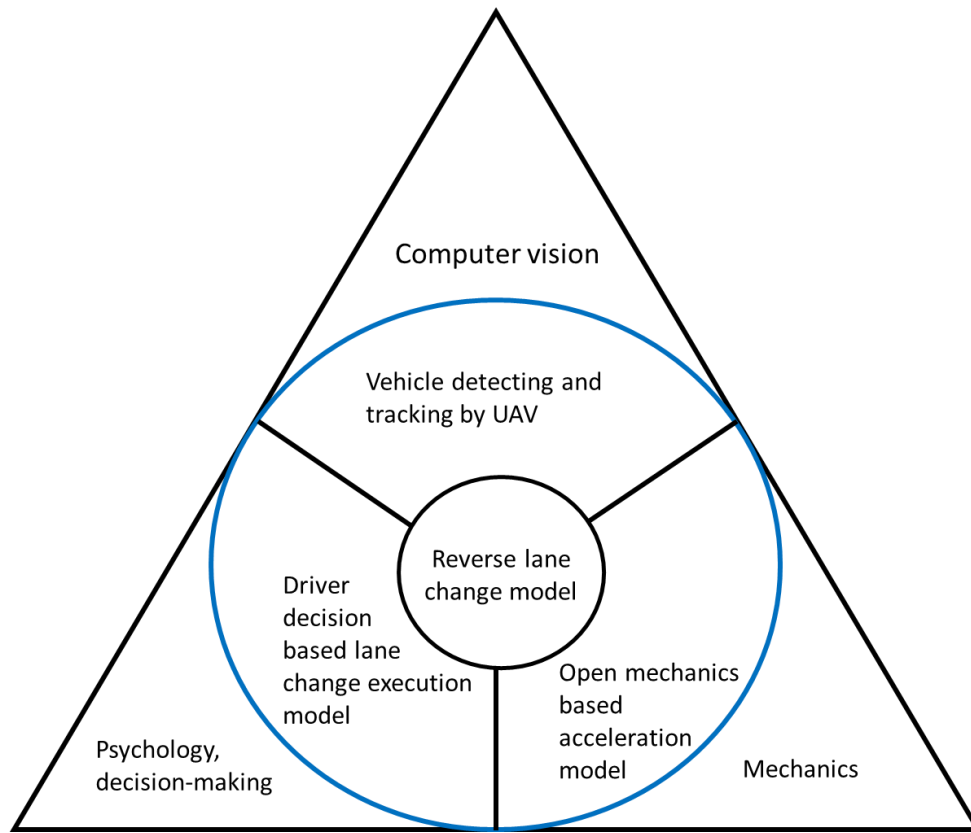


Fig. 0-2 Structure of microscopic simulation research

Open-Mode Integrated Transportation System

The Open-Mode Integrated Transportation System (OMITS) has been proposed in 2009 [5], which has been developed and implemented in cooperation of Columbia University and NDJ Sustainable Engineering LLC, uses emerging information and communication technologies, such as smart phones, Internet services, GPS/GIS, and data mining and fusion technologies, to improve ridership of vehicles and optimize operation of transportation system. This system is designed to provide more effective and intelligent traffic service platform for different specified purpose. In this chapter, Section 2.1 introduces the design philosophy of the OMITS system. Section 2.2 presents an OMITS application to carpool. Section 2.3 describes the social networking aspects in OMITS. Finally, some conclusive remarks are provided in the last Section. This chapter is reproduced from the paper co-authored with Huiming Yin, Paul Maurin, and Heqin Xu, which has been presented in the annual meeting of the Transportation Research Board [99] and published in National Technical Information Service [100]

Design of the OMITS

Design philosophy

New data management systems, navigation technologies, and smart phones provide opportunities to dramatically improve the management of transportation networks without expanding the physical infrastructure. The OMITS system was proposed as a substantial and groundbreaking paradigm shift to change conventional transportation planning and management in three aspects: (i) As vehicle flow in a roadway and one vehicle pick-up/drop-off passengers are in a series sequence. Improving the ridership of vehicle and using group riders with similar transportation demand will parallelize the rider's traveling trajectory and thus optimize travel behavior and save traveling time; (ii) Using the speed difference of information communication and vehicle motion, we can optimize the routing and planning of the trips and thus cut-off travel time for each trip; and (iii) Using social networking, travelers can be grouped for ridesharing with improved traveling experience and safety

Open-Mode Integrated Transportation System

confidence. Similarly to general ITS, the OMITS system has been designed with three major functions, including multimodal travel system for trip planning and carpooling matching, advanced traffic information system for routing and dispatching, and interactive user interface for communication.

Multimodal travel system

Different transportation modes has different features. For example, subway is a type of high-speed and high-capacity public transport generally found in urban areas. However the average distance between stations is long and it cannot cover many suburban residency areas. People who live between stations which will face the “last one mile problem”[101]. Mass transit buses may reach residency areas but the routes and stops are commonly designed to meet the daily transportation demand of the public, and thus too many stops are listed in a static fashion. Any individual stop will cause the time waste of the rest many riders. On the other hand, private vehicles can provide door-to-door service, but the increasing number of vehicles on the road have already significantly devastated traffic jam, parking, and high accident problems. If we can divide a regular trip into several segments with different transportation modes, we may solve the problems in the individual transportation mode. In that sense, the multimodal travel system is required.

Multimodal travel system (MTS) is defined as a combination of different traveler modes and transportation systems operated by various information transport systems. A traveler can use either public (bus, taxi, metro, railway, carpool, and ferry) or private (car, motorbike, bicycle, and walking) transportation modes. The MTS focuses on the distribution of transportation related information and the coordination of regional transportation systems for the benefit of the transportation network users [3].

Travelers need improved means to access the information on alternative transport modes which can be taken their journeys. The MTS is able to increase the utilization of high occupancy vehicle modes. By providing the traffic and transportation service information to travelers, especially regular commuters, prior to embark on their trips, travelers are able to make a most informed choices of modes and routings. Furthermore, trip planning module is a main component of MTS, informing and assisting travelers in choosing the best path to reach their destination based on the real-time or predicted traffic situation. Overall, a well-designed MTS will be an effective

Open-Mode Integrated Transportation System

and efficient method to considerably raise the quality of traveling services and increase the operational efficiency of existing transportation system, and reduce the congestion and pollution as well.

Advanced Traveler Information Systems

Advanced traveler information system (ATIS) is an area of ITS applications. Recent advances in electronics and micro-computing have led to the feasibility of functionally powerful, computer-based advanced traffic information systems as part of the automotive environment. Although these systems range in functionality, they all have the goal of acquiring, analyzing, communicating, and presenting information to assist travelers in moving from a starting location to a desired destination. The systems improve travel safety, efficiency, and comfort and represent a new frontier in ground transportation.

In the highly mobile society of the U.S., travelers have an increasing desire and need for accurate, timely information for trip planning, and traffic reporting. ATIS is designed to meet this need. [102]. The service of ATIS can be classified into static information such as road map, public transportation routes and operation schedules, and dynamic traffic information such as road traffic situation, vehicle real-time position and estimated arrival time.

Real-time road traffic prediction has been an essential components of advanced, smart transportation technologies. It is necessary for network operators and traveler to accurately predict short-term traffic conditions and thus save traveling time. In the past decade, the collection of real-time traffic data was a foremost goal, and now many traffic authorities possess real-time traffic data feeds and information warehouses containing extensive traffic data. The next step will be to use the big data technologies in transportation to crease new services.

Road traffic prediction is the first major step in that direction. However not many tools are available for future predictive information. It is clearly of interest to instruct traffic controllers on how to set signals or various message signs based on expected traffic conditions timely, rather than based on a traffic situation soon to be obsolete [103]. From a traveler's aspect, he/she prefers to being given a route guidance information based on the traffic when he/she gets on the road.

Open-Mode Integrated Transportation System

Interactive user interface for communication

With the development of smart phones, travelers are able to make more activities through it, such as communication with the Internet, detecting roadway geographic information system (GIS) information, and connecting vehicles/riders with global positioning system (GPS) data. The OMITS has built up interactive user interface for communication through mobile applications and the Internet website. The OMITS App will provide drivers with real-time driving directions based on the traffic condition and also riders with vehicle current locations and estimate arrival time.

In addition, the OMITS users are not only able to obtain useful information, but also can request specific services. The OMITS member management system also provides social network features for user communication and dynamic carpool group forming through the OMITS App. For example, using the OMITS-Carpool App, both vehicles and riders can easily send ride offers and requests information, respectively. A driver can check the profiles of riders to approve the carpooling match. With the aid of data mining and fusion, the system can use the traffic data for traveler behavior analysis and traffic prediction, from which an optimal routing direction and ridesharing group can be obtained. In addition, after acquiring user's agreement, the OMITS is able to trace a vehicle's traveling trajectory data, which is an effective way to collect the real-time traffic data. As an on-going work, the user interface will connect users through the social network, which will be explained in detail in Section 2.3.

In summary, the OMITS integrates the availability of multiple public transit modes and private vehicles to provide optimal transportation service to social network-based local communities as well as information service of real-time and future traffic to the riders and the public. The success of this system will provide reliable, safe, efficient, economic and fair transit service to the public and improve the resilience and sustainability of transportation system with broader impacts on gasoline use, greenhouse gas emissions, city parking, transit costs, and traffic congestion relief. The OMITS is still under the development and will be demonstrated in New York metropolitan area and then extended to other megacities through the collaboration with the industry partner – NDJ Sustainable Engineering, LLC. The methodology developed can be also extended to freight transportation and goods delivery.

Open-Mode Integrated Transportation System

Architecture of the OMITS system

The architecture of the OMITS system consists of the information communication framework and the OMITS server performance system which illustrates the main operation system of OMITS. They will be introduced respectively.

Fig. 0-1 illustrates the information communication framework of OMITS. The OMITS server collects transportation demands from riders and matches them with the available services. It also probes the traffic information of road sections through vehicles and simulates the traffic conditions for route direction. The user entities of the OMITS include the follows:

- Public commuters or riders can obtain the ridesharing service integrated with the public transit service at the lowest cost in terms of time or fare.
- Private car or van owners can provide dynamic carpooling or vanpooling service and receive routing service based on traffic situation.
- General members can access the OMITS database for the real-time roadway traffic condition and trip planning.

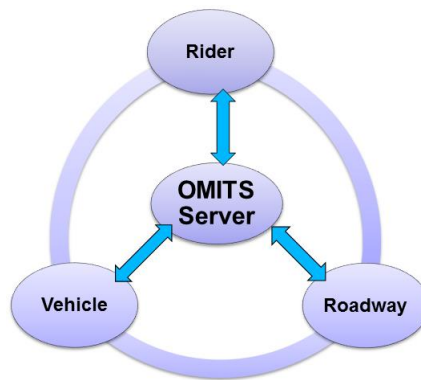


Fig. 0-1 The information communication framework of the OMITS

Notice that, although the system integrates multiple existing transit modes, it only provides the schedule and location information to the OMITS, so their operation and customers will not be affected. The audience of the OMITS system is riders and drivers traveling in city scale, who are open for ridesharing services. Integrating other transit modes into the OMITS system provides passengers the shortest route using all available public transit modes and ridesharing options. In case no ridesharing service available, OMITS can still make the travel plan based on the public transit service. Thus it can guarantee the reliability no lower than the public transit system.

Open-Mode Integrated Transportation System

The OMITS system forms a sustainable information infrastructure for communication within and between the mobile/Internet network, the roadway network, and the users' social network. It manipulates the speed gap between different types of the network: information communication through cellular phones and the Internet is tremendously higher than that of vehicles on roadway, which is much faster than that of the social networking. Using the integrated information communication platform of the OMITS system, the time and spatial limits of traditional transportation system can be overcome by high speed of information communication and data fusion through smart phones and the Internet.

The OMITS server performs the information communication and transportation management through the following three modules as illustrated in Fig. 0-2:

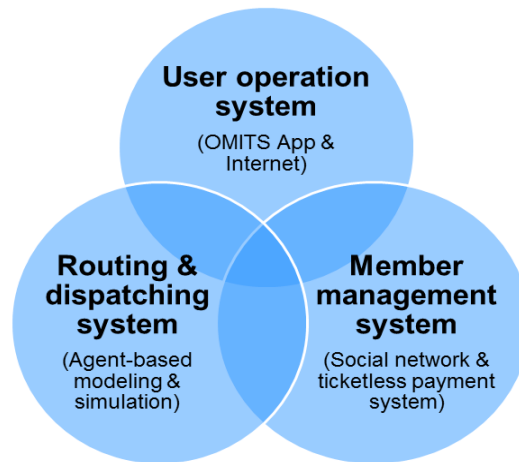


Fig. 0-2 Three modules of the OMITS system for transportation operation and management [5].

The User Operation System provides the interface for users through smart phone apps or the Internet interface. The OMITS App has been developed for iPhone and Android Phone, available for free installation.[38] All drivers are required to use OMITS App for the transit service to provide real-time location and speed of the vehicles. However, a rider, who does not own a smart phone, can still use our Internet interface for transit service. A driver needs to submit a message by the OMITS App to the database server in advance. OMITS server will provide ride-matching information and give driving direction based on the traffic situation through the app. A rider can submit a riding request signal through the OMITS App or the Internet interface at any time. OMITS

Open-Mode Integrated Transportation System

will find a possible ride plan based on the availability of transit services. When a vehicle is in the service, the driver's OMITS App will keep sending its location and speed to the OMITS server.

The Routing and Dispatching System, which keeps running in the background, provides the optimal route for drivers and matches a driver and riders. Using the data of real-time and historic speed on each road section collected by OMITS vehicles, we predict the travel time of the section in future through traffic flow analysis and the support vector regression method, which are used for short-term and long-term traffic prediction, respectively. The schedule of bus will be dynamically updated with the traffic situation. For a driver request, the driving direction will be calculated and recommended by the modified Dijkstra's algorithm using the predicted travel time under the first in first out (FIFO) condition. Once the route is found, it will be transferred into an available service, which is the same as a public transit service. The overall available service forms a network with the temporal and spatial information. When a rider request is received, the Dijkstra's algorithm will be used again to find the best route for the rider, which may cover multiple transit modes.

The Member Management System provides service such as member registration, billing and payment, data reporting and complaint handling. Social network among the member will also be taken into account, so that carpooling among strangers will be avoided. With the clear record in OMITS, no ticket other than the confirmation through the OMITS App is needed at the point of boarding. The payment flow within the OMITS users, both drivers and riders, will go through a monthly bill. Although, the OMITS's ultimate goal is to make a ticketless service for multi-modal transit, corresponding works are anticipated to make it available in the future.

GIS data structure for routing and networking in the OMITS system

The road-net GIS data and routing algorithm are the fundamental components in the OMITS. Most of services are based on them. The basic structure of road-net GIS data and the routing algorithm method in OMITS are introduced respectively.

GIS data structure

A geographic information system (GIS) is a system designed to capture, store, manipulate, analyze, manage, and present different spatial or geographical data. In the transportation, the road information of GIS is widely used in managing, planning, evaluating, and maintaining

Open-Mode Integrated Transportation System

transportation systems [104,105]. The OMITS routing and dispatching system is based on this GIS road map. A small region of GIS data in Manhattan, New York City was firstly uploaded into the OMITS server (Fig. 0-3). To reduce the memory and storage in the OMTIS's data structure, the adjacent list is applied to describe road topological relation. As shown in Fig. 0-3, the structure of the GIS road-net has three hierarchies: road-net, lane and node [106]. Each road section's basic information are stored in the lane module, such as lane number and speed limitation on each direction. The node module includes position's data, such as address and zip code.

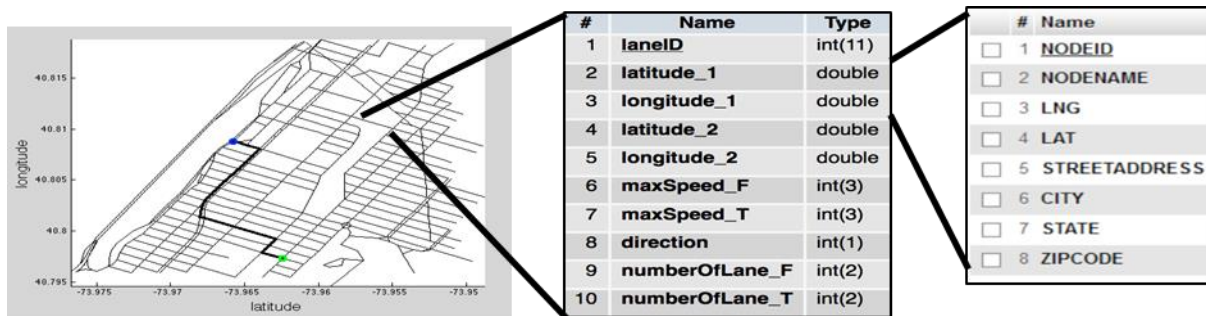


Fig. 0-3 GIS data in OMITS

The integrated dynamic routing method

Within the OMITS system, the existing public transit service can still be handled with the static data integrated with traffic prediction data. A feature is to integrate the carpooling service into the existing available services. The drive routing and rideshare grouping should be provided under the dynamic traffic condition. Given a starting point and the destination, if the speed or travel time on each road section is given, the drive direction can be obtained by the Dijkstra's algorithm, which is based on the open shortest path first protocol.[39]

For example, Fig. 0-4 provides a simple road network with the shortest travel time for each road section under free flow condition. A driver starts at A towards F. Using the Dijkstra's algorithm, we can find the shortest path and travel time is $A \rightarrow E \rightarrow F$; $T=45+45=90$.

Open-Mode Integrated Transportation System

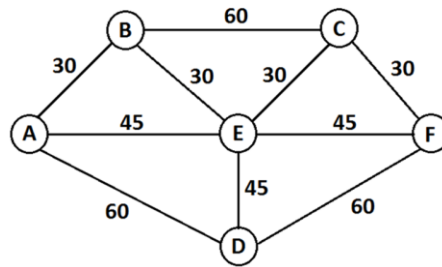


Fig. 0-4 Simple road network with the shortest travel time for each road section

However, in actual traffic situation, the travel time in each road section may change asynchronously, which still satisfies the FIFO condition, i.e. for two riders, who start at t_1 and t_2 ($t_1 < t_2$) and take T_1 and T_2 to travel through the same road section, there exists a condition $t_1 + T_1 < t_2 + T_2$ or $(T_2 - T_1) / (t_2 - t_1) > -1$. Through traffic prediction, we can obtain the travel time for each road section at a certain starting time. For demonstration, the traffic data for the road network in Fig. 0-4 are provided in Table 0-1, which satisfies the FIFO condition. The Dijkstra's algorithm obviously cannot be directly used for dynamic routing. However, under the FIFO condition, a minor modification of the Dijkstra's algorithm will make it applicable to find the shortest path at the same complexity level. The main difference between the modified and traditional Dijkstra's algorithm is that the modified algorithm uses dynamical weight (in the OMITS is traveling time on each road section) based on transportation prediction. Using the data in Table 0-1 for a driver starting at A toward F at 6:00 A.M., the modified Dijkstra's algorithm in the OMITS system is demonstrated step by step. At each step, nodes that are adjacent to the current node are the only ones considered, and other nodes are not updated with a weight of infinity as follows:

1. Assign to every node a tentative travel time value: set it to zero for A and to infinity for B to F. Set the initial node A as current node. Create a set of the unvisited nodes from B to F.
2. Start at the current node A, and update the shortest travel time for all unvisited nodes with start time at 6:00 A.M. $T_{A-B} = 30$; $T_{A-C} = \infty$; $T_{A-D} = 60$; $T_{A-E} = 45$; $T_{A-F} = \infty$. Choose the node B with the shortest time as the current node. Take B from the unvisited node set, which is currently C to F.
3. Start at the current node B, and update the shortest travel time for all nodes with start time at 6:30 A.M.: $T_{B-C} = 70$; $T_{B-D} = \infty$; $T_{B-E} = 30$; $T_{B-F} = \infty$. Only C and E are considered. Starting at A, $T_{A-C} = 100$; $T_{A-D} = 60$; $T_{A-E} = 45$; $T_{A-F} = \infty$. Choose the node D with the shortest time as the current node. Take E from the unvisited node set, which is currently C,

Open-Mode Integrated Transportation System

D, and F.

4. Start at the current node E, and update the shortest travel time for all nodes with start time at 6:45 A.M.: $T_{E-C} = 30$; $T_{E-D} = 45$; $T_{E-F} = 180$. Starting at A, $T_{A-C} = 75$; $T_{A-D} = 60$; $T_{A-F} = 225$. Choose the node C with the shortest time as the current node. Take D from the unvisited node set, which is currently C and F.
5. Start at the current node D, and update the shortest travel time for all nodes with start time at 7:00 A.M.: $T_{D-C} = \infty$; $T_{D-F} = 100$. Starting at A, $T_{A-C} = 75$; $T_{A-F} = 180$. Choose the node C with the shortest time as the current node. Take C from the unvisited node set, which is currently F.
6. Start at the current node C, and update the shortest travel time for all nodes with start time at 7:00 A.M.: $T_{F-C} = 40$. Starting at A, $T_{A-F} = 115$. Finish the calculation.

Therefore, the path of $A \rightarrow E \rightarrow C \rightarrow F$ provides the shortest travel time of 115 minutes.

In general, the nodes used in the algorithm are much more than those of the shortest path. However, the Dijkstra's algorithm does not need to go over all nodes in the map - once the destination node has been marked visited, then stop. The modified Dijkstra's algorithm exhibits the same computational complexity as the traditional one.

However, if the start time is flexible, the total travel time on the road can be much different. For example, if the driver starts at 6:30 A.M., 7:00 A.M., or 7:30 A.M., the shortest paths (travel time) can be obtained in the same fashion, which are $A \rightarrow B \rightarrow C \rightarrow F$ (140 min), $A \rightarrow D \rightarrow F$ (150 min), and $A \rightarrow D \rightarrow E \rightarrow C \rightarrow F$ (145 min), respectively. Using this method, we can provide recommendation for drivers to choose a better start time for traffic control and mitigation.

Once the route is found for a driver, we list it as an available transit service. Traditional transportation assignment can be used to dynamically match riders to private cars and public transit vehicles in the uniform fashion.

Table 0-1 The dynamic travel time for each road section at a specific start time.

Open-Mode Integrated Transportation System

Time	T(A-B;t)	T(A-E;t)	T(A-D;t)	T(B-E;t)	T(B-C;t)	T(C-E;t)	T(C-F;t)	T(D-E;t)	T(D-F;t)	T(E-F;t)
6:00:00 AM	30	45	60	30	60	30	30	45	60	45
6:10:00 AM	30	40	50	30	70	30	30	45	80	60
6:20:00 AM	30	50	40	30	70	30	30	45	80	90
6:30:00 AM	30	60	40	30	70	30	30	45	80	90
6:40:00 AM	30	60	40	30	70	30	30	45	80	180
6:50:00 AM	30	60	40	30	70	30	40	45	80	180
7:00:00 AM	40	90	40	30	70	40	40	45	100	180
7:10:00 AM	40	90	40	40	70	40	40	45	110	180
7:20:00 AM	40	90	40	40	70	40	40	45	110	180
7:30:00 AM	60	100	40	40	70	40	40	45	110	175
7:40:00 AM	60	120	40	40	70	40	40	45	110	170
7:50:00 AM	60	115	40	40	70	40	40	45	110	165
8:00:00 AM	60	115	40	40	70	35	40	45	110	160
8:10:00 AM	60	110	40	40	80	35	40	45	110	155
8:20:00 AM	60	105	40	40	80	35	40	45	110	150
8:30:00 AM	55	100	40	35	80	35	40	45	110	145
8:40:00 AM	55	100	40	35	80	30	40	45	110	140
8:50:00 AM	50	95	40	35	80	30	40	45	110	135
9:00:00 AM	50	140	40	35	90	30	35	45	110	130
9:10:00 AM	45	135	40	30	90	30	35	45	110	125
9:20:00 AM	45	130	40	30	100	30	30	45	110	120
9:30:00 AM	40	130	40	30	100	30	30	45	110	115
9:40:00 AM	30	125	40	30	100	30	30	45	110	110
9:50:00 AM	30	120	40	30	100	30	30	45	100	105
10:00:00 AM	30	115	40	30	100	30	30	45	90	100

OMITS application for Carpooling

The OMITS application design for carpooling has been developed and tested in New York City. The system provides an optimized ridesharing and transit service based on spontaneous transportation demands and service availability.

Background of carpooling

Carpooling can be conceptualized as an arrangement where two or more people, not belonging to the same household, share the use of a privately owned car for a trip (or part of a trip), and the passengers contribute to the driver's expenses [107,108]. Carpooling should be clearly distinguished from car-sharing. In car-sharing, as in carpooling, the same vehicle is used by several different persons but the vehicles are not privately owned. The vehicles usually belong to a car-sharing company and the persons using this service rent them for the duration of their trip. From

Open-Mode Integrated Transportation System

transportation's aspect, carpooling includes the behaviors of picking up and dropping off rider, matching between driver and rider, optimizing route. With respect to formation, carpools can develop casually, through intra-household negotiation, between friends and co-workers, or as part of a structured travel demand management initiative [109].

Road transport, in the European Union, has been estimated to be responsible for approximately 71.4% of CO₂ emissions, which corresponds to more than 20% of global emissions [110]. Private car use accounts for the largest part of kilometers traveled and is considered one of the most important contributors to air pollution [111]. Promoting eco-friendly transportation modes (such as public transportation, bicycle, walking, or carpooling) is becoming more and more frequent. However, even with increasing environmental awareness and concern, many road users are still car-dependent, either by choice or constrained by circumstances [112]. One alternative route for car dependents is carpooling, which has many advantages. The carpooling can reduce the number of kilometers traveled by 12.5% [110]. As a result, such reduction will reduce 7.7% in fuel use, if one person was to be added to each commute [110]. It will also help reduce traffic congestion as well as time and money spent on traveling [113]. Furthermore, it is estimated that people who carpool, for distances of 48 km for example, could save up to 33% of the monthly costs of commuting compared to those who choose to drive alone [114]. Finally, carpooling can reduce driver fatigue, and lead to important social benefits by enlarging carpoolers' social network and increasing their satisfaction [115,116].

Compared with traditional private and public transportation modes, there are three specific features of carpool service. Firstly, the service of carpooling is not fixed. The carpooling service schedule and route are depending on drivers and riders. As a result, a special designed dynamic routing and matching algorithm is required. Secondly, the motivation for a carpooling driver is complex and affected by local transportation policies. For example, if the city introduced high-occupancy vehicle (HOV) lanes in which only vehicles with two or more passengers are allowed to use. HOV lane can create strong practical incentives for carpooling by reducing travel time and expenses, which should be considered in the carpooling routing and matching service. Thirdly, the social network plays an important role in the carpooling service. Since people will feel uncomfortable with a totally unknown person in the same vehicle, a reliable and trustable social network is required. Unlike normal media social network, such as Facebook and Twitter, the

Open-Mode Integrated Transportation System

carpooling social network should have more cautious ID authentication and more reliable relationship between users.

OMITS App and web interface

The development of wireless communications, Internet services, global positioning systems (GPS), geographic information systems (GIS), and large-scale database systems creates us an exciting opportunity to integrate our transportation system for higher levels of efficiency and sustainability [117–119]. The free OMITS App has been developed and published at Apple store and Google Play for free downloading. Once it is installed on a smart phone, the information communication can be conducted between users and the OMITS server. In the meantime, an OMITS web page is also developed, the address is <http://ndjse.com/omits.php>.

Using an app of smart phones or web interface, OMITS customers can communicate with the OMITS server, detect roadway traffic conditions, and receive driving directions. With the aid of data mining and fusion, the system can use the traffic data for traveler behavior analysis and traffic prediction, from which the optimal routing direction and ridesharing group can be recommended.

Data structure and working mechanism of the OMITS system

For the customized design of carpooling, a data structure has been developed. Fig. 0-5 illustrates the entity-relationship (ER) diagram of the OMITS system for the design and development of its database. Starting at the bottom, the road network is made of RoadSections, which are the links on the map including specific speed limit and historic, current and predicted travel time data. The link connects two Nodes, which can be either StopNode or ParkSite associated with a ZoningGroup to facilitate node grouping. An adjacency list is provided for each node, which forms the road network. A Route for RideSharing typically consists of multiple links. A member of OMITS may own a PrivateVehicle to serve as an OMITS driver or simply present as a rider. FrequentTrips are also reported for each member for easy input of service request. When a member demands a RideDemand, it will match with RideSharing and ServiceRoute containing the related nodes. Besides PrivateVehicle, AllVehicle also lists the types of PublicVehicle, which are owned by different TransitProviders and serve for different ServiceRoute.

Open-Mode Integrated Transportation System

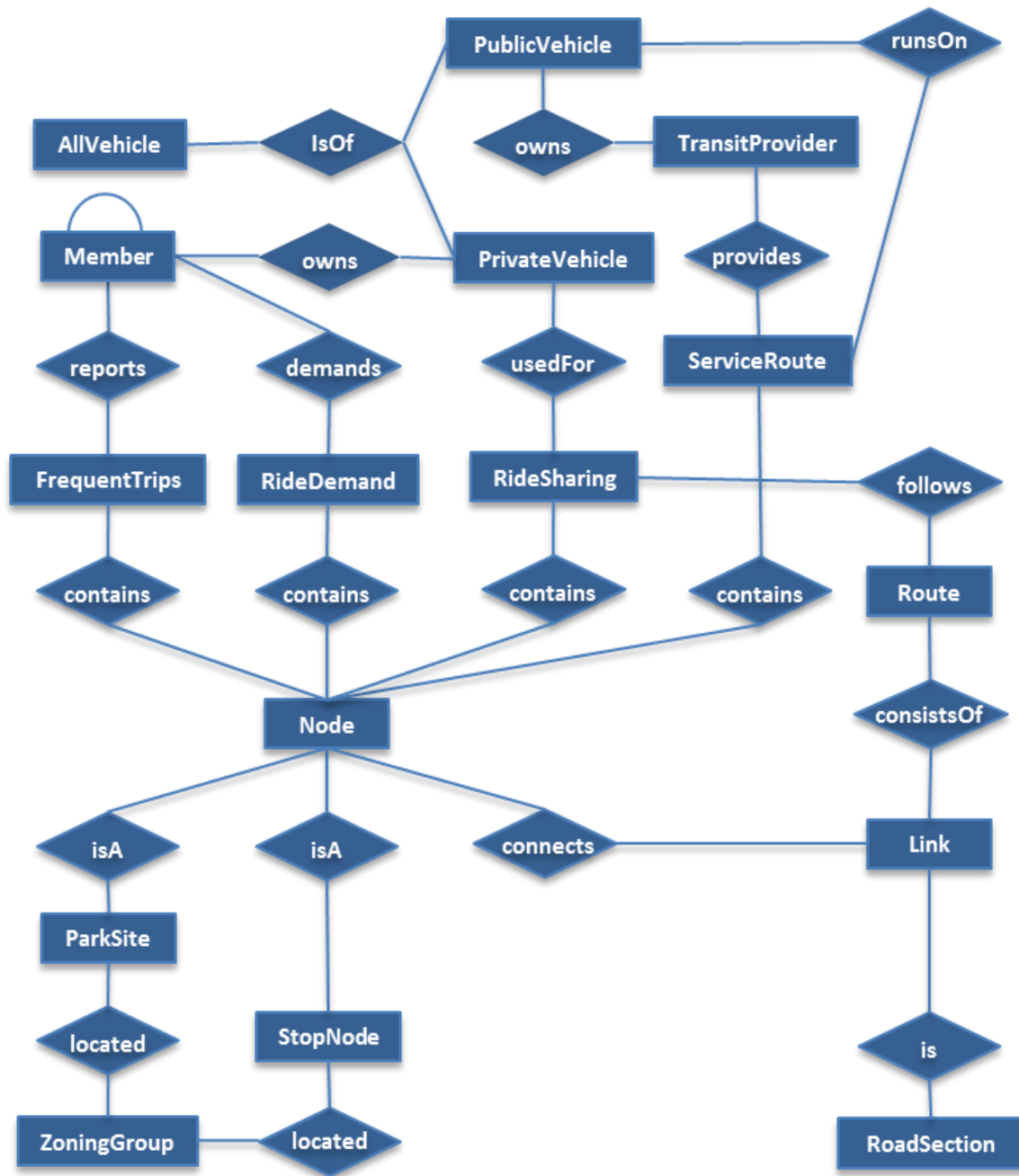


Fig. 0-5 Entity-relationship diagram of the OMITS

Using the OMITS App in Fig. 0-6 together with the public transit databases, the OMITS system integrates carpooling into the public transit systems for dynamic transit services to the public. The social network among users has been recorded through membership invitation and registration. To match a ride between a driver and riders, their social relationship and route information (both service time and location) will be considered, so that friends and colleagues will

Open-Mode Integrated Transportation System

have more chance to share rides, so as to alleviate the nervousness and hesitation of drivers to provide ridesharing service. The OMITS can find a ride for rider requests with a lower cost and higher reliability, so that it is a more preferable choice for users.



Fig. 0-6 Interface of the OMITS App on smart phones (a) member management, (b) new service request, (c) service information, (d) rider information for carpooling, and (e) dynamic route direction and pick-up sites

Fig. 0-6(a) shows the OMITS App's user interface of user profile for member management. We can update the profile as needed. "Trip" button is used to request or provide a carpooling service. The user can type departure and destination addresses manually in Fig. 0-6(b). If the user is to repeat a frequent route, the most frequent trips are shown in a descent order of trip frequency. Each trip item contains the departure time, departure address and destination address as Fig. 0-6(c). Once a carpooling service is produced, the driver can see the rider's information in Fig. 0-6(d) in "Ride" button. "Route" button will show the current vehicle location and driving direction to pick-up and drop-off riders as Fig. 0-6(e). The "Info" button provides some common information for public transit providers, OMITS contact and emergency information.

Social network

A social network is a relational connection between individuals, including every relationships related to the exchange of information such as those among friends or colleagues [120,121]. The social network perspective provides a set of methods for analyzing the structure of whole social

Open-Mode Integrated Transportation System

entities as well as a variety of theories explaining the patterns observed in these structures. Social network analytics are useful to a broad range of research enterprises. In social science, these fields of study include, but are not limited to anthropology, biology, communication studies, economics, geography, information science, organizational studies, social psychology, sociology, and sociolinguistics [122]. As above stated, for a user, carpooling is not only a transportation mode, but also an important opportunity to extend social benefits by enlarging carpoolers' social network.

The social relationship among members is also recorded with primary relationships, including "neighbor", "coworker", "ride-sharer", and "stranger" in order. The relationship may change with the ridesharing service. For example, once strangers share rides, their relationship is upgraded to "ride-sharer". "Neighbor" and "coworker" means they share close home and work addresses, respectively, but their relationship can be overridden by one member for unhappy experience and thus be downgraded to "stranger" to avoid future ridesharing. Each member has an adjacency list for the relationships with other members, which forms a social network. To improve a social network's reliability and trust, the social network member could be limited into an authentic group, such as a school or a company.

During ridesharing match, the member with a closer relationship will have higher priority to get a ridesharing service. In this way, direct or indirect friends can share ride and thus have improved ride experience. Each member can invite their friends to become member and associate with other members into friend groups, so that we can provide dynamic transit service based on the social network. Accordingly, Dijkstra Algorithm [123] in social network is applied to find out the best match between riders and drivers.

Fig. 0-7 and Table 0-2 is one example of the social network between faculties of School of Engineering and Teachers College. Social relationship network is limited by one person's working, entertainment, and living etc. As a result, the relationship between two different groups is relatively weak. In the left circle, the Engineering school faculties know each other very well, but between the two groups of people, there is only one direct connection between A and G. This social phenomenon limits the amount of the OMITS users. According to the Dijkstra Algorithm, we introduce the road-network shortest route concept to social network. For example, In Table 0-2, each connection between two persons has a weight. The bigger weight means this kind of relationship is harder to extend than the smaller weight. In the OMITS, we apply Dijkstra algorithm

Open-Mode Integrated Transportation System

in social network to provide the shortest relationship between two persons, and minimize the sum of weight values in one carpooling vehicle. As a result, instead of direct relationship between two people, the OMITS applies the shortest relationship chain. In this example, the relationship connection between D and H is D-E (Coworker), E-A (Coworker), A-G (Neighbor), and G-H (Friend). This information of the relationship chain will be showed on smart phone of each rider and driver. The improved social relationship network system will reduce the opportunity to be a “stranger” between two persons, and also enforce the relationship after each ridesharing service.

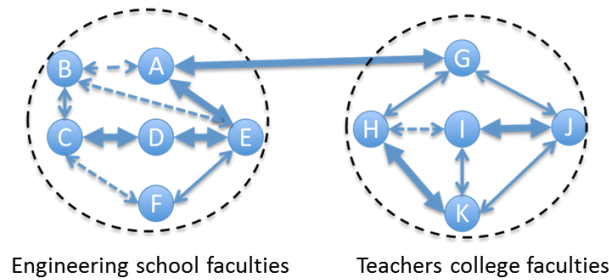


Fig. 0-7 Social relationship network sample

Table 0-2 Weights of Social relationship network at different relationship

Relationship	Weight	Symbol
Neighbor	1	↔
Coworker	1	↔
Friend	2	↔
Ride-sharer	3	⋯↔

Conclusions

The structure and the main features of the Open-Mode Integrated Transportation System are presented in this chapter. The OMITS is designed for improving the traffic condition of roadways by increasing ridership of vehicles, and optimizing transportation modes through smart services integrating emerging information communication technologies, big data management, social networking, and transportation management. A carpooling based OMITS prototype has been developed and tested in New York City. It can provide an optimized ridesharing and transit service based on spontaneous transportation demands and service availabilities. Actual application and implementation of the OMITS is underway through the collaboration with NDJ Sustainable

Open-Mode Integrated Transportation System

Engineering LLC. The OMITS is far beyond a carpooling system. Using the OMITS App, it integrates the carpooling service into the public transit system with the aid of taxi system and emergency service system and provides real-time transit service. OMITS aims to find a ride for all rider requests with a lower cost and higher confidence. The charge and credit of the carpooling riding service will be managed by the system, and no money flows between riders and drivers directly, which makes it possible for a fair rule. The member management system provides service for drivers to briefly check the information of riders, so as to alleviate the nervousness and hesitation of drivers to provide carpooling riding service. OMITS also provides an ideal platform for social networking to promote carpooling and improve traveling experience.

As a core function, the operation of the OMITS relies on the accurate prediction of the traffic on the roadway. Although the OMITS App also performs as a probe for vehicle trajectory data acquisition, the information is discrete and limited. We have developed alternative methodology using unmanned aerial vehicles for collecting detailed and continuous trajectory data of vehicles on a road section, which will be introduced in Chapter 3. As key components in optimizing traveling routing and matching in the OMITS, traffic simulation and prediction are carried out to understand each individual vehicle's behaviors at the microscopic level and to accurately simulate and predict the traffic. Accordingly, the acceleration and lane change execution models as two central components of vehicle's behaviors will be introduced in Chapter 4 and Chapter 5, respectively. The influence of incident-induced traffic flow are important for accurate traffic simulation and prediction in OMITS. To study such an influence, Chapter 6 will develop a reverse lane change model to simulate driver behaviors at a two-way-two-lane road section where one lane is blocked by a traffic incident.

Vehicle trajectory data collection by UAV

In this chapter, a vehicle trajectory data collection system based on image data collected by UAV is presented. Although, cell phone's GPS can provide vehicle's trajectory data in the OMTS, however, limited by its precision and users distribution, such data can only be used to indicate traffic flow states, such as the average travel time and speed, but cannot be used in traffic simulation analysis. As a result, a UAV-based vehicle trajectory data collection method is designed. This system uses consecutive frames to generate a vehicle's dynamic information, such as positions and velocities. Four major modules have been developed: image registration, image feature extraction, vehicle shape detecting, and vehicle tracking. Three image features have been introduced into this system to customize the vehicle and traffic flow and to jointly use them in multiple consecutive images to increase the system accuracy of detecting and tracking vehicles. This chapter is reproduced from the paper co-authored with Fangliang Chen and Huiming Yin, which was being reviewed by Automation in Construction [124].

Introduction

With the ongoing growth of our metropolitan road network, it is indispensable to have a comprehensive monitoring system for the complex transportation. However, there are many limitations based on the current monitoring systems. Firstly, the range of traditional road traffic monitoring is restricted to the sensor's distributions, such as induction loops, radar sensors and traffic cameras. According to the sparse distribution of the current traffic monitoring system, there are many blind regions on a city road network. In certain cases such as emergency mitigation, it is required to temporarily supervise the detailed traffic situations at the "hotspots", such as the regions of traffic incidents, sources and/or destinations of traffic flow, and the emergency locations with damage of ground infrastructure [125], etc. Secondly, most traffic sensors are designed to

Vehicle trajectory data collection by UAV

collect the traffic information on a fixed road section or a limited road length. As a result, it is convenient to obtain the traffic data at the lane's level, including each lane's average speed, density and flow, but it is hard to obtain traffic data at vehicle's level based on these discretely distributed sensors, such as vehicle's trajectory data.

The vehicle's level data is the fundamental data for both intelligent transportation systems (ITS) and transportation management [126]. Therefore, a monitor method designed for traffic data at vehicle's level is of significance in transportation engineering. On the other hand, in the research of driving behaviors, a detailed and accurate vehicle trajectory data is also necessary. Driving behavior models capture drivers' tactical maneuvering decisions in different traffic conditions, and the models are essential components in microscopic traffic simulation systems. Due to the limited availability of detailed trajectory data, most models are not validated rigorously[6]. Data availability has posed a significant obstacle to the advancement of driving behavior modeling. Therefore, a system for detecting and tracking vehicles from UAV can on one hand compensate the disadvantage in the existing transportation monitoring system, while on the other hand can also fulfill the data requirements in the research of driving behaviors modeling.

As a useful and powerful aerial robot, UAV plays important roles on data and image acquisition. For example, they have been widely used in the research of agriculture, geology, hydrology, and cinematography etc. [12–17]. Compared with traditional transportation sensors located on the ground or low angle cameras, UAV exhibits many advantages, such as low cost, easy to deploy, high mobility, large view scope, uniform scale, etc. UAV can record different lengths of road by adjusting flying altitude to fulfill different research requirements. Compared with low angle cameras, the video recorded by UAV has less influences on the block of vehicles in a lane, and could measure vehicle's position more accurately from the top view [18]. However, UAV is rarely applied in the transportation monitoring. One of the main reasons is the lacking of an effective and robust method to detect and track vehicles in the UAV's image data.

Usually, the traffic data captured by UAV contains much complex information than those by traditional monitoring system. UAV's videos include not only the traditional data such as the average speed, density and traffic flow, but also the each vehicle's level data, such as vehicle's trajectory data, lane change data and car following data on the road. In addition, the data from a frame of UAV's video contains multiple vehicles and the frame frequency of UAV's video is very

Vehicle trajectory data collection by UAV

high, thus the data size from the UAV's video is very large. Moreover, the data from UAV's video contains the fundamental information of transportation research and management, and play an important role in several other fields of transportation science and engineering, including safety studies and capacity analyses [6,127,128]. Considering such features, the data collection, reduction and analysis can be considered as an important component in the big data analysis in transportation. It can be extended to other civil engineering applications.

Compared with traditional traffic surveillance systems, detecting and tracking vehicles through the images captured by UAV has specific challenges. First of all, the camera of UAV surveillance platform changes frequently because the camera in the UAV may rotate, shift and roll during video recording. In addition, sudden shakes might also happen due to wind fluctuations, which can cause negative effects in the vehicle tracking. On the other hand, in driver behavior research models, such as car following and lane change models, each car's accurate trajectory data is needed. Missing car data and tracking error could affect the accuracy of the model parameters settings. Therefore, a high resolution of images is crucial for accurately calculating vehicle speed and lateral position of vehicles in the process of vehicle detecting and tracking.

Overall, detecting and tracking vehicles in traffic by UAV's videos and photos has been attracting increasing attention among transportation research community. However, many problems have not been solved yet. Firstly, the accuracy of vehicle recognition is low. Normally, the detecting accuracy of the existing technology is lower than 90% [36,38,39,46], and the driver's detailed trajectory data cannot be obtained [47,48]. On the other hand, traffic information, such as road, traffic flow and driver behavior features, have not been included in these methods [29,43,49]. To the best knowledge of the author, a well-developed vehicle detecting and tracking method for actual transportation application has not been developed yet.

This chapter introduces a method attempting to address these problems. It combines many features in different optical methods into an integrated system, which consists of four modules: image registration, image feature extraction, vehicle shape detecting, and vehicle tracking. Complementary advantages of different optical methods considerably improve the accuracy by this method. In addition, vehicle and traffic flow features and the corresponding specifications have been implemented in the system. In what follows, Section 3.2 will introduce the experiments with the UAV; Section 3.3 will present the methodology of vehicle detection and tracking in traffic.

Vehicle trajectory data collection by UAV

Section 3.4 will demonstrate the numerical results based on the experimental data for the vehicle detection and tracking. Finally, some conclusions of this work are provided.

Experiments

A UAV traffic monitoring system has been set up to study traffic information, which consists of the quadrocopter, camera mount, image transfer system, and camera as shown in Fig. 0-1(a), where the camera mount and the camera are enlarged in Fig. 0-1(b).



Fig. 0-1 The UAV traffic monitoring system used in this experiment: (a) the whole set-up and (b) the camera mount and camera

The quadrocopter used in the experiments of this paper is the DJI Phantom 2. It includes motors, battery, electronic parts, and the connection port for the camera mount. The core control part of UAV is the flight control unit, which is a lightweight multi-rotor control platform specially designed for this lightweight UAV. The flight control unit combines the main controller (MC), a gyro-accelerometer, and a barometric altimeter. The basic information of the machine is listed in the Table 0-1.

The second device is the camera mount. A 3-axis H3-3D gimbal (Fig. 0-1(b)) powdered by built-in Inertial Measurement Unit (IMU) and special servo module was applied, which can compensate movement of the quadrocopter and provide stable quality visual video during the data collection. The camera used in the experiment is a GoPro 3 in silver version. The camera parameter settings in the experiments are listed in Table 0-2.

Table 0-1 Parameters of quadrocopter in the experiments

Parameter	Range
-----------	-------

Vehicle trajectory data collection by UAV

Operating temperature	-10°C ~50°C
Take-off weight	<1000g
Hovering accuracy (GPS Mode)	Vertical: $\pm 0.8\text{m}$, Horizontal: $\pm 2.5\text{m}$
Max yaw angular Velocity	200 °/s
Max ascent/descent Speed	Ascent: 6m/s, Descent: 2m/s
Max flight velocity	10m/s
Diagonal distance	350mm
Weight with battery	800g
Max flight time without load	25 min

Table 0-2 Camera parameters in experiments

Parameter	Range
Resolution	1920×1080
Frequency	30 fps
Optical zoom	1x
Horizontal degree of field of view	94.4
Vertical degree of field of view	55.0
Diagonal degree of field of view	107.1
Dimensions	177mm×100mm×100mm
Weight	590g

The third part of the UAV used in the experiment is the image transfer system. It transmits real time video and UAV's flight data back to the controller. The information displayed on the controller's screen is shown in Fig. 0-2(a). In addition, the more important real-time flight data is superimposed on the video. The information includes power voltage, channel, distance between aircraft and home points, height, control mode, fail-safe mode, pitch attitude, roll attitude, flight velocity, GPS satellite, video input, vertical velocity, attitude line and aircraft nose direction. During the test, as the UAV must remain stable in the air, its position has significant influence on the results, therefore the height and aircraft nose direction are key to the experiment. In order to control the UAV more precisely, reference lines are added on the screen. The video monitor is attached with the quadcopter's remote controller, and the working image is shown in Fig. 0-2 (b).

Vehicle trajectory data collection by UAV

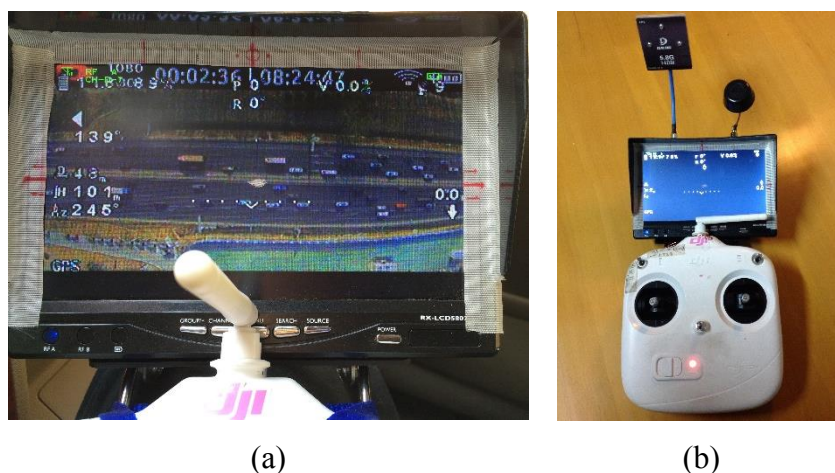


Fig. 0-2 Image capture and transfer system: (a) image taken during the experiment and (b) the remote controller of quadcopter and video monitor

Considering the capability restrictions of image transfer system, the video is stored in the camera's SD card, and only the low-resolution images could be obtained in the monitor during the experiment. So the vehicle tracking and detection method cannot be operated in real-time with current experiment devices. However, with a more powerful image transfer system, the video could directly transfer into a computer. Therefore, the vehicles' real-time detecting and tracking could be possible using the method introduced in this paper.

Vehicle detection and tracking methodology

In this section, the whole procedures of the method for vehicle detection and tracking are presented. The workflow chart of the system is illustrated in Fig. 0-3, which consists of four major modules: image registration, image feature extraction, vehicle shape detecting and vehicle tracking. Each part will be elaborated subsequently.

Two factors of this method are worthy noting. First, three image features are used, including edge, optical flow and the local feature point which are elaborated in Section 3.2. These features work together to increase the accuracy of vehicle recognition. On the other hand, vehicle detecting and vehicle tracking are analyzed as two modules in this method. It is better to make specific adjustments based on their different objective. For instance, vehicle detection aims to accurately identify each vehicle's shape in a single frame, while vehicle tracking focuses on each vehicle's motion between consecutive frames. Therefore, each module of the present method is based on the

Vehicle trajectory data collection by UAV

combination of computer vision and transportation. The properties of traffic flow and driver behavior have also been taken into account in this method.

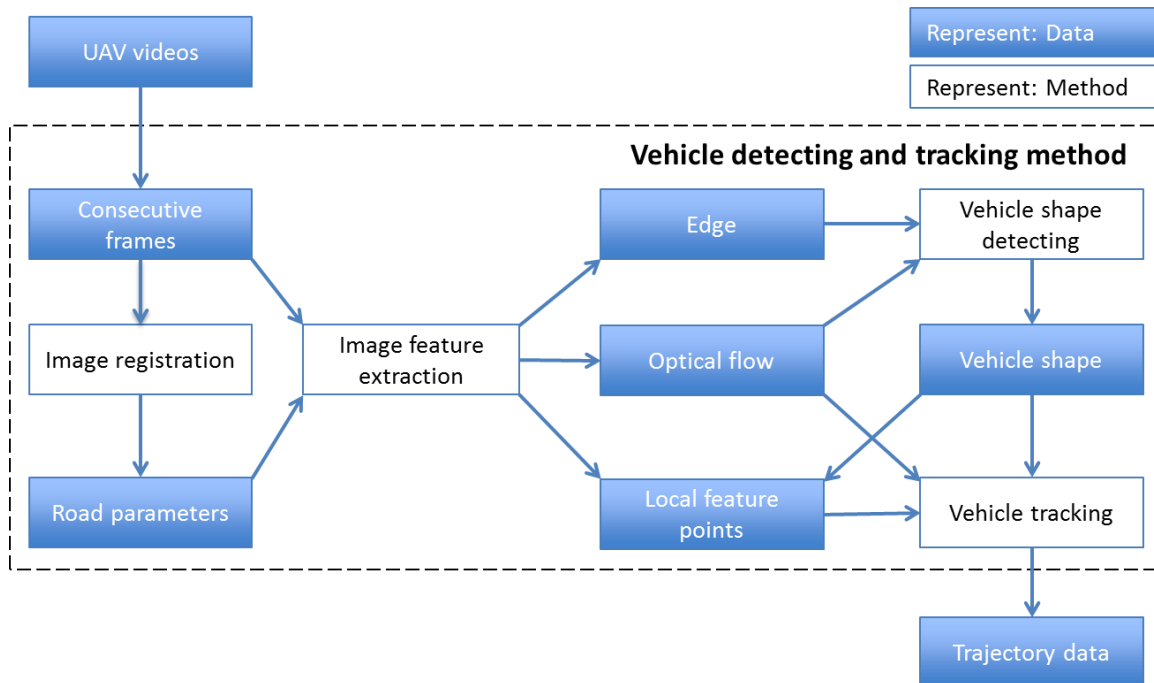


Fig. 0-3 Workflow chart for vehicle detection and tracking in a UAV system

Image registration

Because of the instability of the UAV flying in the air, the vehicle motion recorded in the video is actually the sum of the real motion of the vehicle and that of the camera. In order to obtain each vehicle's trajectory data, the camera motion should be separated and eliminated from the vehicle motion in the video. This section describes a sequential and automatic framework aiming at the precise registration of a road area. In the computer vision science, these processes of transforming different sets of frames into one coordinate system are called as image registration, which includes transformation models and matching point selection[129,130]. Three types of transformation and corresponding applications are introduced. The methods of matching point selection in road environment are also discussed.

Transformation models

Normally, the general transformation between two images could be expressed in the following equation[131]:

Vehicle trajectory data collection by UAV

$$X_{a,p} = TX_{b,p} \quad (0.1)$$

where $X_{a,p}$, $X_{b,p}$ are the image coordinates of the point p in the frame a and frame b ; T is the transformation matrix, which includes the information of rotation matrix from a to b , translation vector from a to b , and camera's intrinsic parameter matrices, etc.

Because all optical imaging system strongly rely on the weather and illumination conditions during the experiment[49], there is no uniform transformation model could be applied for all UAV's videos and all traffic situations, and the matrix T in Eq.(0.1) has different expressions correspondingly. Theoretically, a complex T could be more compatible for complex situations, but has higher probability to fail, while a simple T could only be used in specific situation, but is relatively stable in the image registration [49].

For an arbitrary object, the relationship of a fixed point in an image and a reference image is following a fundamental matrix [129,132]. However, if considering the road surface in a UAV's video is a planar, and the scene height differences are relatively small compared to the UAV's flight height, the image transformation process could be assumed as a homography transformation problem [49]. The homography transformation matrix could be expressed as Eq.(0.2) [49,133].

$$\begin{bmatrix} x' \\ y' \\ 1 \end{bmatrix} = \begin{bmatrix} h_1 & h_2 & h_3 \\ h_4 & h_5 & h_6 \\ h_7 & h_8 & 1 \end{bmatrix} \begin{bmatrix} x \\ y \\ 1 \end{bmatrix} \quad (0.2)$$

where h_1 to h_8 are parameters needed to be determined. At least four corresponding points are required to determine the homography matrix, while three of them must be non-collinear[133].



Fig. 0-4 Two frames in a UAV experiments: (a) the 120st frame, (b) the 1530th frame

Vehicle trajectory data collection by UAV

Because of the camera mount in a UAV system, some camera movements along some specific directions could be well controlled by adjusting the operational parameters. As shown in Fig. 0-4, the camera's rotation along the road lateral direction is very small, and the main camera's movement is on the road lateral direction. In that situation, the lines along the longitudinal direction of the road are always parallel and follow the linear transformation requirements. Although the lines in the frame are not always parallel on the lateral direction, considering the road length is much longer than width in the video, and the vehicle's width is relatively small, we still can assume this is an affine transformation and the transformation model could be expressed by Eq.(0.3) [131].

$$\begin{bmatrix} x' \\ y' \\ 1 \end{bmatrix} = \begin{bmatrix} a_1 & a_2 & t_x \\ a_3 & a_4 & t_y \\ 0 & 0 & 1 \end{bmatrix} \begin{bmatrix} x \\ y \\ 1 \end{bmatrix} \quad (0.3)$$

where the 3×3 matrix is the affine transformation matrix. The parameters a_1 to a_4 define scale, rotation, and sheering effects of the combination of any linear transforms, and t_x and t_y are translation parameters on the x and y directions. In the Eq.(0.3), there are 6 parameters needed to be determined.

If the wind during the experiment is very small and the whole UAV system is well optimized, the camera mount could isolate the UAV's movement and accurately maintain the camera always vertically facing to the ground (Fig. 0-5). In that situation, the transformation model can be considered as a scale-rotation transformation, which can be mathematically expressed in Eq.(0.4) [131].

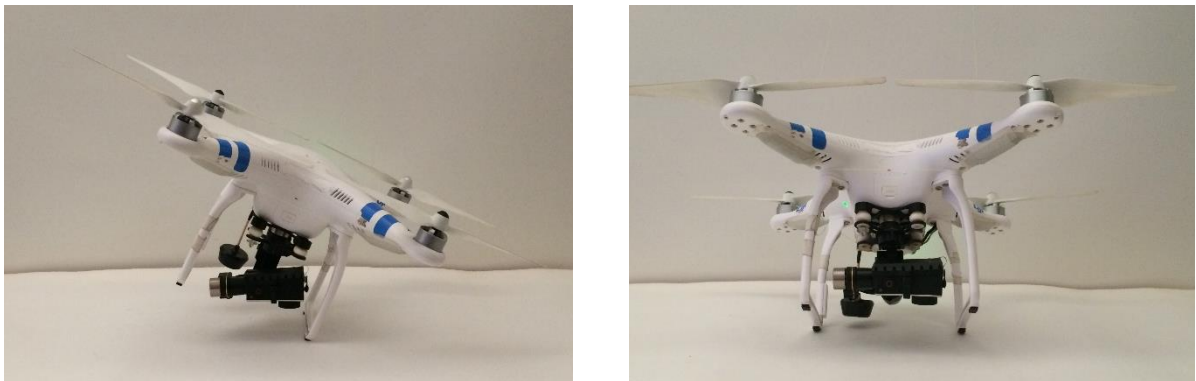


Fig. 0-5 The camera mount isolate of the quadcopter

Vehicle trajectory data collection by UAV

$$\begin{bmatrix} x' \\ y' \\ 1 \end{bmatrix} = \begin{bmatrix} s \cdot \cos\gamma & s \cdot (-\sin\gamma) & t_x \\ s \cdot \sin\gamma & s \cdot \cos\gamma & t_y \\ 0 & 0 & 1 \end{bmatrix} \begin{bmatrix} x \\ y \\ 1 \end{bmatrix} \quad (0.4)$$

where the transformation matrix has four unknown parameters. Besides t_x and t_y , s represents the scale changes, and γ is the rotation angle of camera. Two matching points are required to determine the matrix.

For a real UAV video, the transformation model selection is based on the quality of the video. Table 0-3 lists the three most possible image transformation models could be used in the image registration. Considering the field test environment and the stability of UAV's video, the scale-rotation matrix has been implemented in our simulation in the following part of this paper.

Table 0-3 Transformation models in the image registration

Transformation Model	Minimum matching points	Requirements
Homography	4	The observed road in a plane or the height of the observed object is relatively small compare with UAV's altitude.
Affine	3	The camera rotation along the road lateral direction is small
Scale-rotation	2	The camera could always vertically face to the ground

Matching point selection

Normally, the altitude of the UAV is more than 100 meters, and the region of road is only a small part of the whole view scope of UAV's camera. Therefore, the scene covers a large amount of unnecessary information, which might cause errors in the process of image registration [49]. On the other hand, repeated patterns are also a severe problem, which could lead to the failure of algorithm. The road area of a freeway severely suffers from this problem, because there are several similar road elements, such as landmarks and lights. For these reasons, traditional image registration methods, such as SIFT-based matching [134] and Kanade–Lucas–Tomasi (KLT) based matching [135] will have many difficulties in parameter determination [49].

To improve the accuracy and robustness of image registration for the UAV's video, two methods are proposed in the matching point selection. First, the road features are selected to

Vehicle trajectory data collection by UAV

calculate the camera motion. To reduce the error caused by the repeated pattern, the elements of road could be used as matching points, including road width, road direction angle θ and lane mark. However, the relatively high objects on the road, such as signal boards, are not recommended as matching points, because the height of signal board is usually higher than 10 meters, which not accurately satisfy the plane assumption of homography transformation that all objects in the image should be in the same plane. For example, the two signal boards in Fig. 0-6(b), which have been marked in green boxes, are not proper matching points.

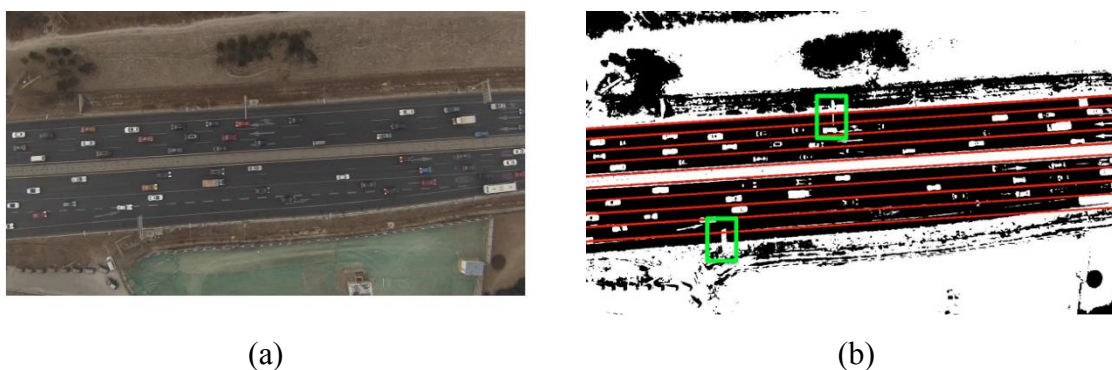


Fig. 0-6 Traffic flow in UAV's frame: (a) the original UAV's frame and (b) the BW figure by setting the threshold of $V=0.35$

Furthermore, the color form of the video is recommended to transform into HSV, which represents hue, saturation and value. Compared with other color forms, HSV is easy to capture the road features, because the road materials are usually selected to absorb light and avoid reflecting and lane marks are selected to reflect light clearly. The road area shows much lower value of V than others. As a result, by setting a suitable threshold for V , the road information can be easily captured. Fig. 0-6(a) illustrates an example of image registration; whereas Fig.6(b) shows the result of setting the threshold of V as 0.35, which is set according to the illumination and the camera parameters.

Image feature extraction

After the image registration, the next step is to extract the image features, including, edge, optical flow and local feature point. The image features will be used in the modules of vehicle detection and vehicle tracking. In this section, the concepts of the three image features are briefly

Vehicle trajectory data collection by UAV

introduced. Considering the characteristics of traffic flow to be investigated, some specific modifications are made in the process of image feature extraction.

Edge

Edge detection has been carried out by a set of mathematical methods, which aim at identifying points in a digital image at which the image brightness changes sharply or, more formally, exhibits discontinuities. The points at which image brightness changes sharply are typically organized into a set of curved line segments termed edges [136]. In this method, the operator of Prewitt edge detection [130] is applied. Mathematically, the Prewitt operator uses two 3×3 kernels that are convolved with the original image to calculate approximations of the derivatives - one for horizontal changes, and the other for vertical, which could be expressed by Eq. (0.5) [130].

$$G_x = \begin{bmatrix} -1 & 0 & 1 \\ -1 & 0 & 1 \\ -1 & 0 & 1 \end{bmatrix} * A \text{ and } G_y = \begin{bmatrix} -1 & -1 & -1 \\ 0 & 0 & 0 \\ 1 & 1 & 1 \end{bmatrix} * A \quad (0.5)$$

where * here denotes the 2-dimensional convolution operation; A is an a grayscale digital image, which is converted from the original UAV's video; and G_x and G_y are two images which at each point contain the horizontal and vertical derivative approximations.

In this method, we only analyze the direction vertically to the longitudinal direction of the road. Therefore, the edge required in the method can be calculated by

$$G_{lat} = G_x \sin\theta + G_y \cos\theta \quad (0.6)$$

where θ is the angle from x -coordinate to the road longitudinal direction, the value is obtained in the process of image registration in Section 4.3.1.

Then based on each pixel's $G_{lat}(i, j)$, it is possible to generate the edge binary image with a proper threshold δ , where i and j are the pixel indexes at x -axis and y -axis separately. The value of δ is affected by experimental environments and operational parameters of UAV's camera. Each pixel's value in the binary image can be calculated by Eq.(0.7) and a frame of the resulted edge is shown in the Fig. 0-7.

Vehicle trajectory data collection by UAV

$$F_{edge}(i, j) = \begin{cases} 1 & G_{lat}(i, j) \geq \delta \\ 0 & G_{lat}(i, j) < \delta \end{cases} \quad (0.7)$$

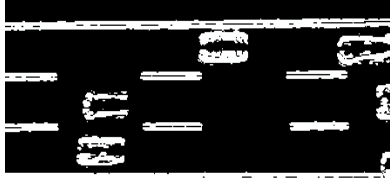


Fig. 0-7 Edge feature in the lateral direction of the road

Although Fig. 0-7 only shows the vehicles' lateral boundary and the vehicle shape is not very clear, the vehicle shape could be easily recognized together with the optical flow result. The Optical flow will be introduced in the following section.

Optical flow

Optical flow is the pattern of apparent motion of objects, surfaces, and edges in a visual scene caused by the relative motion between an observer (an eye or a camera) and the scene[137]. For a 2D with time dimension case a voxel at location (x, y, t) with intensity $I(x, y, t)$ will move by Δx , Δy and Δt between the two consecutive image frames, and the following brightness constancy constraint. Assuming the movement is small, the image constraint at $I(x, y, t)$ with Taylor series can be expressed by Eq.(0.8) [137].

$$I(x + \Delta x, y + \Delta y, t + \Delta t) = I(x, y, t) + \frac{\partial I}{\partial x} \Delta x + \frac{\partial I}{\partial y} \Delta y + \frac{\partial I}{\partial t} \Delta t + O(\Delta x^2, \Delta y^2, \Delta t^2) \quad (0.8)$$

Eq.(0.8) can be rewritten into

$$\frac{\partial I}{\partial x} V_x + \frac{\partial I}{\partial y} V_y + \frac{\partial I}{\partial t} = 0 \quad (0.9)$$

where V_x, V_y are the x and y components of the velocity.

Eq.(0.9) is known as the optical flow equation [135]. Because there are two unknown variables V_x and V_y , an additional equation is required, given by some other constraints. Different optical flow methods introduce different extra conditions for that.

Vehicle trajectory data collection by UAV

The Lucas-Kanade operator [135] is applied in this method. It assumes that the flow is essentially constant in a local neighborhood of the pixel under consideration, and solves the basic optical flow equations for all the pixels in that neighborhood, by using the least squares criterion. The optical flow equation for pixel p can be assumed to hold for all pixels within a region Ω centered at p . Namely, the local image flow vector (V_x, V_y) could be obtained by calculating the minimum value of the following weighted item [135].

$$\sum_{x,y \in \Omega} W^2(x)(I_x V_x + I_y V_y + I_t)^2 \quad (0.10)$$

where W is an $n \times n$ diagonal matrix containing the weights $W_{ii} = \omega_i$ to be assigned to the equation of pixel q_i . Usually more weight to the pixels that are closer to the central pixel p . The Lucas-Kanade method obtains a compromise solution by the least squares criterion [135]:

$$A^T W^2 A V = A^T W^2 b \quad (0.11)$$

where $A = (\Delta I(q_1), \dots, \Delta I(q_n))^T$, $W = \text{diag}(W(q_1), \dots, W(q_n))$, $b = -(\frac{\partial I(q_1)}{\partial t}, \dots, \frac{\partial I(q_n)}{\partial t})^T$ and V is obtained as Eq.(0.12) [135]:

$$V = (A^T W^2 A)^{-1} A^T W^2 b$$

$$\begin{bmatrix} V_x \\ V_y \end{bmatrix} = \begin{bmatrix} \sum_i I_x(q_i)^2 & \sum_i I_x(q_i)I_y(q_i) \\ \sum_i I_y(q_i)I_x(q_i) & \sum_i I_y(q_i)^2 \end{bmatrix}^{-1} \begin{bmatrix} -\sum_i I_x(q_i)I_t(q_i) \\ -\sum_i I_y(q_i)I_t(q_i) \end{bmatrix} \quad (0.12)$$

Each vehicle's speed includes two directions: longitudinal and lateral. The latter is equal to zero unless the driver wants to make a lane change. In that case, the lateral speed should be still very small comparing with the longitudinal speed. In the UAV's video, most movements in the lateral direction belong to the camera motion. To minimize the errors, only the vehicle's velocity along the road longitudinal direction is considered, and which can be expressed by

$$V_{lon} = V_x \cos\theta + V_y \sin\theta \quad (0.13)$$

Although it is possible to obtain each pixel's velocity in Eq.(0.13), because of the instability of the optical flow at pixel level it is hard to directly obtain each vehicle's speed accurately from

Vehicle trajectory data collection by UAV

the result of optical flow [138]. Therefore, in this method, the optical flow is used to detect the shape of each vehicle, and the value of V_{lon} will transfer into binary value according to a proper threshold in Eq.(0.14). Fig. 0-8 is the final binary figure for one frame.

$$F_{OF}(i,j) = \begin{cases} 1 & V_{lon}(i,j) \geq \tau \text{ and } V_{lon} \leq \sigma \\ 0 & \text{otherwise} \end{cases} \quad (0.14)$$

where τ and σ are the maximum and minimum rational speeds, which relate to the UAV's altitude and the stability after the image registration. Higher altitude leads to smaller τ and σ , while the lower stability requires bigger σ to eliminate the camera motion.

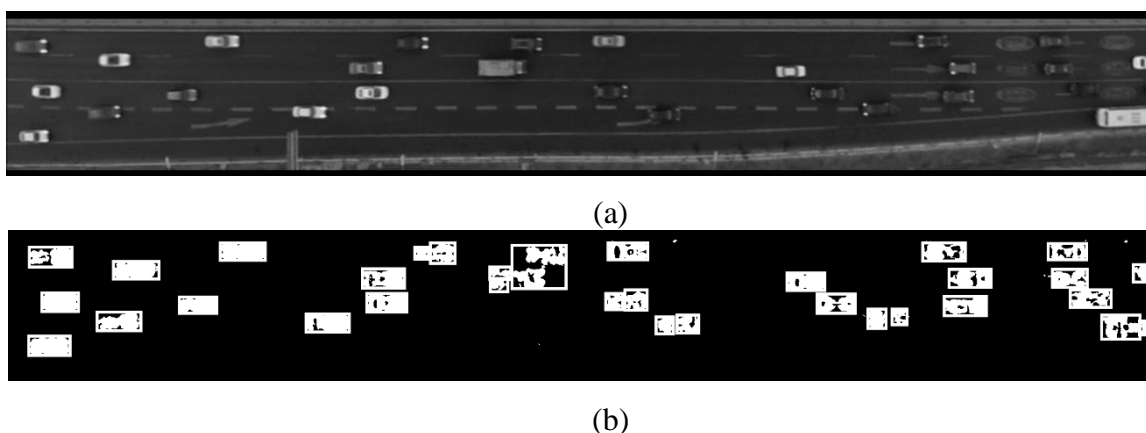


Fig. 0-8 Optical flow in the longitudinal direction of the road. (a) The original grayscale frame; (b) The optical flow result.

Local feature point

Scale-invariant feature transform (SIFT) is an algorithm in computer vision to detect and describe local features in images. The algorithm was published by David Lowe in 1999 [139]. SIFT has been widely used in many applications, including object recognition, image stitching, 3D modeling, gesture recognition, video tracking, individual identification of wildlife and match moving [32]. SIFT is selected as the feature detector and matching method in the present system due to its advantages over other methods. The local feature points are invariant to image scaling, translation, and rotation, and partially invariant to illumination changes and affine or 3D projection [140]. The stability of local feature could compensate the negative effects caused by the movement and vibration of the UAV's camera in the air. Furthermore, because each vehicle in the video will change its position as proceeding forward, from the perspective of the camera the angle of a vehicle changes accordingly. This situation is illustrated in Fig. 0-9, in which the image of a vehicle has a

Vehicle trajectory data collection by UAV

transparent change as it proceeds. The obvious angle change of a vehicle in the video is challenging to the vehicle tracking accuracy. However, SIFT local feature points are immune to image rotation and remain invariant in this situation. Also, the UAV's camera setting could slightly change during recording video, such as brightness and white balance. As SIFT doesn't rely on the absolute values of brightness and colors, it can handle these differences in the process of matching.

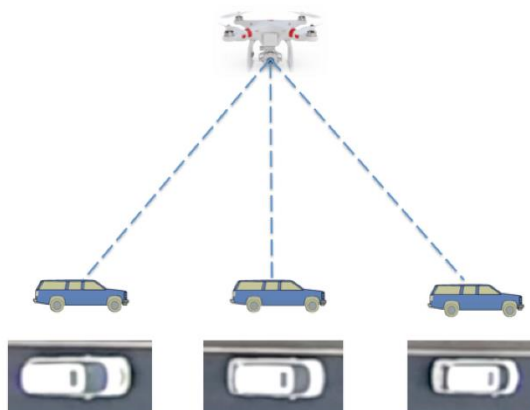


Fig. 0-9 Different relevant angles between vehicle and UAV

In conclusion, three image features are used in the method, which includes edge, optical flow and local feature point. The input, required orientation, calculation range and applications of each feature are summarized in Table 0-4.

Table 0-4 The summary of three types of image features

Features	Input	Orientation	Range	Application
Edge	One frame	Vertical to the road longitudinal direction	On the vehicle shape detection region	Vehicle shape detection
Optical flow	Consecutive frames	Parallel to the road longitudinal direction	All the road region	Vehicle shape detection and vehicle tracking
Local feature point	Consecutive frames	No direction	Inside detected shape of each vehicle	Vehicle tracking

Vehicle trajectory data collection by UAV

Vehicle shape detection

In this module, the method detects the boundary of vehicle appeared in vehicle shape detection region. And to solve the potential problems in vehicle shape detection, both features of optical flow and edge are used.

Vehicle shape detection region

Considering the vehicle is a rigid body, each vehicle's shape will not change in the following processors after determined. As a result, vehicle shape detection can be conducted in a region of interest, which is called as vehicle shape detection region in this method.

There are two requirements for the vehicle shape detection. The first is that the length of the region should be longer than the longest vehicle during the experiment; whereas the second is that the vehicle shape detection region should be an area where vehicles prefer to stay in the center of the lane in the shape detection region when they do not intend to change lanes. In this method, the features of image edge are used to refine the result of vehicle shape. A region of a vehicle edge with less lane mark interrupted could increase the accuracy of vehicle shape detecting. As shown in Fig. 0-10, the left side part of red line is the vehicle shape detection region in this test, we choose the left (upstream) 300 pixels width as shape detection region.

Vehicle shape detection with optical flow and edge

From the image feature result of optical flow obtained in Section 3.2.2, it is possible to identify the rough vehicle shape information. However, the result of optical flow has some potential errors in the process of vehicle shape recognition.

Firstly, the similar brightness inside a vehicle implies that the matrix A in Eq.(0.11) is singular, where A is defined as the difference of intensity around the subject point. When pixels intensity are similar insider a vehicle's region, the matrix A will be close to zeros and singular. The velocity at this point, $V = (A^T W^2 A)^{-1} A^T W^2 b$, is considered as zero [138]. Consequently, when the middle area of a long vehicle has few recognized features from the top view, the optical flow method could recognize the long vehicle as two separated parts. Thus it is possible that one vehicle will be recognized as two short vehicles. Another error is when two vehicles are close to each other, in which case the optical result can't accurately identify the boundaries of the two close vehicles. For example, two cars move on two adjacent lanes with a similar speed, and the distance

Vehicle trajectory data collection by UAV

between the two vehicles is short. Due to the vehicle shadow and the camera angle, the gap between two vehicles is invisible in the result of optical flow. This method will mistakenly recognize two cars as one. These two optical flow potential errors are shown in top in Fig. 0-11(b).

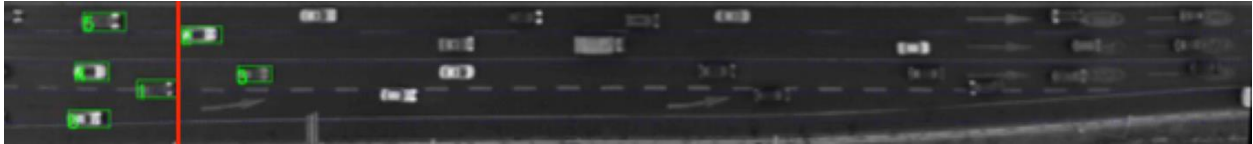
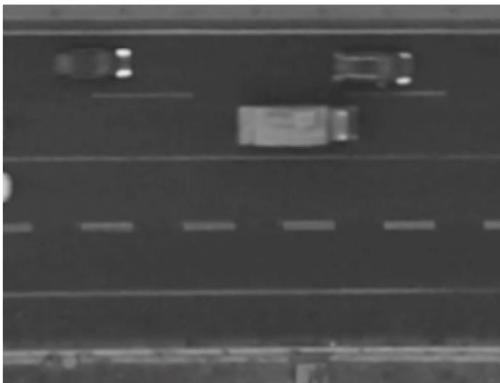
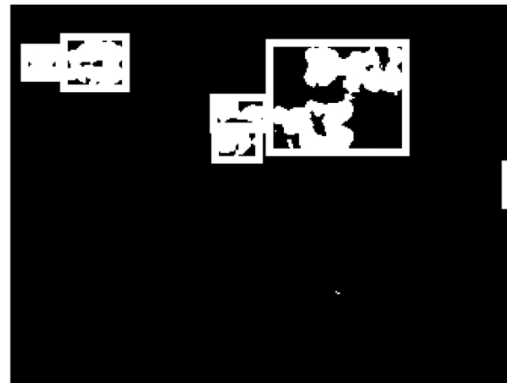


Fig. 0-10 The result of vehicle shape detection

In order to quantify the two potential errors in optical flow, the edge feature (Fig. 0-11(c)) is used as a supplement to the optical flow method. The pseudo code of the framework is listed in Table 0-5. The code from line 4 to 6 can solve the first potential error, and that from line 7 to 8 can solve the second potential error. The result of vehicle shape detection is shown in Fig. 0-11(d). After one vehicle shape is confirmed, the system will move to the next step of vehicle tracking.



(a)



(b)

Vehicle trajectory data collection by UAV

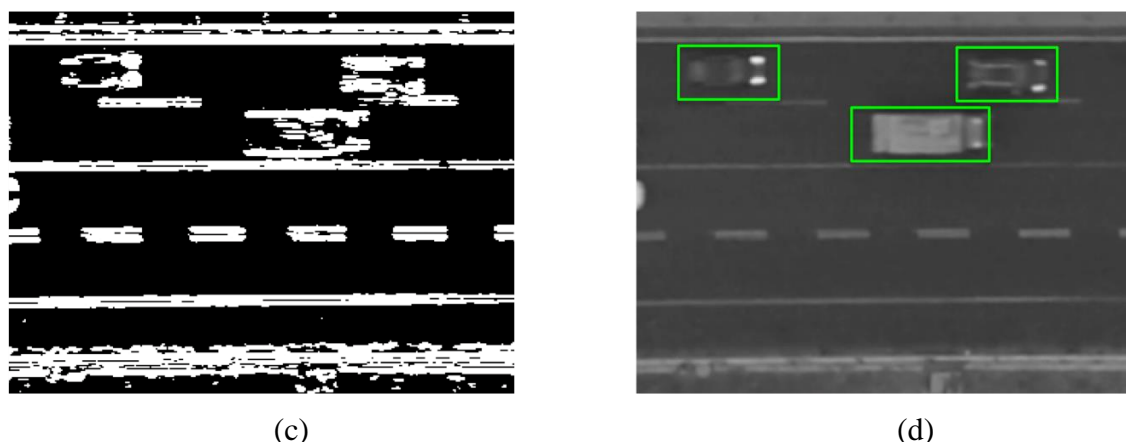


Fig. 0-11(a) The original figure; (b) the optical flow result; (c) the edge feature result; (d) the final detection result.

Table 0-5 Framework of the Vehicle shape detection with optical flow and edge

0	Input: optical flow feature in road longitudinal direction and edge feature in road lateral direction
1	For $i =$ first frame to last image
2	Recognize vehicle shape set $\{B_j\}$ based on result of optical flow in each frame
3	For $j =$ all vehicle shape B_j
4	For $k =$ all vehicle shape B_k close to B_j , where $B_k \in \{B_j\}$
5	If B_j and B_k share two continuous edge lines
6	Link the areas of B_j and B_k as one vehicle.
7	If the width of B_j is bigger than the threshold λ (in the calculation $\lambda = 4m$)
8	Separate B_j according to the result of edge, and recalculate the vehicle shapes
9	Output: the confirmed vehicle shape with a unique ID

Vehicle tracking

To improve the accuracy and decrease the error rate, both features of local feature point and optical flow are used in the vehicle tracking module. Occlusion is also considered in this method. The workflow of vehicle tracking is illustrated in Fig. 0-12. The local feature points are matched in two consecutive frames in each vehicle shape, and the matched points are selected in vehicle tracking. There are some traffic signs or bridge that may block a vehicle's shape. To avoid these occlusion's negative effects, this method will check each matched local feature point, and identify the occlusion point. Then the recognized occlusion local feature point will be stored into a database, which will be helpful to recognize the occlusion point in the following steps. Because the matched

Vehicle trajectory data collection by UAV

local feature points are not reliable in the process of vehicle tracking, as a backup method, optical flow could also help to track vehicle. The verification of each vehicle's tracking result will be demonstrated.

Update speed with matched local feature points

In the step of vehicle tracking, we use the matched local feature points to detect the movement of the vehicle in consecutive frames. As shown in Fig. 0-13(a), the blue local feature points belong to the frame at time n , and the red local feature points belong to the frame at time $n + \Delta t$, where Δt is the time between two consecutive frames. The matched local feature pair is considered as the same point on the vehicle. As a result, the distance between the matched local feature pairs is considered as the distance of vehicle movement during Δt . In Fig. 0-13(b), two consecutive frames are shown in cyan-red figure.

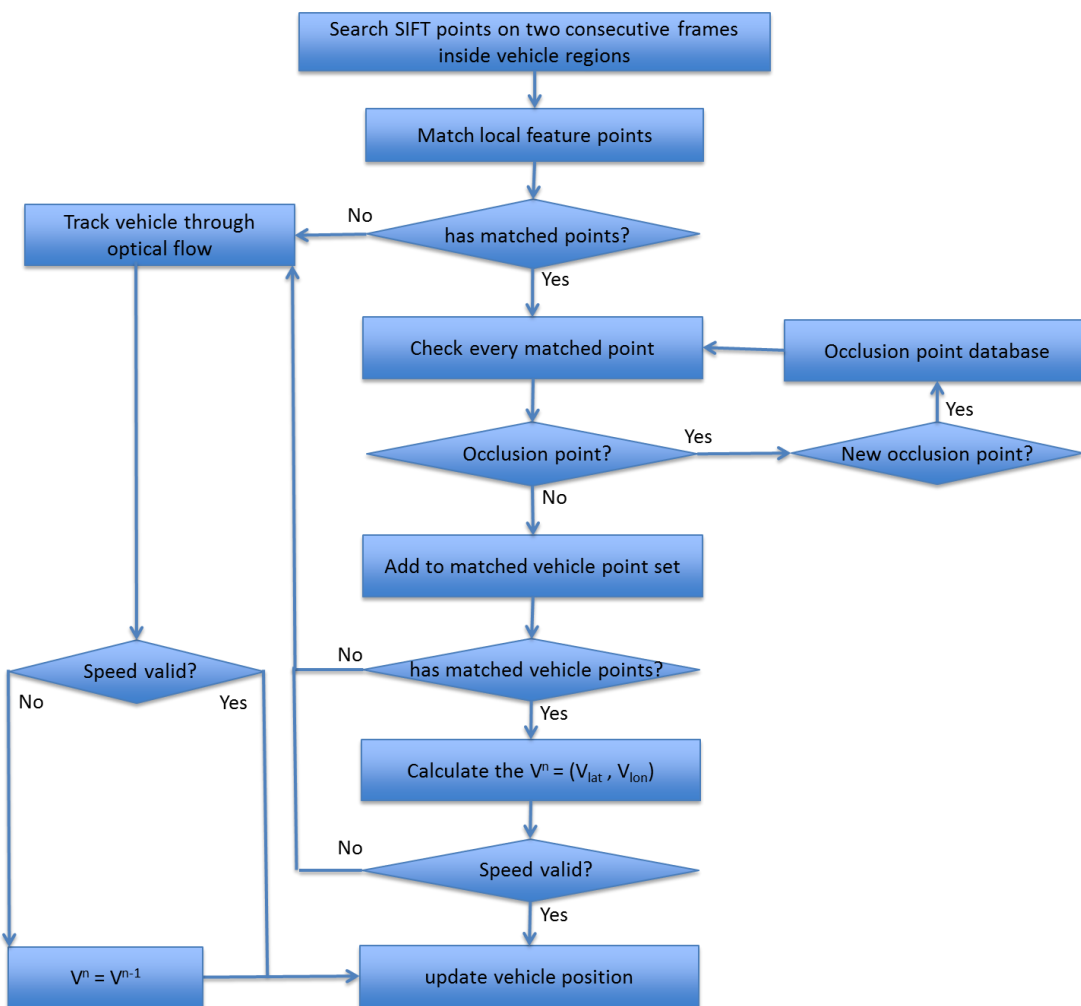


Fig. 0-12 Workflow of vehicle tracking

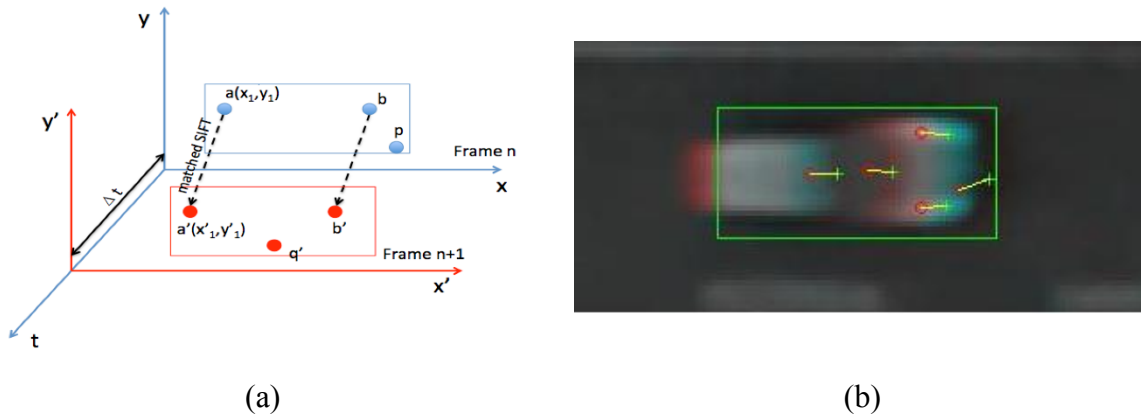


Fig. 0-13 (a) The demonstration of vehicle tracking based on matched local feature points. (b) one example to track vehicle with matched local feature points.

Occlusion with traffic signs

In some situations, part of the vehicle will be occluded by the traffic signs in the video. Then the matched local feature points on the vehicle will be clustered into two groups. One group remains moving in the original speed and the other group is static, because these matched local feature points are from the traffic signs. Several steps are taken to solve this problem. In the first place, these matched local feature points of the traffic signs are removed and the matched local feature points left are used to track the vehicle. If no matched local feature points are left, the vehicle's previous speed would be used to track the vehicle. Then, the matched local feature points of the occlusion will be stored in the occlusion point database. If the same occlusion point appears in the following frames, the computer will easily recognize it and eliminate the negative influences of the occlusion point directly.

Track vehicle through optical flow

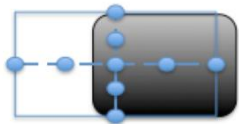
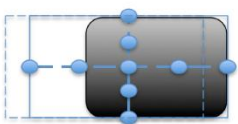
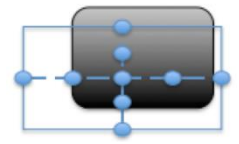
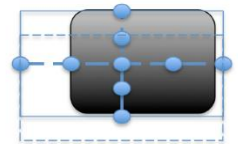
As is known, the SIFT method is a powerful tool in the research of feature point. However, in the process of finding the matched local feature points, there exist many restrictions and requirements [32,141]. If the resolution of the image is not enough or the altitude of UAV is too high, the pixels for each vehicle will be fairly limited. As a consequence, it will be difficult to identify matched local feature points in the region of detected vehicle shape. Thus, it is impossible

Vehicle trajectory data collection by UAV

to track vehicle based on SIFT method. To deal with such problem, the optical flow will be included in vehicle tracking.

As shown in Table 6, the vehicle optical flow results at time $t+\Delta t$ are demonstrated as black block, the blue box is the vehicle position at time t , and the dashed box is the estimated vehicle position at time $t+\Delta t$. By the rule, each vehicle shape at time t is marked with 9 points (Table 0-6). There are 5 points on both longitudinal and lateral directions. In the longitudinal direction, if one optical flow block covers 3 of the 5 points, this block is considered as part of the car and this optical flow block could be used in tracking this vehicle. The same rule is applied in the lateral direction. If the vehicle speed is low or the video frequency is high, one optical flow block will be considered as part of the car only when it covers at least 4 of the 5 longitudinal points.

Table 0-6 The rule of vehicle tracking based on optical flow

Original situation	Adjustment result
	
	

This is a relatively conservative rule to avoid the failures in the vehicle tracking process. However, because only the optical flow block occupied 3 of the 5 points could be used in vehicle tracking, the vehicle trajectory result is not very smooth compare with compare with updating speed with local feature points. Considering optical flow is only a backup method in vehicle tracking process and to avoid tracking failure, this rule is reasonable.

Vehicle speed validation

In order to test whether the tracking results are reasonable, each vehicle movement is required to satisfy certain basic criteria. If the acceleration value of a vehicle is larger than the threshold, the vehicle tracking result is considered as a failure. In this situation, previous step's speed will be used. The vehicle movement limitations used are based on the parameters of the Gipps car

Vehicle trajectory data collection by UAV

following model. The maximum acceleration is 6 m/s^2 and the maximum deceleration is -7 m/s^2 [142].

Results and discussions

To demonstrate the present vehicle detecting and tracking system, field tests were conducted and the modeling results are compared with the actual observations. The location of the field tests was selected as the north part of the 5th Ring Road in Beijing, China. The testing road has two direction traffic flows, which is an arterial road and the traffic flow is large. The side stretching from west to east has four lanes with an additional merging lane and a shoulder lane. The other side of the road has four lanes with a shoulder lane. This road section includes complex traffic marks on the lane, such as the number of speed limit and direction sign. Nearby the merging lane, there is a traffic signal board. The image of the experiment road is shown in Fig. 0-14.



Fig. 0-14 The location of the field test (altitude is 150m)

From 2014 Dec to 2015 May, the road was monitored by 66 times and the total videos length is over 850 minutes. Limited by the battery capacity, each test was about 13 minutes. Excepting the time of taking off, landing and adjustment, the length of each valuable video on vehicle detecting and tracking is about 10 minutes. Considering the conditions of traffic flow, weather and sunshine, the tests were chosen at the morning time from 6:30 a.m. - 7:20 a.m.

Considering its convenience and portability, a MacBook Pro laptop was selected in the tests. The processor is 2.7 GHz Intel Core i7, memory is 16 GB 1600 MHz DDR3, Graphics is Intel HD

Vehicle trajectory data collection by UAV

graphics 4000 1536MB. The method is programmed in MATLAB. The basic image feature extraction methods used in the program are listed in the following Table 0-7.

Table 0-7 The main image feature extraction method applied in the code

Image feature	Method	Code
Edge	Prewitt edge detection	MATLAB
Optical flow	Lucas-Kanade operator	MATLAB
Local feature point	SIFT	VLFeat [143]

The running time depends on the traffic situation of the observed road section and the frame frequency of the video. Considering the road section length is 228 meters (UAV's altitude is 120m), about 25 vehicles on each frame (only consider on direction traffic flow); and video frame frequency is 30 Hz, and the resolution is 1920×1080. In such conditions, a 10 min UAV video requires 142 minutes of the image process, which equals to 0.47 second/ frame.

Vehicle detection results

For the evaluation of the vehicle detection and tracking algorithms, the values for correctness, completeness and quality are calculated for different scenes from several campaigns. They are defined in Eq.(0.15)-(0.17) from the Reference [39], with true positives being the number of vehicles detected, false positives the number of non-vehicle detections and false negatives the number of vehicles missed.

$$Correctness = \frac{true\ positives}{true\ positives + false\ positives} \quad (0.15)$$

$$Completeness = \frac{true\ positives}{true\ positives + false\ negatives} \quad (0.16)$$

$$Quality = \frac{true\ positives}{true\ positives + false\ negatives + false\ positives} \quad (0.17)$$

The vehicle detection results are listed in Table 8 and are validated manually. It is worthy to note that through the camera horizontal degree of field of view is 94.4 degree (Table 0-2), however, after the correcting the image deformation, the observed road section length will be reduced. From

Vehicle trajectory data collection by UAV

the Table 0-8, the results of correctness are all 100% at different altitude, which means every vehicle recognized is correct. Because each detected vehicle needs to be verified by optical flow and lateral edge. In transportation research, the correctness is more important than completeness in vehicle shape detection, because one false positive failure (consider a non-vehicle as a vehicle) will directly cause the failure of vehicle tracking in the following steps, since vehicle tracking is depending on the vehicle detecting result. Furthermore, this false positive detected “vehicle” (this isn’t a vehicle in the video) is like a “ghost” vehicle, and will generate unpredictable errors, which could cause difficulties in the traffic flow analysis.

There are two main reasons that may cause false negative failures. On one hand, when vehicle is crossing the lane mark in the vehicle shape detection region, the lane mark will have negative effects in vehicle detecting. Especially in vehicle lateral edge figure, the computer cannot tell the vehicle shape with lane mark edge. On the other hand, if a vehicle shape is very different from the typical vehicle, it will cause false negative failure. For this reason, a predefined vehicle width threshold is set in the vehicle shape detecting. If vehicle is over that limitation, the vehicle will not be recognized. For example, in the 120 m-altitude video, the vehicle recognized width limitation is 30 pixels to 45 pixels.

Table 0-8 Vehicle detection results

UAV altitude (m)/ Road section length(m)	100/ 190	120/ 228	150/ 285
Vehicle average speed (m/s)	12.4	11.2	12.0
True positives	1999	1877	1520
False positives	0	0	0
False Negatives	2	3	61
Correctness	100%	100%	100%
Completeness	99.9%	99.8%	96.1 %
Quality	99.9%	99.8%	96.1%

Overall, vehicle detecting could provide acceptable accuracy when the UAV's altitude within the range of 100 m-120 m. But when the UAV’s altitude increases to 150 m, the accuracy decreases to 96.1%. Because each vehicle’s occupied pixels in video is reduced (in 150m-altitude video, each vehicle occupies only about 150 pixels), correspondingly the optical flow and lateral edge are

Vehicle trajectory data collection by UAV

not accurate enough for vehicle detection. Theoretically, a higher resolution camera could increase the accuracy of detection results in higher altitude.

Vehicle tracking results

Because this method separates the vehicle detection and tracking into two different processes, the vehicle tracking results will be demonstrated individually. However, there's no exact method or standard to evaluate the result of vehicle tracking. Indirectly, the concept of "lost vehicle"[79,81,144] is introduced in macroscopic traffic simulation, which is defined as a vehicle moving out of the lane, or superimposed on another one, or staying in a position for an irrationally long time. The number of "lost vehicles" can be an indicator to evaluate the vehicle tracking algorithms. The results of vehicle tracking at different altitudes are listed in Table 0-9. Vehicle tracking accuracy will decrease when the UAV altitude increases. But the presented method could still generally keep a higher accuracy in tracking each vehicle from 100 m – 150 m altitude.

Table 0-9 Vehicle tracking results

UAV altitude (m)/ Road section length (m)	100/ 190	120/ 228	150/ 285
Number of vehicles	1999	1877	1520
Number of "lost vehicle"	0	11	32
Error	0%	0.6%	2.1%

For each vehicle tracking result, both vehicle longitudinal and lateral positions are recorded in an equal time interval sequence. Fig. 0-15 is a typical vehicle tracking result. This vehicle moves from the second lane to the third lane and takes about 20 seconds through the research region (200 m). It is clear that during the lane change the vehicle decreases speed for a proper gap to enter. The average speed at the second lane is about 14 m/s, and the average speed at destination lane (third lane) is about 12 m/s. However, when gathering vehicle positions, whatever the technique used, the observed points happen to be dispersed in the neighborhoods of the actual points and the path drawn on the observed positions inevitably fluctuates around the true path followed by the vehicle [145]. Therefore there are two types of limitations of the raw experiment results. Firstly, the vehicle's trajectory position and speed vibrate greatly, and two consecutive frames have great differences (Fig. 0-15). Secondly, the measurement error is more obvious in the

Vehicle trajectory data collection by UAV

vehicle lateral direction. Comparing vehicle's longitudinal speed, the vehicle's lateral speed is relatively very small. As shown in Fig. 0-15 (b), the maximum lateral speed is only 10% of the maximum longitudinal speed, which means that the same measurement error will occupy higher percentage in vehicle lateral speed. On the other hand, vehicle lateral position is hard to predict. A driver may change lateral speed and direction at any time, which means that it is hard to set a limitation to eliminate unreasonable lateral movement.

In general, the raw vehicle trajectory data could describe vehicle's main behavior, such as speed change, lane change, etc. However the raw trajectory data still has some limitations and disadvantages for microscopic transportation research with higher accuracy requirements. A proper assessment and optimize method for raw vehicle trajectory data is thus highly demanded in the transportation analysis.

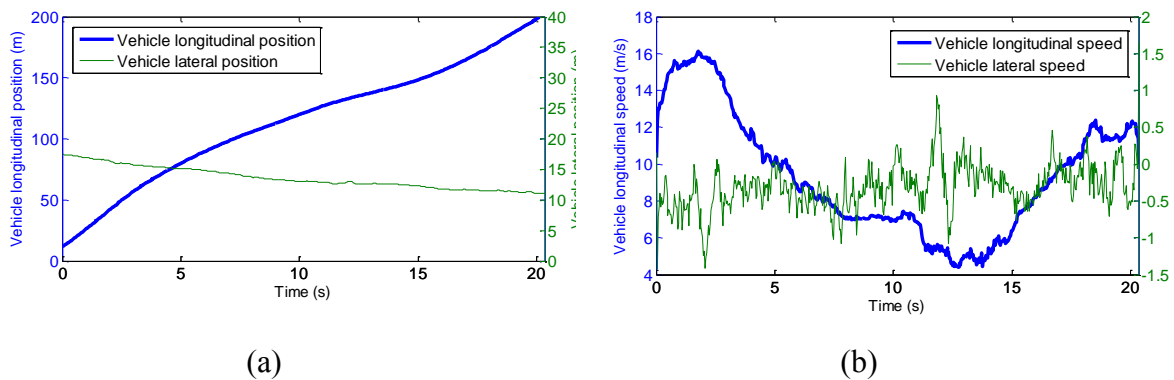


Fig. 0-15 A typical vehicle trajectory data; (a) vehicle position trajectory data; (b) vehicle speed trajectory data

Conclusions and discussions

A UAV-based vehicle detecting and tracking system has been presented with many advantages in both traffic monitoring system and driver behavior research. The method extracts vehicle trajectory data from the UAV's video at different altitudes with different view scopes. Three significant features of the method have been demonstrated:

- Three image features, including edge, optical flow and local feature point, work jointly in this method to detect and track vehicles in a UAV's video. Compared with traditional single image feature methods, the presented method considerably improve the recognition accuracy and the system robustness.

Vehicle trajectory data collection by UAV

- This method is specifically designed for vehicle detection and tracking. Based on the analysis of road, traffic flow and driver behavior characteristics, some adjustments, such as transforming image's color form into HSV to obtain road features, extracting longitudinal direction feature of Optical flow for vehicle detection, vehicle shape detection region and checking vehicle speed based on the Gipps acceleration model have been introduced in the model to further improve efficiency and accuracy.
- The vehicle detection and tracking results based on the present method showed that considerable improvement of the detecting accuracy has been reached. Three road section lengths 190 m, 228 m and 285 m, were studied, all the test results are very reliable, and the vehicle detection error is lower than 3.9% and vehicle tracking error is lower than 2.1%.”

The presented method provides a convenient and reliable way to acquire each vehicle's information. The trajectory data could be used in most transportation research and traffic data analysis. The research demonstrates a high potential of this system to be used in actual traffic monitoring in dense metropolitan areas or emergency mitigation cases. Nevertheless, as a novel equipment emerging in traffic monitoring system, there still exist certain limitations of applying UAV in vehicle detecting and tracking:

- UAV's behavior is sensitive to the testing environment. Based on the field experiences, the video vibration increases as the wind velocity increases. As a consequence, it might cause the image registration failure[49]. Additionally, the UAV might not properly work in bad weather conditions, such as foggy or snowy conditions.
- The UAV's continuous working time is limited by its battery capacity. As a traffic-monitoring device, the short continuous working time is not able to provide enough consecutive data for a long-term monitoring of a road section. The UAV used in this test is only 15 minutes. To the authors' knowledge, UAV as a traffic-monitoring device is still in research level, but has not been widely used in city road today.
- The shadow will have negative effects on vehicle tracking and detecting accuracy. Intensive research is required to effectively address this issue in the computer vision[146].
- In macroscopic transportation analysis, a longer road section is required [147]. However it is

Vehicle trajectory data collection by UAV

hard to extend the observation scope by increasing a UAV's altitude while keeping enough resolutions for each vehicle. Multiple UAVs are eventually needed.

- With the advance of technology, the UAV's stability and endurance might be improved considerably in the near future, thus the effect of weather conditions and battery capacity limitations can be overcome. To address the shadow problem, the infrared waveband camera might be an alternative way, where each vehicle can be detected and tracked by extracting its engine's heat. In order to extend the observation scope, a multiple-UAV system could be applied.

An open mechanics-based acceleration model

Traffic simulation and prediction are the key components in optimizing traveling routing and matching in the OMITS. In order to accurately simulate and predict the traffic, one needs to understand each individual vehicle's behaviors at the microscopic level, since traffic phenomena are the accumulation of relevant vehicle's behaviors. In the following, two central components of vehicle's behaviors, acceleration and lane change execution, will be introduced in Chapter 4 and Chapter 5, respectively. In this Chapter, an open mechanics-based acceleration model is developed to consider longitudinal motion of vehicles on a road for microscopic traffic simulation. Five general factors, say (1) subject vehicle's speed, (2) acceleration sensitivity, (3) safety consideration, (4) relative speed sensitivity, and (5) gap reducing desire, are identified to simulate driver behavior on the roadway. By introducing feeling gap, multilane acceleration behavior is included in the presented model. These factors describe a driver's preferences and interactions between vehicles, and each of them may function as a trigger to change vehicle's speed. Inspired by the similarity of vehicle interactions and particle interactions, a mechanical system with force elements is introduced to quantify the vehicle acceleration. Based on Newton's second law of motion, the subject vehicle's longitudinal behavior can be simulated by the present open mechanics-based acceleration model. This chapter is reproduced from the paper co-authored with Fangliang Chen and Huiming Yin [148].

Introduction

A vehicle acceleration model describes the longitudinal behavior of vehicles on the road [50]. It is an essential component in the microscopic traffic simulation and plays an important role in transportation science and engineering, including safety studies and capacity analysis [21,22,51–54]. Over the past decades, as a fundamental research topic in transportation, a large number of

An open mechanics-based acceleration model

vehicle acceleration models have been developed to describe vehicle longitudinal behaviors in different traffic conditions. Some of them have already been applied in commercial software for microscopic traffic simulations, which have been serving as basic tools in design of advanced vehicle control, safety systems and intelligent transportation systems [149].

The optimal velocity (OV) model, introduced by Bando et al. [150] has received considerable attention in the acceleration behavior researches. OV model assumes that each vehicle has an optimal velocity, and that a driver seeks to minimize the difference between the desired measures and the actual states[50]. The OV model can describe many characteristics of real traffic flow such as the stop-and-go traffic and the evolution of traffic congestion[151]. In order to overcome the shortage of OV model that may lead to impractical high acceleration and unrealistic deceleration , Helbing and Tilch [152] developed a generalized force (GF) model by considering negative velocity difference on the basis of OV model. Both OV and GF models cannot explain the instance that if the leading car is much faster, then the car will not brake, even if its headway is smaller than the safe distance pointed out by Treiber et al.[63], so Jiang et al. [153] put forward full velocity difference (FVD) model by considering both negative and positive velocity difference, which can give a better description of starting process than OV and GF models [154] .

These classical models are very charming for their simplicity, because they can simulate most macroscopic level traffic phenomena. However, it is well known that the each driver's acceleration behavior on the way is different and complex, which may be affected by various factors. An ideal acceleration model is expected to be able to reflect a driver's behavior at different situations, such as different traffic situations, driver characteristics (ages, genders, health states, temper and perception) and even specific behaviors during driving, like distraction, fatigue, talking in phone. Although a large number of acceleration models have been developed over the past few decades, two obvious limitations are often exhibited in the current models. Firstly, many of them were developed in a rigid form by only considering certain factors, such as the Gazis-Herman-Rothery (GHR) model [55,56] and the Gipps model [53], while other relevant or emerging factors is not able to be accounted for or integrated. As a result, driver's psychological behaviors driver behavior [65–73,75] are usually ignored.

Furthermore, most acceleration theories are developed to model the motion of vehicles following each other on a single lane without any overtaking. It is based on the assumption each

An open mechanics-based acceleration model

driver reacts in some specific fashion to a stimulus from the vehicle ahead of him in the same lane [153]. However, real-world traffic usually contains multilane system and lane change phenomena. In multilane and lane-changing available traffic systems, as is well-known, it's not possible to control drivers' driving behavior and for the sake of better driving conditions drivers can hardly run on a fixed lane without lane-changing. Thus, to study real traffic, single-lane models should be extended to lane-changeable multilane models. Most of the researches are based on cellular automaton model [155–157] and energy method [154], but they are not adaptable to lane change process very well [10,54,76]. As a result, most lane change models have to introduce specific parameters and formulas to describe vehicle's longitudinal behaviors in the lane change process [77,78].

To overcome those limitations in the existing acceleration models, a vehicle acceleration model based on a mechanical system is developed. The remainder of this chapter is organized as follows: Section 4.2 will introduce the proposed open mechanics-based acceleration model, including five main factors, feeling gap in multilane acceleration, governing equation and relative parameter studies. Section 4.3 will present the information of field experiment and parameter selection. Based on the present acceleration model, a microscopic simulation program will be developed with MATLAB in Section 4.4. Finally the conclusions will be presented in Section 4.5.

Open mechanics-based acceleration model

The structure of the present acceleration model is shown in Fig.0-1. The traffic conditions are the inputs of the model, which includes the leading and subject vehicles' states, their relative speed and distance, and local traffic rules, etc. The traffic conditions can be described by five general factors, say subject vehicle's speed and acceleration sensitivity, safety consideration, relative speed sensitivity, and gap reducing desire, which will change the driver behavior on the road. Each of them are treated as force elements and synthesized in to a mechanical system. Based on Newton's second law of motion, the subject vehicle's governing equation of longitudinal motion can be simulated by this open mechanics-based acceleration model. By introducing the feeling gap, the factor of multilane acceleration behavior is also included in the presented model.

An open mechanics-based acceleration model

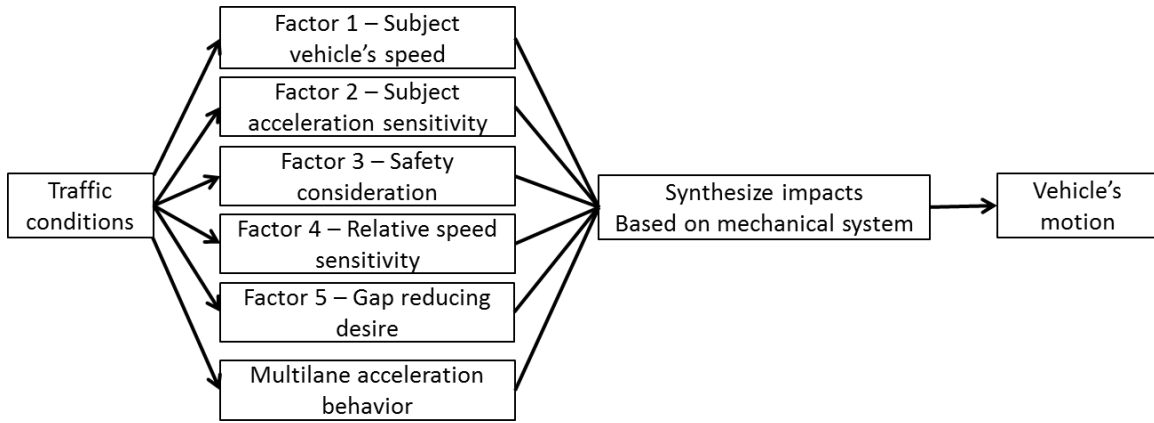


Fig.0-1 Structure of the present acceleration model

Vehicle acceleration factors

There exist many factors, which might affect a driver's longitudinal behaviors[158–160]. It is very challenging to integrate all of them into a single model. Based on the existing acceleration models, five factors are taken into account, including subject vehicle' speed and acceleration sensitivity, safety consideration, relative speed sensitivity, and gap reducing desire. These factors describe the driver's preferences and interactions between vehicles, and each of them may function as a trigger to change the vehicle's speed. To describe the traffic states, the traffic condition at time t is the input of the model, and can be expressed as $[x_x^t, v_s^t, a_s^t, x_l^t, v_l^t, a_l^t]$, representing subject vehicle position, speed and acceleration, and leading vehicle position, speed and acceleration at time t , respectively. In the following, we will model each of the five factors with a force element.

Subject vehicle's speed

Normally, a driver has a target speed v_o on a road. The value of v_o represents a driver's personal preferences of the speed, and it is affected by many factors, such as road speed limitation, vehicle condition and driver's time schedule [53,160]. If the current speed v_s^t is lower than v_o , the driver may prefer to increase speed; while if current speed is higher than v_o , the driver may tend to decrease speed correspondingly. This concept of subject vehicle's speed has been introduced in the desired measures models [50,55,61,161]. The subject vehicle's speed impact in this model is expressed in Eq.(0.1).

$$F_1 = -\alpha' (v_s^t - v_o) \quad (0.1)$$

An open mechanics-based acceleration model

where v_0 is the subject driver's target speed. α' is a parameter reflecting a driver's desire to reach the target speed. A larger α' means that this driver has a strong and strict requirement of speed, while a smaller α' means that this driver does not really mind the vehicle speed. The force in Eq. (0.1) can be simulated by a dashpot with a reference speed at v_0 and damping coefficient α' , which is illustrated in Fig. 0-3 later.

Acceleration sensitivity

Usually, a cautious driver prefers to a smooth driving speed and tries to avoid a sudden acceleration or deceleration. Such driver's preferences could be defined as the acceleration sensitive factors. The concept of acceleration sensitivity has been presented in some speed difference models[82,162]. It is noteworthy that some literatures has proved that the acceleration and deceleration are not completely symmetric for a driver [163,164]. The asymmetric feature will be caused by the safety consideration factor in this model. In this model the acceleration sensitivity impact can be expressed in Eq.(0.2).

$$F_2 = -\beta' a_s^t \quad (0.2)$$

where β' is the parameter for a driver reflecting the attitude with vehicle speed. A larger β' indicates that this driver has a strong motivation to drive smoothly; a smaller β' means that this driver is used to the speed change. The force in Eq.(0.2) can be simulated by a mass β' moving at an acceleration $-a_s^t$, which is also illustrated in Fig. 0-3 later.

Safety consideration

When the gap to the leading vehicle is small, a driver will try to increase the gap with the leading vehicle for a safety consideration. Such impact has been demonstrated in many existing acceleration models. For example, in the collision avoidance models, the safety factor was considered by introducing a buffering distance to avoid crash at the most dangerous scenarios [50,53,161]. In the safety distance models, the safety factor was introduced as a minimum safety distance that a driver seeks to keep [50,59]. Actually, the concept of safety consideration is not simply stated as "the larger the gap, the safer the feeling of the driver". In fact, a driver can obtain safety feeling from following a leading vehicle with a target gap, such as maintaining visual contacts with a leading vehicle can assist driver's decision making [165], and leading vehicle can

An open mechanics-based acceleration model

help the driver of the subject vehicle to control the vehicle at a stable speed [166,167]. As a result, a target distance will be introduced for the safety reasons, which means that the driver of subject vehicle seeks to minimize the difference between the target distance and the actual distance [62,168]. When the actual distance is smaller than the target distance, a compressive force will be induced to increase the distance, and vice versa.

Based on the above observation, we can introduce the Lennard-Jones potential to describe the safety consideration factor. The Lennard-Jones potential is a model that approximates the interaction between a pair of neutral atoms or molecules [169], which is expressed in Eq. (0.3):

$$V_{LJ} = 4\xi\left[\left(\frac{\sigma}{r}\right)^{12} - \left(\frac{\sigma}{r}\right)^6\right] \quad (0.3)$$

where V_{LJ} is the Lennard-Jones potential; ξ is the depth of the potential well; σ is the finite distance at which the inter-particle potential is zero, r is the distance between the two particles. The Lennard--Jones force F_{LJ} between two molecules is given Eq (0.4), which is the derivative of Eq. (0.3).

$$F_{LJ} = -24\xi\left[2\frac{\sigma^{12}}{r^{13}} - \frac{\sigma^6}{r^7}\right] \quad (0.4)$$

The shapes of the Lennard-Jones potential and force are shown in Fig. 0-2. $r_m = 2\sigma$ is the distance that the potential reaches its minimum and the interaction force is 0 (Fig. 0-2(b)).

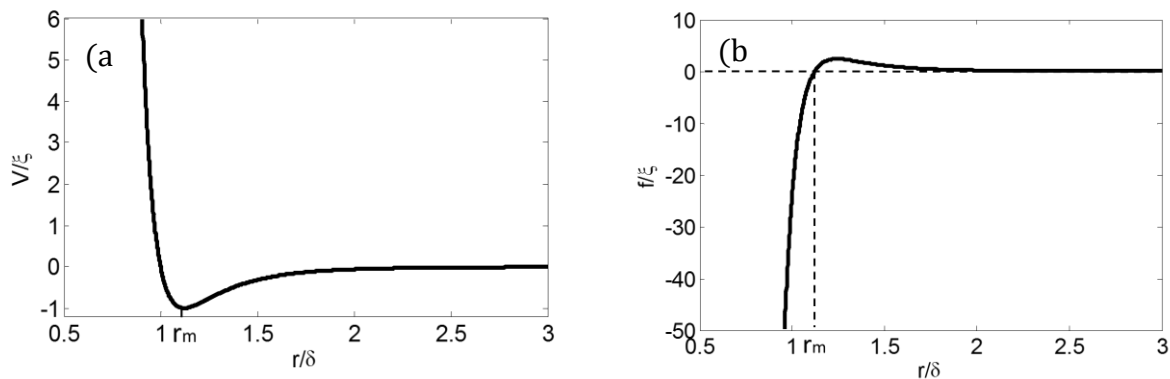


Fig. 0-2 The Lennard-Jones potential and force. (a) Potential, (b) Force

The Lennard-Jones potential and force were developed for three dimensional cases of molecule/atom interactions. When the distance is smaller than the target distance, rapidly

An open mechanics-based acceleration model

increasing compressive force will be induced, which is much higher than the realistic situation of one-dimensional vehicle interactions on the roadway. As the first step for simulation, the potential of safety V_{SC} is assumed as Eq. (0.5).

$$V_{SC} = 4\lambda\delta' \left[\left(\frac{\sigma}{x_i^t - x_s^t} \right)^2 - \left(\frac{\sigma}{x_i^t - x_s^t} \right)^1 \right] \quad (0.5)$$

where δ' is a parameter reflecting a driver's safety considerations. A larger δ' means a driver is defensive, and would like to make more effort to maintain the gap with the leading vehicle. Here λ is a cut-off parameter indicating a vehicle's following state, which is defined as

$$\lambda = \begin{cases} 1 & \text{when } g \leq 2g_0 \\ 0 & \text{otherwise} \end{cases} \quad (0.6)$$

where g_0 is the length of the following gap in a uniform flow. Based on the Gipps model[53], the g_0 could be expressed in Eq.(0.7).

$$g_0 = \left(\frac{b - \hat{b}}{2b\hat{b}} \right) (v_s^t)^2 + \frac{3}{2} \tau v_s^t \quad (0.7)$$

where b is the most severe braking that the subject vehicle wishes to undertake; \hat{b} is an estimation of the severe braking that the leading vehicle wishes to undertake estimated by subject driver; and τ is a reaction time for all drivers in the Gipps model.

The following three factors, including the safety consideration, relative speed sensitivity, and gap reducing desire are affected by the gap between the subject vehicle and the leading vehicle. If the gap is too large, these three factors are negligible. In this model, the but-off of the gap is considered as $2g_0$.

By differentiating Eq. (0.5), the safety consideration force F_3 can be mathematically expressed in Eq.(0.8)

$$F_3 = -4\lambda\delta' \left[2 \frac{\sigma^2}{(x_i^t - x_s^t)^3} - \frac{\sigma}{(x_i^t - x_s^t)^2} \right] \quad (0.8)$$

An open mechanics-based acceleration model

Similarly to r_m in the Lennard-Jones force, g_0 is defined as the gap that safety consideration force is zero in the acceleration model. Substituting the relationship into Eq. (0.8), one can identify $r_m = 2\sigma$, so that $\sigma = g_0/2$. Thus, the safety consideration force can be written as

$$F_3 = -2\lambda\delta' \left[\frac{g_0^2}{(x_l^t - x_s^t)^3} - \frac{g_0}{(x_l^t - x_s^t)^2} \right] \quad (0.9)$$

The value of g_0 is mathematically expressed in Eq.(0.7).

Relative speed sensitivity

Generally, drivers on the roadway may follow each other to maintain same speed as possible. When the leading vehicle increases speed, the subject vehicle prefers to follow up. This factor has also been introduced in the speed difference models[57,158]. Such factor can be mathematically expressed in Eq.(0.10) in this model.

$$F_4 = \lambda\varepsilon' (v_l^t - v_s^t) \quad (0.10)$$

where ε' is a driver parameter reflecting a driver's desire to avoid gap changing. A larger ε' means that a driver has a strong will to keep a steady gap with leading vehicle and prefers to keep the same speed with the leading vehicle. The force in Eq.(0.10) can be simulated by a dashpot with a reference speed at v_l^t , damping coefficient ε' , and a cut-off distance $2g_0$, which is illustrated in Fig. 0-3 later.

Gap reducing desire

In a real traffic situation, a driver's acceleration behavior is not only affected by the leading vehicle at the same lane, but also influenced by the vehicles at the adjacent lanes. According to the lane change researches, in a heavy traffic flow, a driver will try to reduce the gap with the leading vehicle to avoid a new lane change vehicle moving in front of the subject vehicle [82,87,170,171]. Similarly, the lane change vehicle desires to get advantages in lane change by reducing the gap with the leading vehicle [81,93,172]. In this model, the gap reducing desire will be simplified as Eq. (0.11).

$$F_5 = \mu\lambda\gamma' (x_l^t - l_l - x_s^t) \quad (0.11)$$

An open mechanics-based acceleration model

where l_l is the length of the leading vehicle, γ' is a parameter representing driver's wish to reduce the gap. A larger γ' means that this driver has strong will to reduce gap with the leading vehicle. μ is a cut-off parameter indicating the gap reducing state, which is defined as

$$\mu = \begin{cases} 1 & \text{gap reducing is required} \\ 0 & \text{otherwise} \end{cases} \quad (0.12)$$

Here the force in Eq. (0.11) can be simulated by a spring with a reference length at l_l , spring coefficient γ' , and a cut-off distance $2g_0$, which is illustrated in Fig. 0-3 with the other four cases together. Therefore, the five factors can be simultaneously taken into account for simulating driver's acceleration behavior.

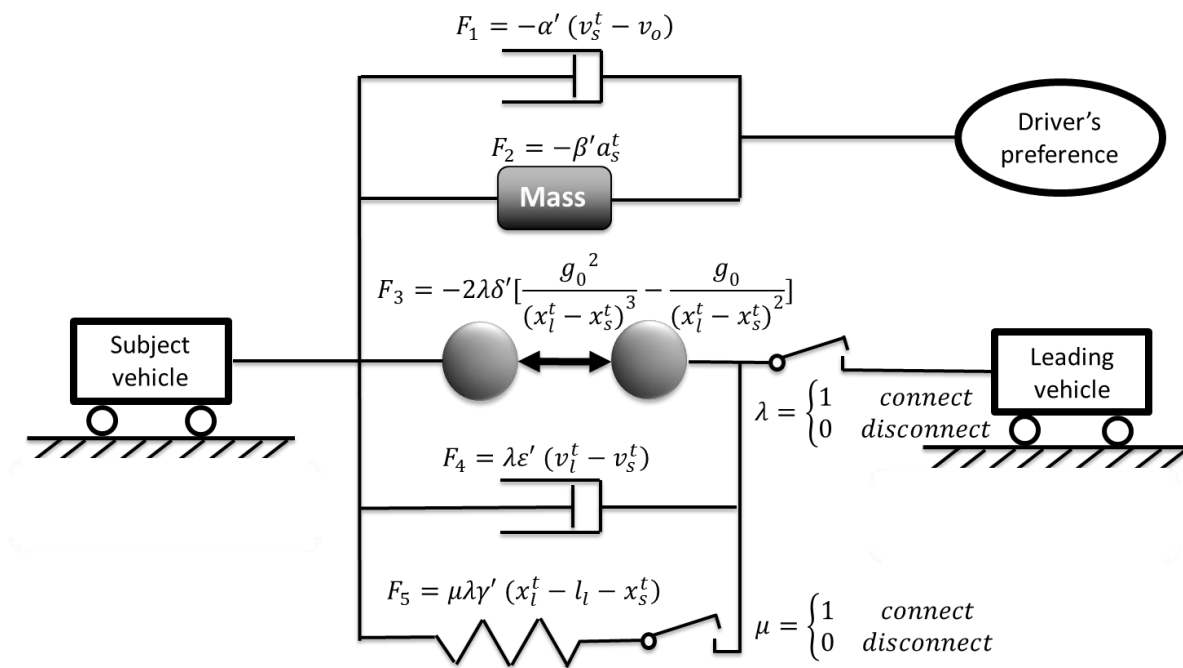


Fig. 0-3 The force elements to simulate the 5 factors in the open mechanics-based acceleration model

Feeling gap in multilane acceleration behavior

In a real traffic situation, lane change behaviors are very common phenomena in a multilane road sections. During a lane change process, one vehicle might follow another vehicle in a different lane. For example, as shown in Fig. 0-4 (a), vehicle S plans to make a lane change, where vehicle

An open mechanics-based acceleration model

S considers vehicle L as the leading vehicle. Since the lateral offset w , vehicle S will have different acceleration behaviors compare with single-lane behaviors.

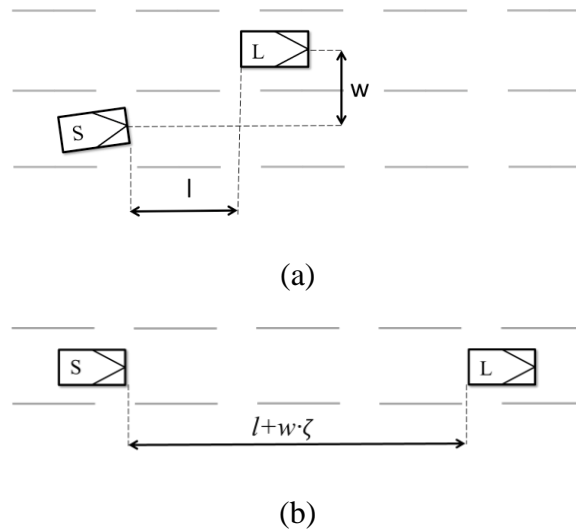


Fig. 0-4 Multilane acceleration behavior in a lane change scenario. (a) The original multilane acceleration situation, (b) The equivalent scenario of the multilane acceleration situation for driver S

To model driver's behavior in a multilane situation, the concept of feeling gap is introduced, which includes both longitudinal gap and lateral offset. Multilane acceleration behaviors for a driver is a complex process in reality, which is usually affected by traffic rules, vehicle states, driving courtesy and driver's characteristic. However, it is hard to accurately quantify these influences in a multilane acceleration behavior. To circumvent this problem, a "feeling gap" is introduced to describe multilane acceleration behavior, which is defined as a driver's feeling gap on a real physical one and directs a driver's driving acceleration behaviors. The "feeling gap" can reflect a driver's personal experiences and preferences during a multilane car following process. Generally, a driver has different feelings with certain lateral offset w and longitudinal distance l during a multilane acceleration process (Fig. 0-4 (a)). In this respect, a parameter ζ is introduced to describe such a difference, which is defined as an equivalent longitudinal rate with respect to a unit lateral offset.

If w and l are the lateral offset and longitudinal gap between leading vehicle and following vehicle. The equivalent gap based on the "feeling gap" can be expressed in Eq. 4.13

An open mechanics-based acceleration model

$$FG = \zeta * w + l \quad (0.13)$$

where FG is the equivalent gap between two vehicles in different lanes; l and w are the real longitudinal and lateral offset between leading and following vehicles. As a result, Fig. 0-4 (b) is equivalent scenario of the multilane situation shown in Fig. 0-4 (a). In a normal one lane car following scenario, since the lateral offset w is close to zero, the “feeling gap” is equal to the longitudinal gap with leading vehicle.

Governing equation in the mechanical system

As mentioned in Section 4.2.1, the five factors are treated as force elements of a mechanical system. Actually, the open mechanics-based acceleration modeling method is general and is open to any new factors, which can be added into the model as a force element. Based on Newton’s second law of motion, the governing equation of the subject vehicle’s longitudinal behavior can be described as:

$$\sum_{i=1}^5 F_i = ma_s \quad (0.14)$$

where m is a parameter, which can be calibrated by the driver’s behavior, although it is originally corresponding to the inertia in the Newton’s second law of motion. By substituting Eqs. (4-1) - (4-2), (4-9) - (4-11) and (4-13) in Eq. (4-14), one obtains

$$\begin{aligned} a_s \left(1 + \frac{\beta'}{m} \right) + v_s \left(\frac{\alpha' + \lambda \varepsilon'}{m} \right) + x_s \lambda \mu \frac{\gamma'}{m} + 2\lambda \left[\frac{g_0^2}{((x_l^t - x_s^t - l_l) + w \cdot \zeta)^3} - \frac{g_0}{((x_l^t - x_s^t - l_l) + w \cdot \zeta)^2} \right] \frac{\delta'}{m} \\ + \left[-\frac{\alpha'}{m} v_0 - \mu \lambda \frac{\gamma'}{m} ((x_l - l_l) + w \cdot \zeta) - \lambda \frac{\varepsilon'}{m} v_l \right] = 0 \end{aligned} \quad (0.15)$$

To get rid of the parameter m in the governing equation, parameters $\alpha = \alpha'/m$, $\beta = \beta'/m$, $\gamma = \gamma'/m$, $\delta = \delta'/m$, $\varepsilon = \varepsilon'/m$ are introduced. Thus, the final governing equation of the subject vehicle can be simplified as

$$\begin{aligned} a_s(1 + \beta) + v_s(\alpha + \lambda \varepsilon) + x_s \lambda \mu \gamma + 2\lambda \left[\frac{g_0^2}{((x_l^t - x_s^t - l_l) + w \cdot \zeta)^3} - \frac{g_0}{((x_l^t - x_s^t - l_l) + w \cdot \zeta)^2} \right] \delta \\ + [-\alpha v_0 - \mu \lambda \gamma ((x_l - l_l) + w \cdot \zeta) - \lambda \varepsilon v_l] = 0 \end{aligned} \quad (0.16)$$

An open mechanics-based acceleration model

which is an ordinary differential equations (ODE) of $x_s, v_s = \dot{x}_s$ and $a_s = \dot{v}_s$ that can be numerically solved with the iterative method. The initial values of x_s, v_s, a_s can be chosen as x_s^t, v_s^t, a_s^t .

Parametric analysis

As shown in the governing equation, six parameters $\alpha, \beta, \gamma, \delta, \varepsilon$ and ζ , simultaneously affect the vehicle's acceleration behavior. It is necessary to analyze each parameter's influence. To this end, three typical scenarios in real traffic situations are studied in this section to illustrate effects of these five parameters.

Free-flow scenario

In a free-flow scenario, without the interactions with other vehicles, the subject vehicle will finally reach a driver's optimal speed. Different α reflect different speed impacts for a driver. When α is relatively larger, say $\alpha = 0.35$, a driver has a strong speed desire (the solid line in Fig. 0-5). It takes less than 18 seconds to reach the target speed (25 m/s) from the static state. When α is relatively small, say $\alpha = 0.15$, the driver is not sensitive with speed impact, such as a loaded truck or bus driver (the dotted line in Fig.3). It takes more than 35 seconds to reach the same optimal speed. Furthermore, the speed shape of the vehicle also matches with real vehicle's behavior: at a lower speed, the acceleration is large, while when the driver closes to the optimal speed, the acceleration also decreases. In the simulation shown in Fig. 0-5, the other parameters are $\lambda = 0, \mu = 0, \beta = 1.25, v_0 = 25, v_s(t = 0) = 0$.

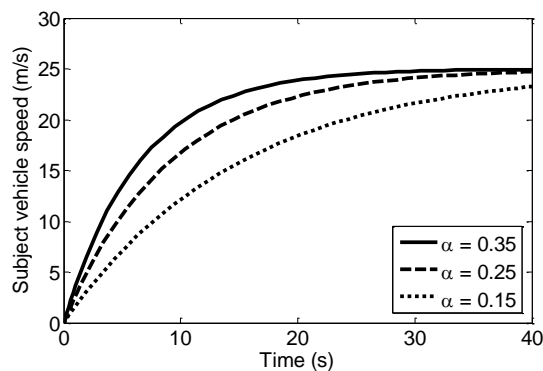


Fig. 0-5 The impact of parameter α in free-flow scenario

Gap increase scenario

In the car following state, when a new vehicle moves in front of the subject vehicle from an adjacent lane, if the new gap is relative small, the subject vehicle will try to increase the gap to the leading vehicle. Such a scenario is considered as the gap increasing. Here, the initial gap is selected as 35 m, and the initial subject vehicle speed is 20 m/s for this scenario.

Different δ represents different driver's safety considerations. When δ is relatively larger, say $\delta = 50$, the driver is very cautious (solid lines in Fig. 0-6). When a new vehicle moves in, this driver will try to slow down the speed and keep a longer safety gap. As a consequence, the new gap will be extended from 30 m to about 44 m. On the other hand, when δ is relatively small, say $\delta = 30$ m, the driver will have a relatively weak safety desire (dotted lines in Fig. 0-6). The driver will not be sensitive with the gap reducing, and following the leading vehicle with a smaller gap. In the simulation shown in Fig. 0-6, the other parameters are $\lambda = 1, \mu = 0, \alpha = 0.25, \beta = 1.25, \gamma = 0.1, \varepsilon = 0.2, v_0 = 25, v_s(t = 0) = 20, v_l = 20$. Because the subject vehicle wants to increase the gap, the value of μ is 0, which means that the impact of gap reducing desire are not considered in the simulation.

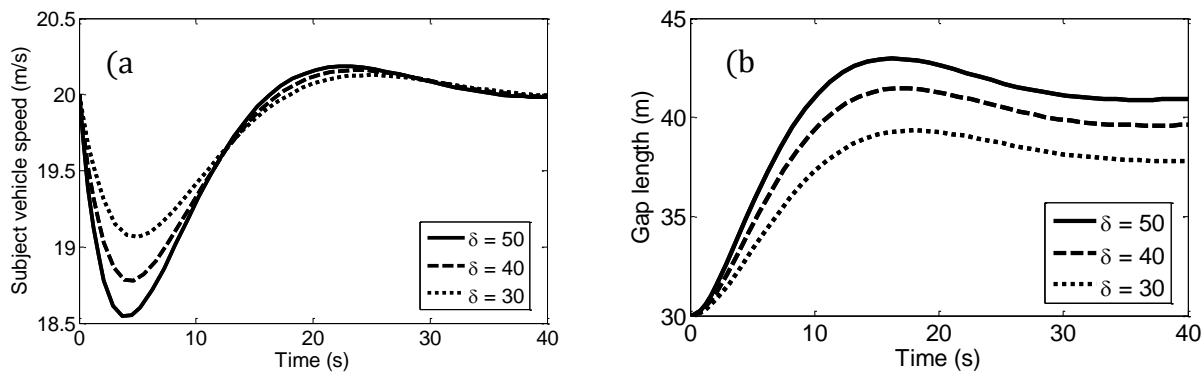


Fig. 0-6 The impact of parameter δ in a gap increase scenario. (a) Subject vehicle speed; and (b) Gap length.

The parameter ε reflects the difference of speed change sensitivity with the leading vehicle. When ε is relatively larger, say $\varepsilon = 0.3$, a driver has a strong desire to keep the same speed with the leading vehicle and avoid the gap changing with the leading vehicle (solid lines in Fig. 0-7). Although all of the three cases convert to gap length about 34 m, the processes are different. When ε is larger, the subject vehicle can reach the stable state with less oscillation at both speed and gap. As shown in Fig. 0-7, the speed change sensitivity factor plays the damping's function in the

An open mechanics-based acceleration model

mechanical system. In the simulation shown in Fig. 0-7, the other parameters are $\lambda = 1, \mu = 0, \alpha = 0.25, \beta = 1.25, \gamma = 0.1, \delta = 40, v_0 = 25, v_s(t = 0) = 20, v_l = 20$.

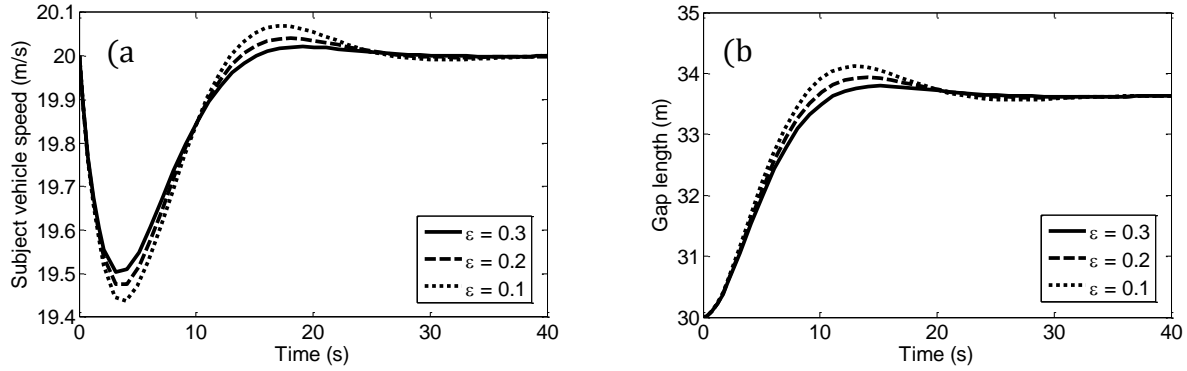


Fig. 0-7 The impact of parameter ε in a gap increase scenario: (a) Subject vehicle speed; and (b) Gap length.

Gap decrease scenario

In the car following state, when a leading vehicle moves to an adjacent lane, the subject vehicle will try to reduce the gap to a new leading vehicle. Such a scenario is considered as the gap decreasing. Here, the initial gap is selected as 95 m and the initial speed of the subject vehicle is 20 m/s for this scenario.

Different values of γ reflect different gap reducing impacts. When γ is relatively larger, say $\gamma = 0.15$, a driver will have a strong desire to reduce the gap with the leading vehicle (the solid lines in Fig. 0-8). Generally, to reduce this gap, a driver will prefer to take a larger acceleration to reduce the gap quickly, and keep a smaller gap. As shown in Fig. 0-8, a larger γ will also increase the frequencies of both speed and gap oscillations. This feature can explain the phenomenon that when a driver wants to reduce the gap with the leading vehicle, the driver's behavior is more active[20]. In the simulation shown in Fig. 0-8, the other parameters are $\lambda = 1, \mu = 1, \alpha = 0.25, \beta = 1.25, \varepsilon = 0.1, \delta = 40, v_0 = 25, v_s(t = 0) = 20, v_l = 20$.

An open mechanics-based acceleration model

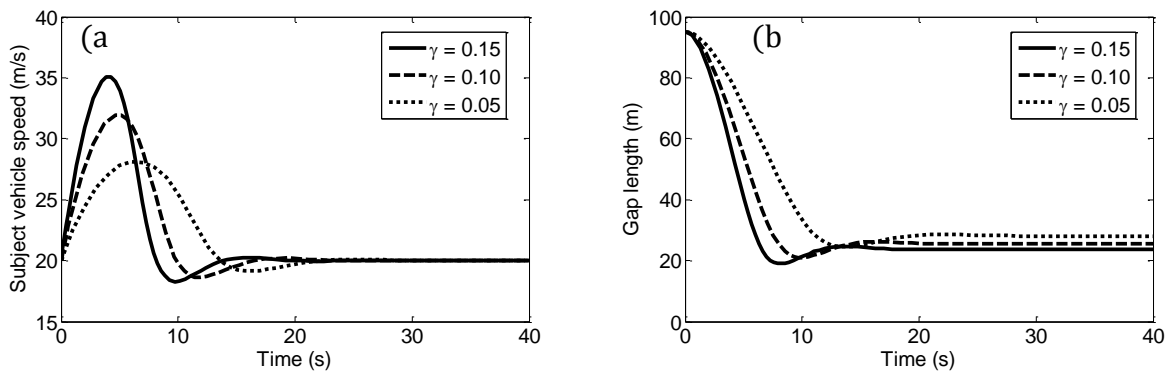


Fig. 0-8 The impact of parameter γ in a gap decrease scenario. (a) Subject vehicle speed; and (b) Gap length

Generally, a driver prefers to a smooth driving speed while tries to avoid a sudden acceleration or deceleration. Different values of β reflect different acceleration sensitivities. When β is relatively larger, say $\beta = 2$, a driver will have a strong preference to drive smoothly (solid line in Fig. 0-9). There are two features for the driver with a larger β . The first one is that the frequencies of both speed and gap oscillations are lower. The second one is that the speed changing is smoother. In the simulation shown in Fig. 0-9, the other parameters are $\lambda = 1, \mu = 1, \alpha = 0.25, \gamma = 0.1, \varepsilon = 0.2, \delta = 40, v_0 = 25, v_s(t = 0) = 20, v_l = 20$.

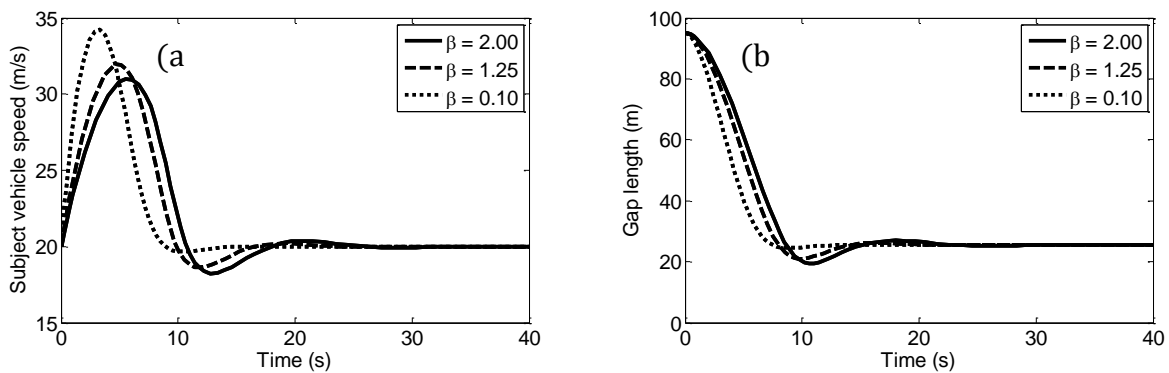


Fig. 0-9 The impact of parameter β in a gap decrease scenario. (a) Subject vehicle speed; and (b) Gap length

Multilane car following scenario

In the car following state, when a testing vehicle moves to an adjacent lane, the testing driver will consider the leading vehicle on the target lane as the leading vehicle. Such scenario is considered as the multilane car following scenario (Fig. 0-10). Here, the initial lateral offset w with

An open mechanics-based acceleration model

vehicle L is selected as 3.5 m and the initial longitudinal distance l with vehicle L is 40 m. The speed of vehicle L is 20 m/s, and the initial speed of vehicle S is 20 m/s. Lateral speed of vehicle S is selected as 0.5 m/s. Vehicle S starts to make a lateral movement from the beginning of the simulation.

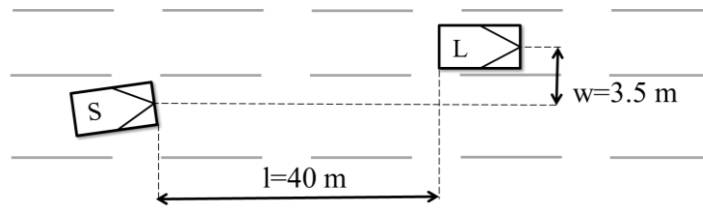


Fig. 0-10 Lane change scenario

Different values of ζ reflect S driver's different feeling of lateral offset. When ζ is relatively larger, say $\zeta = 5$, a driver considers that the lateral distance with leading vehicle on the target lane is equivalent a longer longitudinal gap (the dotted lines in Fig. 0-11). During a lane change, the driver usually prefers to increase speed before entering the target lane. When ζ is relatively small, say $\zeta = 1$, a driver consider the lateral offset is equivalent a shorter longitudinal gap (the solid lines in Fig. 0-11), the driver prefers to decrease speed before entering a target lane. In the simulation shown in Fig. 0-11, the other parameters are $\lambda = 1, \mu = 1, \alpha = 0.25, \beta = 1.25, \varepsilon = 0.1, \delta = 40, v_0 = 25, v_s(t = 0) = 20, v_l = 20$.

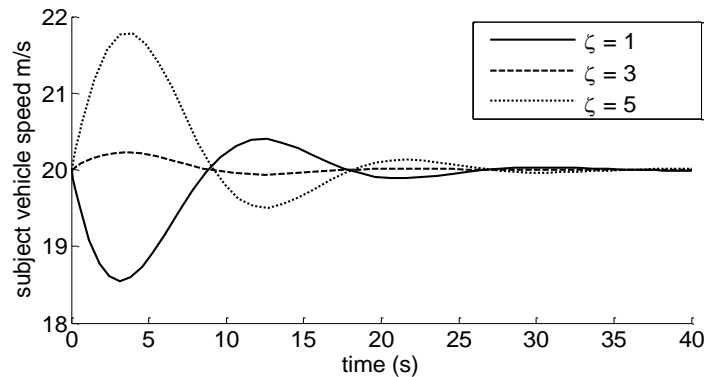


Fig. 0-11 The impact of parameter ζ in a lane change scenario

An open mechanics-based acceleration model

Field experiments and parameter calibration

Since the parameters in the present model describe the driver's detailed acceleration behaviors, macroscopic traffic data cannot be used to calibrate such parameters. As a result, to collect detail driver behaviors, an integrated data collection system is designed.

Experiment design

The testing vehicle is a 2009 Highlander, Toyota SUV, which is equipped with three devices including a camera, a handheld LIDAR rangefinder and ECU data collection system. All the testing devices are shown in Fig. 0-12.

Fig. 0-12 (a) is a LIDAR rangefinder. It is handheld by a researcher in the testing vehicle and provides measured distances from the device to the leading vehicle, with the testing error less than 0.5 m. The real gap between the subject vehicle and the leading vehicle is the measured distance subtracting the distance d (shown in Fig. 0-12 (c)), where d is the length from the bumper of the subject vehicle to LIDAR rangefinder. During the test, one researcher needs to target the LIDAR rangefinder at the rear part of the leading car. The data can only be acquired manually and the maximum frequency is about 1 Hz. Fig. 0-12 (b) is a video camera, which is fixed on the top of the test vehicle and captures the subject vehicle's front side states. The video data could be used to qualitatively analyze the driver's acceleration behaviors. Fig. 0-12 (e) is an ECU data collecting system. In automotive electronics, electronic control unit (ECU) is a generic term for any embedded system that controls the electrical system and subsystems in a motor vehicle. It is an effective way to capture a vehicle's states and a driver's real-time operations in ECU. The ECU data will be obtained by a CAN bus and displayed in a laptop. As shown Fig. 0-12 (e), the CAN bus has an USB-adapter to link with a PC on one side and a port which can be connected to the On-Board Diagnostics (OBD) adapter of the test vehicle on the other side. The position of OBD adapter is marked with red circle.

An open mechanics-based acceleration model

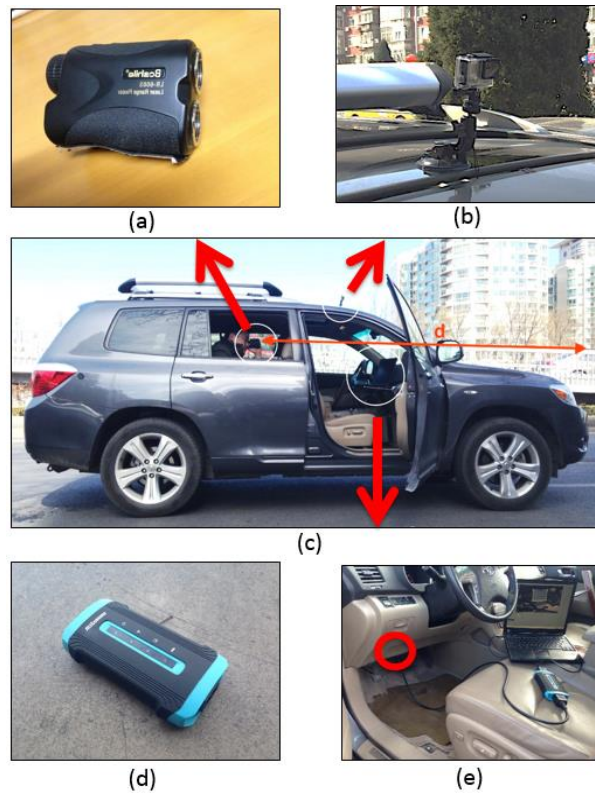


Fig. 0-12 Data collection system. (a) Handhold LIDAR rangefinder, (b) Video camera, (c) Testing vehicle, (d) CAN bus and (e) ECU data collecting system

Two researchers and a testing driver participated in the field test. One sat at the passenger seat at the first row to collect the vehicle ECU data, and to instruct the testing driver. The other one sat at the center seat of second row and operated the LIDAR rangefinder. Two different types of road environments were studied: an urban arterial road (speed limit is 80 km/h, no pedestrians, no intersections) and an urban distributed road (speed limit is 55 km/h, with intersections, less traffic flow). The urban arterial road was selected for the gap increasing and gap reducing scenarios, while the urban distributed road was selected for free-flow scenario without influence from the leading vehicle. Five free-flow scenarios and six gap changing scenarios were analyzed in field test data. The whole test time was about 40 mins. In the first 15 mins, the driver drove the testing vehicle on the road without any instruction to get familiar with the vehicle and the testing devices. Thereafter, test data were collected by the ECU and LIDAR data collection systems. The collected test data include the vehicle speed data from ECU and the data of gaps with leading vehicle from LIDAR.

Parameters calibration

Considering the free-flow scenario includes only two parameters α and β ($\lambda = 0$) in the governing equation, the parameter selection starts from free-flow cases. After α and β are obtained, the parameters γ , δ and ε will be determined from the gap increase and decrease cases.

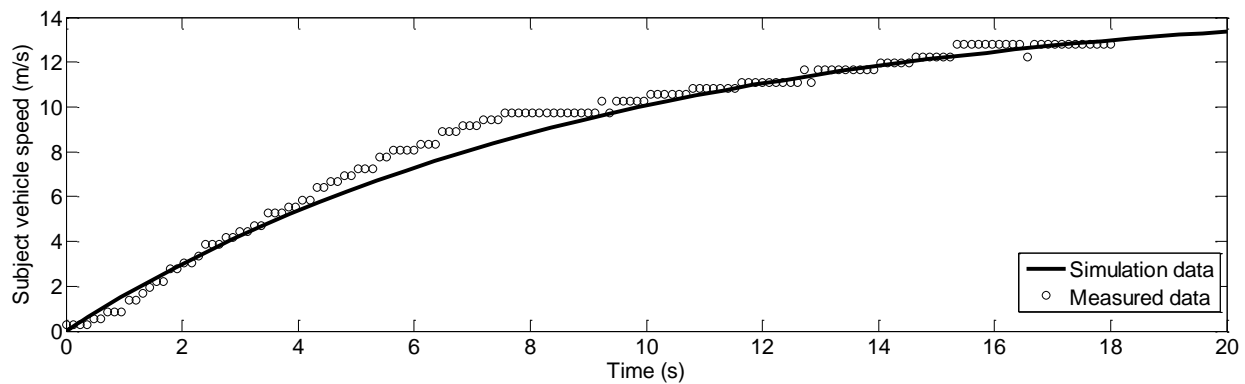


Fig. 0-13 Simulation and measured data in free-flow scenario

In the free-flow case, the driver's optimal speed is selected as the road speed limit, i.e., $v_0 = 15m/s$ (55 km/h). The vehicle was running from a stop status to the optimal speed. A typical testing result is shown in Fig. 0-13 with the solid line, where the subject vehicle's speed increases from 0 to 15m/s. The subject vehicle's acceleration is decreasing as its speed increases. Note that there is a slight pause during the acceleration at about 8 second. Such a pause might result from the transmission changing gears. By fitting the simulation results with the case introduced above based on the five field test results, parameters α and β are determined as $\alpha = 0.25$, $\beta = 1.25$. The simulation result is shown in Fig. 0-13 with the dotted line. Overall, the simulation results well match the field test results.

After α and β are determined, the parameters γ , δ and ε will be obtained from the gap increase and decrease cases. The increasing gap case starts at the moment that the testing vehicle changes to the adjacent lane with a short gap to the leading vehicle in the target lane. Then the testing driver tries to extend the gap until a stable speed and gap to the leading vehicle is reached. A typical testing result is shown in Fig. 0-14 with the solid line. At the first 2 seconds, the testing vehicle decreases speed in order to extend the gap to the leading vehicle, thereafter the testing vehicle smoothly increases its speed to follow the new leading vehicle. The simulation results are presented in Fig. 0-14 with dotted lines. By fitting the simulation results with the case introduced

An open mechanics-based acceleration model

above based on the field test result, parameters $\varepsilon = 0.2, \delta = 40$ are determined as $\varepsilon = 0.2, \delta = 40$. The simulation result is shown in solid line in Fig. 0-14.

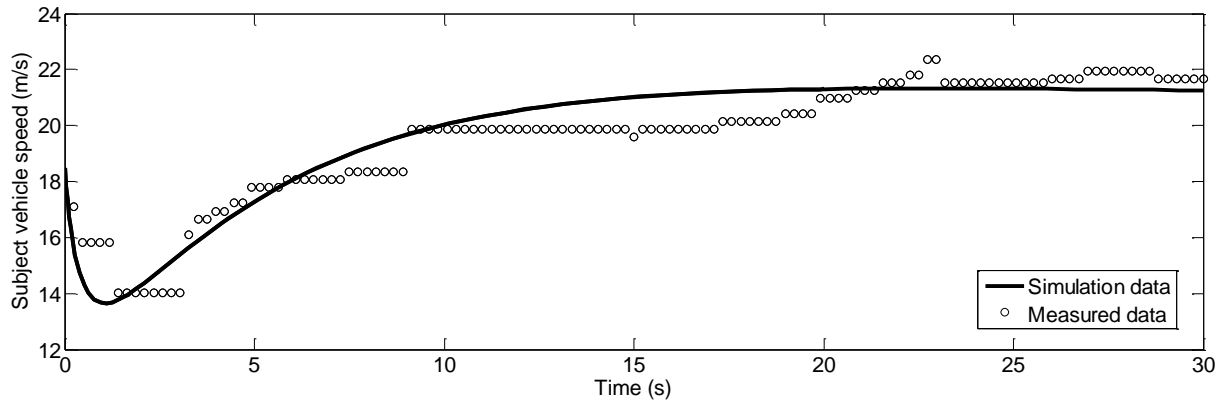


Fig. 0-14 Simulation and measured data in gap increases scenario

When a leading vehicle moves to an adjacent lane, the testing vehicle (the following vehicle) will adjust speed with the new leading vehicle on target lane. A typical testing result is shown in Fig. 0-15 with solid line. The lateral offset is 3.6 m, lateral movement finishes at 4th second. From beginning to 3rd second, the subject vehicle increases its speed to catch up the new leading vehicle. Then the testing vehicle will adjust its speed to follow the new leading vehicle in the same lane. Note that from the 6th to 18th second, subject vehicle shows a speed oscillation around 18 m/s. The simulation results are presented in Fig. 0-15 with dotted lines. By fitting the simulation results with the case introduced above based on the field test result, parameters γ and ζ are determined as $\gamma = 0.1, \zeta = 4.1$. The simulation result is shown in solid line in Fig. 0-15. The parameter based on the testing driver's acceleration behaviors are selected as $\alpha = 0.25, \beta = 1.25, \varepsilon = 0.1, \delta = 40, \gamma = 0.1, \zeta = 4.1$.

An open mechanics-based acceleration model

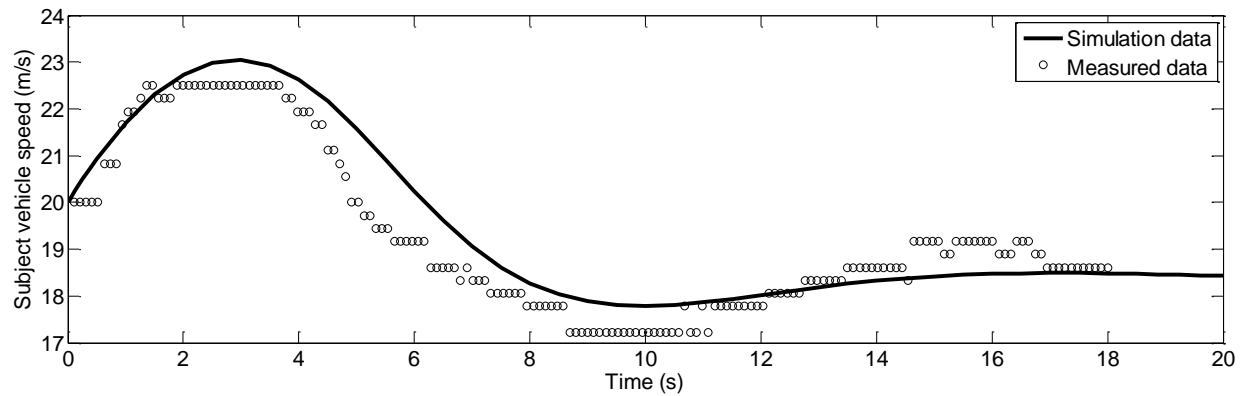


Fig. 0-15 Simulation and measured data in gap decreases scenario

Simulation

To demonstrate and validate the present model, a microscopic simulation program is developed with the MATLAB. The simulation structure system and the results will be discussed in this section.

Simulation results at different traffic situation

The open mechanics-based acceleration model is developed with the MATLAB. Each vehicle is considered as an individual object in the model. The model's parameters are used from the field test results: $\alpha = 0.25$, $\beta = 1.25$, $\gamma = 0.1$, $\varepsilon = 0.2$, $\delta = 40$, $v_0 = 22$ m/s.

A screenshot of the simulation platform is shown in Fig. 0-16. In this study, a one-lane road with traffic direction from left to right is considered. The road with a length of 2 km is divided into four sections with 500 m for each section for better illustrations. To get rid of the initial setting effects, the first 30-min data are not recorded. The simulation time is 30 min with an interval of 1/3 sec. Based on the initial set, if the gap is longer than the predefined generation gap, a new vehicle is generated at the beginning of the lane. By adjusting the generation gaps, different traffic conditions can be simulated. The simulation results are shown in Table 0-1.

An open mechanics-based acceleration model

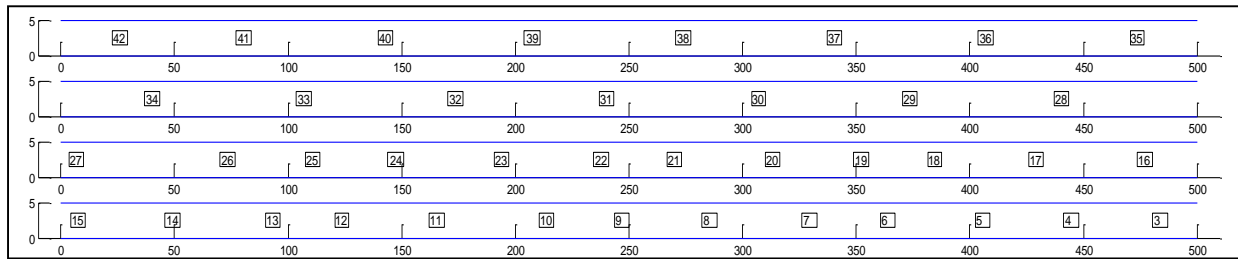


Fig. 0-16 A screen shot of simulation result

Table 0-1 Simulation results at different traffic conditions

Generation gap (m)	10	15	30	45	60	90	120	180
Traffic Flow (vehicle/hour)	432	656	1368	1296	929	684	540	480
Average traffic density (vehicle/km)	62.5	45.5	35.2	31.2	10.4	6.6	6.2	5.3

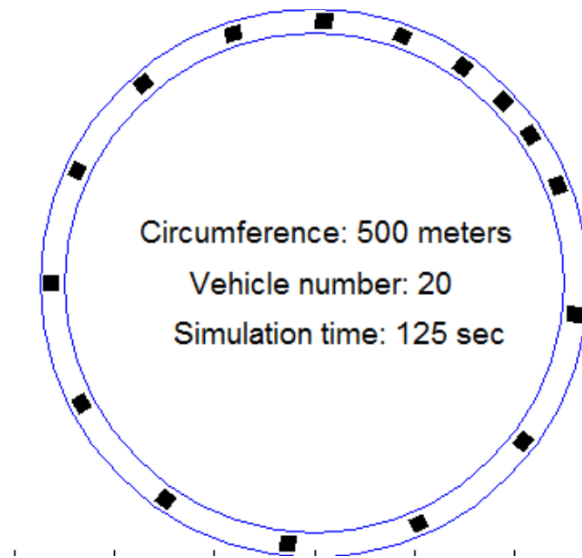
As shown in Table 4-1, when the average density increases from 62.5 vehicle/km to 35.2 vehicle/km, the traffic flow increases from 432 vehicle/hr. to 1368 vehicle/hr. When the average density is lower than 31.2 vehicle/km, the traffic flow decreases as the average traffic density decreases. The maximum traffic flow is about 1368 vehicle/hour happened at 35.2 vehicle/km. The test results shown in Table 0-1 shows that the traffic flow tendency is reasonable and the capability of the simulation road is also within a realistic region.

Shockwaves in simulation result

Shockwaves in traffic flow are observed in real traffic situations especially in congestion and queueing scenarios [173–176]. On the urban freeway, shockwave can be recognized as a transition from a flowing, speedy state to a congested, standstill state. It is an important phenomena in the traffic acceleration behavior analyses [177–180].

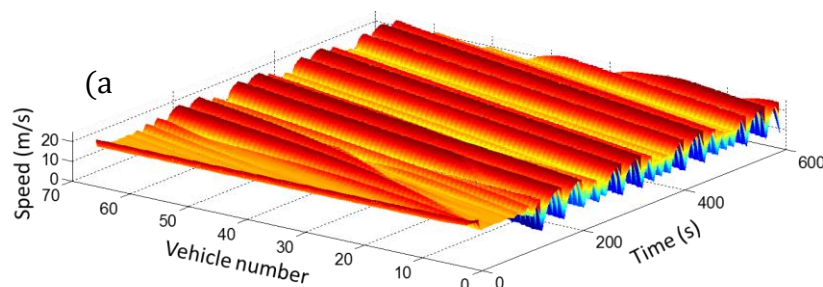
To simulate the shockwave phenomena, a loop road is programed in the MATLAB. A small scale experiment is tested in the simulation, and the simulation results are recorded in Video.1. In the simulation, the shockwave happens at about 100th sec, and the position of shockwave moves along the road in the following simulation time.

An open mechanics-based acceleration model



Video. 1 Simulation result of shockwave generation in a loop road

The shockwave phenomenon in the traffic flow is sensitive with traffic flow density [179]. Usually, when the traffic flow density is relatively high, such phenomenon appears. A larger scale simulation with 2000 m long loop road is simulated at different initial traffic flow densities, and the results are shown in Fig. 0-17. The shockwaves are obvious when the initial traffic flow density is 33 vehicle/km (Fig. 0-17 (a)); when the traffic flow density is 29 vehicle/km (Fig. 0-17 (b)), the shockwave phenomena is still be observed, but the intensity is much less; but when the traffic flow density is lower to 24 vehicle/km (Fig. 0-17 (c)), each vehicle is able to maintain a stable speed and the interaction between vehicles is relatively weak. As a result, the shockwave is not shown in the simulation results. In general, the present open mechanics-based acceleration model can simulate the generation process of traffic flow shockwaves and simulate different intensities of shockwaves in different traffic situations.



An open mechanics-based acceleration model

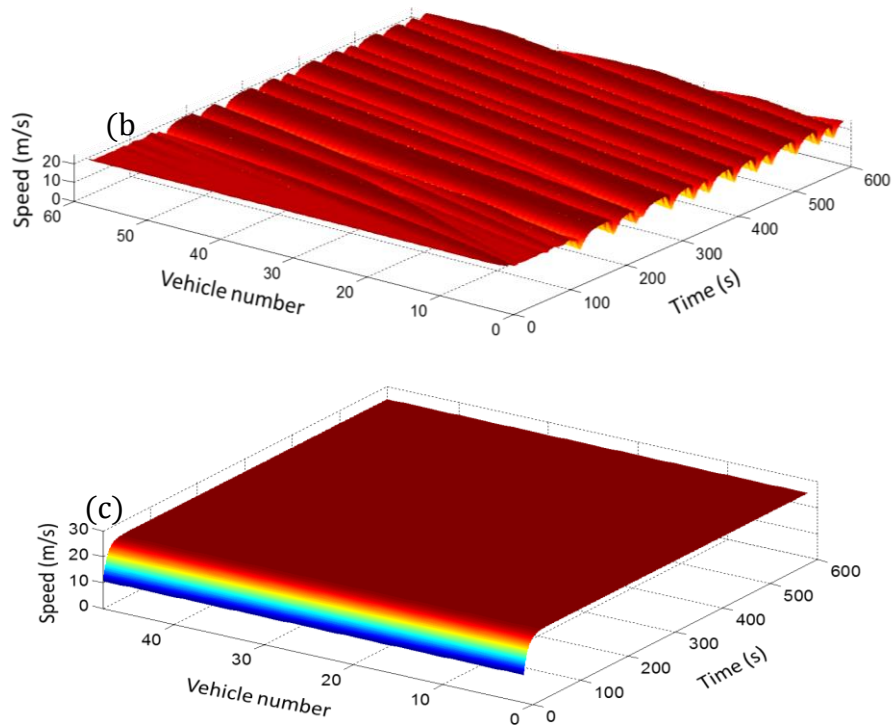


Fig. 0-17 Loop road car-following simulation results at different traffic flow densities

(a) 33 vehicle/km, (b) 29 vehicle/km, (c) (b) 24 vehicle/km

Conclusions and Summary

In this study, an open mechanics-based vehicle acceleration model is presented to consider longitudinal behaviors of vehicles on a road for the microscopic traffic simulation. Five important factors are taken into account, including subject vehicle's speed and acceleration sensitivity, safety consideration, relative speed sensitivity, and gap reducing desire. Each of these factors can describe the driver's preferences and interactions between vehicles, and each of them can function as a trigger to change the vehicle's behaviors. A mechanical system with force elements is introduced to quantify the vehicle motions. Based on Newton's second law of motion, the subject vehicle's governing equation of longitudinal behavior is derived in this open mechanics-based acceleration model. To demonstrate and validate the proposed model, a microscopic simulation program is developed with the MATLAB. The simulation results showed that the traffic flow and the road capacity are reasonable and can fit realistic conditions. In addition, traffic shockwaves were observed.

An open mechanics-based acceleration model

Comparing with traditional acceleration model, five significant characteristics of this open mechanics-based acceleration model have been demonstrated:

- The open mechanics-based acceleration modeling method is general and is open to any new factors, which can be added into the model as a force element.
- Five fundamental factors, which could influence driver's acceleration behavior, are simultaneously considered in the model. Each of them reflects a driver's preference during car following scenarios.
- Model parameters can be calibrated based on a special designed individual vehicle data collection system, including LIDAR rangefinder, video camera and ECU data collection.
- The parameter calibration of the presented model is based on the vehicle's dynamical behaviors, as a result, the model can accurately capture a driver's dynamical driving behavior in car following scenarios.
- The presented model is adapted with both single lane and multilane car following scenarios.

Although the simulation results demonstrate the high potential of the present model to be used in the driver's behavior analysis and microscopic traffic analysis, the following limitations and future work are suggested:

- Vehicle acceleration behavior is very complex. To understand and accurately predict vehicle behaviors, more factors may be considered besides the present five general factors.
- Compared with other methods, this model requires higher computational cost in simulation because the governing equation can only be numerically solved.
- To accurately calibrate the parameters used in the model, more tests need to be conducted for different traffic patterns, geographic regions, and cultures.

A driver decision-based lane change execution model

In this chapter, a driver decision-based lane change execution model is developed to describe the leading vehicle and the subject vehicle's behavior in a lane change process. A lane change execution can be analyzed as a driver's decision making process, which consists of four main steps, including desire point setting, priority decision-making, corresponding actions and achievement of consensus analysis. This chapter is reproduced from the paper co-authored with Fangliang Chen and Huiming Yin [181].

Introduction

Lane changing behaviors have fundamental impacts on microscopic characteristics of traffic flows due to the interference effect they have on surrounding vehicles [19,79]. It is also an important component of driving behavior to meet driver's tactical and operational maneuvering decision in different traffic situations [6]. A reasonable and adaptable lane change model has significant meaning in study of driver behaviors, driving safety, capacity analysis and traffic predictions, etc.

Generally, a lane change simulation often consists of two main steps: the target lane and gap selection and lane change execution [19]. The first step mimics a driver's thought before making lane change, which includes a lane change request and target lane and gap selection. The second step simulates the lane change operational process, such as changing speed and lane change selection. Driver's decisions, safety considerations, lane change priorities and courtesies are the main research topics in the study of execution of lane change. In general, the process of lane change selection has been well developed in the literature [21]. Different lane change selection theories and models can be applied for different driver features in different traffic situations [80,81]. However, compared with the studies on lane change selection, the investigation on lane change

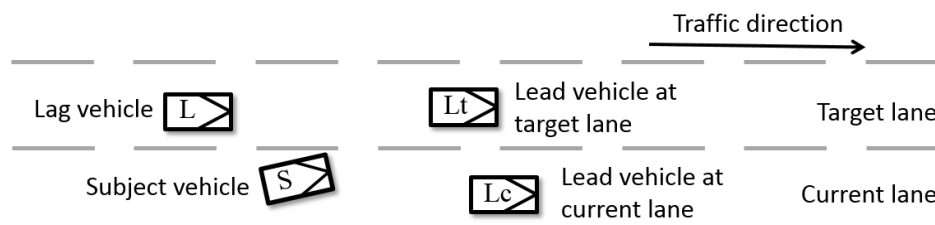
A driver decision-based lane change execution model

execution is limited in literature. The present study mainly focuses on the lane change execution model.

A lane change process is actually a behavior such that the subject vehicle wants to get the lag vehicle's permission to break into the original order in the target lane and take the lag vehicle's original position. In this sense, the lane change is a series of interactions between subject and lag vehicle. Although a large amount of lane change models have been introduced as stated above over the decades, most existing models considered the lag vehicles as certain parameters, but ignored the interactions between subject and lag vehicles. Furthermore, during a lane change process, a vehicle's lateral position will keep changing, which will play an important role in the whole lane change process. However, such lateral position effects were mostly ignored in existing lane change execution models. To overcome these limitations in the current models and better reflect the communication and interaction among vehicles during a lane changing process, a new lane change model is highly demanded. To this end, a driver decision-based lane change execution model has been developed in this study. The remainder of this study is organized as follows: Section 5.2 will introduce the proposed driver decision-based lane change model and describe in detail the four main procedures. Section 5.3 will discuss the information of parameter determinations. Based on the present lane change execution model and modified acceleration model, a microscopic simulation program will be developed with MATLAB. Several cases will be simulated and discussed in Section 5.4 and the conclusions will be presented in Section 5.5.

Driver decision-based lane change model

Generally, four types of vehicles will be involved in a lane change process as shown in Fig. 0-1: a subject vehicle (S) plans to move from its current lane to the target lane and wants to replace the original order of the lag vehicle (L) in the target lane. These two vehicles will be constrained by the two leading vehicle: a leading vehicle at target lane (Lt) and a leading vehicle at the current lane (Lc).



A driver decision-based lane change execution model

Fig. 0-1 Notations of the lead, lag and subject vehicles during a lane change

According to game theoretic analysis and the merging-giveaway interaction model [95], the lane change can be recognized as a game between vehicle S and vehicle L. In other words, these two vehicles can be considered as two competitors to obtain the road right to directly follow Lt in the target lane. According to the studies presented in [16, 17], vehicle S and vehicle L have to choose an option from strategies P_S and P_L separately in a lane change [95,182]

$$P_S = \{merge, pass\} \text{ and } P_L = \{giveaway, do not giveaway\} \quad (0.1)$$

where P_S and P_L are the options chosen by vehicles S and L during a lane change, respectively. Considering that there is only one vehicle is able to directly follow Lt at one time, they might eventually have a collision during a lane change if vehicle S chooses “merge” and vehicle L choose “do not giveaway”. To avoid such a situation, their decisions must satisfy certain achievement of consensus in a lane change.

Based on such interpretation of a lane change, a driver decision-based lane change execution is introduced. According to the decision-making concept [183–185], four main steps are constructed in the lane change execution procedure in the present model by following the structure of Delphi method [186–188], which include the desire point setting, priority decision-making, corresponding actions and achievement of consensus analysis. Each part will be introduced in this section. The structure of the method is shown in Fig. 0-2. Generally speaking, vehicle L and S will not exchange their decisions and thoughts during a lane change process [95]. Accordingly, vehicle L and S are considered in this analysis to individually follow the four steps shown in Fig. 0-2. Subsequently, they will have their own desire point positions, decision-makings, corresponding actions and achievement of consensus.

A driver decision-based lane change execution model

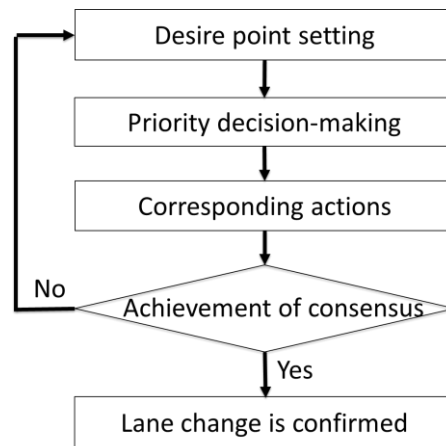


Fig. 0-2 Structure of driver decision-based lane change execution model

Desire point setting

Generally, a lane change process is the lateral movement of vehicle S toward the target lane [189,190]. To complete this process, a desire point [19], alternatively named as the converge point [182], collision point [95] or conflict point [191], is usually predefined as shown in Fig. 3, through which vehicle S enters into vehicle L's route.

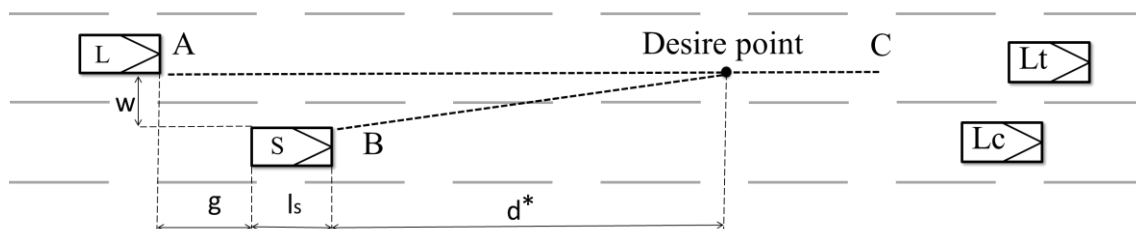


Fig. 0-3 Interpretation of lane change

To simplify the analysis, it is assumed that vehicle L will not take any lateral movement during a lane change. Therefore, the desire point is located in the AC line, and the lateral distance between vehicle S and the desire point is w (Fig. 0-3). The longitudinal distance between vehicle S and the desire point is defined as d^* . It is worth noting that d^* is the longitudinal distance from vehicle S to the desire point; $* \in \{L, S\}$ reflects different point of views from different vehicles, i.e., d^L represents the longitudinal distance from vehicle S to the desire point based on vehicle L's decision while d^S represents the longitudinal distance from vehicle S to the desire point based on

A driver decision-based lane change execution model

vehicle S's decision. In the following, all the terms with the superscript * are defined in this way. The length of d^* should be longer than two restricted distance d_v^* and d_{sc}^* :

$$d^* \geq \max(d_v^*, d_{sc}^*) \quad (0.2)$$

where, d_v^* and d_{sc}^* are the shortest longitudinal distances restricted by vehicle S's lateral and longitudinal speed and safety considerations, respectively.

Lateral and longitudinal speed of Vehicle S

Vehicle lateral speed is a vehicle's speed along the vertical direction during a lane change process. A nonzero lateral speed will be generated when a vehicle starts to move toward a target lane. If vehicle S plans to cross line AC, d_v^* will be affected by vehicle S's lateral and longitudinal speed: a vehicle with a higher lateral speed requires a shorter d_v^* , and a vehicle with a higher longitudinal speed requires a longer d_v^* . Mathematically, the length of d_v^* can be expressed in terms of vehicle S's lateral and longitudinal speed in Eq. (2).

$$d_v^* = \frac{w}{v_{lat_S}^*} v_{lon_S} \quad (0.3)$$

where $v_{lon_S}(t)$ is the longitudinal speed of vehicle S in the lane change process; $v_{lat_S}^*$ is an estimated average lateral speed of vehicle S, which can be assumed as constant values [172,192]; w is the lateral distance between vehicle S and the desire point (Fig. 0-3).

Safety considerations

As shown in Fig. 0-4, the longitudinal distance from the desire point to vehicle L can be considered as a "buffering distance" for vehicle L to adjust its speed and follow vehicle S with a safety gap. If vehicle S is slower than vehicle L, a "buffering distance" will be required for vehicle L and S to avoid collisions. To illustrate such safety considerations, an extreme case is considered. As shown in Fig. 0-4, where vehicle S arrives at the desire point (represented by S' at the moment), and vehicle L at position L', vehicle L and S have the same speed v_{PMP} and the gap between them is 0. In this case, the relationship between vehicle L and vehicle S can be mathematically expressed in Eqs. (0.4) and (4). Eq. (3) describes the motion of vehicle S with an increasing speed from v_{lon_S} to v_{PMP} . Eq. (4) describes the motion of vehicle L with a decreasing speed from v_{lon_L} to v_{PMP} .

A driver decision-based lane change execution model

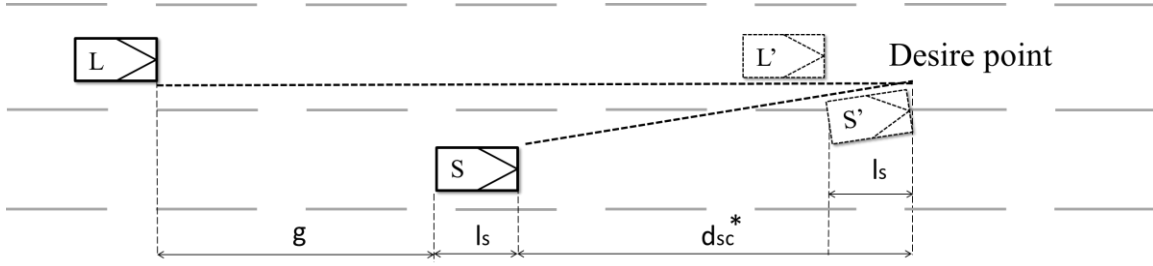


Fig. 0-4 The most dangerous situation considered in desire point setting

$$\begin{cases} \frac{(v_{PMP})^2 - (v_{lon_S})^2}{2a_{max_S}^*} = d_{sc}^* & (0.4) \\ \frac{(v_{lon_L})^2 - (v_{PMP})^2}{2d_{max_L}^*} = g + d_{sc}^* & (0.5) \end{cases}$$

where v_{lon_L} is the current longitudinal speed of vehicle L; v_{lon_S} the current longitudinal speed of vehicle S; $a_{max_S}^*$ is the maximum estimated acceleration of vehicle S that will be applied in the lane change process, and the value is different for vehicle S and vehicle L; $d_{max_L}^*$ is the maximum deceleration vehicle L will apply; v_{PMP} is the final speed of vehicle S and vehicle L, when vehicle S reaches the desire point; g_{min}^* is the minimum acceptable gap for vehicle L when vehicle S reach the desire point, the value is different for vehicle S and vehicle L; d_{sc}^* is the shortest longitudinal distance from vehicle S to the desire point.

By substituting Eq. (0.5) into Eq. (0.4), d_{sc}^* can be expressed in Eq. (0.6). It is considered as a safe scenario when $v_{lon_L} \leq v_{lon_S}$, therefore l_{min}^* is defined as 0.

$$d_{sc}^* = \begin{cases} \frac{(v_{lon_L})^2 - (v_{lon_S})^2 - 2d_{max_L}^* \cdot g}{2(a_{max_S}^* + d_{max_L}^*)} & \text{if } v_{lon_L} > v_{lon_S} \\ 0 & \text{otherwise} \end{cases} \quad (0.6)$$

Eq.(0.6) describes the safety considerations of driver S and driver L respectively based on their personal driving behaviors and experiences. Although some parameters are introduced to describe the same driving aspect, they have different meanings for vehicle S and L:

- $d_{max_L}^*$ is the maximum estimated deceleration of vehicle L in the process of a lane change. Because driver L can directly control the behavior of vehicle L, the value of $d_{max_L}^L$ will be

A driver decision-based lane change execution model

totally dependent on driver L's decision. However, for driver S, $d_{max_L}^S$ is an estimated parameter and cannot be directly controlled. An egoistic or a risk-prone S driver might believe vehicle L will definitely slow down to cooperate in the process of a lane change, which means that a larger value of $d_{max_L}^S$ is estimated in Eq.(0.6). In contrast, a prudent S driver might not want to take risk the safety issues on other vehicle's cooperation. In this sense, a smaller $d_{max_L}^S$ is considered in Eq.(0.6).

- $a_{max_S}^*$ is the estimated maximum acceleration for vehicle S in the process of lane change, which has different meanings for vehicle L and vehicle S. Driver S can directly control the behavior of its vehicle, therefore the value of $a_{max_S}^S$ is fully depending on driver S's desire and vehicle S's capability. However, $a_{max_S}^L$ is a predicted value for vehicle L. A risk-averse L driver always estimates a small $a_{max_S}^*$.

There are two features needed to be clarified about the desire point position. Firstly, the desire point is a virtual expected point before an actual lane change happens. The position of the desire point doesn't require a clear space in the road. Secondly, it is an estimated position, while the real merge point may vary as the speed of vehicle S and traffic condition change.

Priority decision-making

After the desire point is determined, both vehicle S and vehicle L will decide that who will have the priority to firstly arrive at the desire point based on their priority decisions. To express a driver's characteristics and preference in a priority decision-making, a "feeling distance" is introduced in driver's priority decisions.

Feeling distance

The priority decision-making process for a driver is a very complex process in reality, which is usually affected by traffic rules, vehicle states, driving courtesy and even driver's characteristic. However, it is hard to quantify these influences in a lane change execution process. To circumvent this problem, a "feeling distance" is introduced in this model, which is defined as a driver's feeling distance on a real physical one and directs a driver's driving behaviors. Compared with a real distance, the "feeling distance" reflects a driver's personal experiences and preferences during a lane change process.

A driver decision-based lane change execution model

Based on a direction of two measured points, it is possible to classify a distance into two categories: longitudinal and lateral distances. Generally, a driver has different feelings with certain lateral distance and longitudinal distance during a lane change process, where a lateral distance generates a longer “feeling distance” comparing with longitudinal distance. In this respect, a parameter *SELR* (*Subject vehicle Equivalent Lateral Rate*) is introduced to describe such a difference, which is defined as an equivalent longitudinal distance with respect to a unit lateral distance. Specifically, the value of $SELR^*$, $* \in \{S, L\}$ reflects a driver's different "feel distance" of w shown in Fig. (2), i.e., $SELR^L$ and $SELR^S$ represents the equivalent lateral rate of subject vehicle to the desire point based on vehicle L and vehicle S's decision, respectively.

Priority decision-making

As a “competition” to reach the desire point between vehicle S and vehicle L, the most straightforward criterion for the priority decision is that, based on current states, the vehicle that is able to reach the desire point prior to the other one has the priority. By introducing the feeling distance, the priority decision-making can be mathematically expressed in Eq.(0.7), where 1 means that vehicle L has priority and 0 means vehicle S has priority.

$$Priority\ decision = \begin{cases} 1 & \frac{SELR^* \cdot w + d^*}{v_{lon_S}} \geq \frac{d^* + g + l_S}{v_{lon_L}} \\ 0 & otherwise \end{cases} \quad (0.7)$$

where $SELR^* \cdot w$ is the feeling distance of the lateral distance from current position to the desire point.

A small $SELR^S$ denotes that a driver is very confident of his skill to change the lane and thus tends to take risky behaviors in a lane change. In contrast, a large $SELR^S$ indicates that a driver is very cautious and keeps a higher safety level for vehicle S in a lane change. Correspondingly, $SELR^L$ is considered as an expectation for other subject vehicles. A small $SELR^L$ means that a driver thinks the competitor is very aggressive and risky as vehicle S, while a large $SELR^L$ means the driver thinks the competitor is a courtesy driver as vehicle S.

Generally, a driver's characteristics can be qualitatively classified into four types as listed in Table 0-1. A driver with a large $SELR^S$ and a large $SELR^L$ (Type 1) is considered as a rational

A driver decision-based lane change execution model

driver, which is also applied to a driver with a small $SELR^S$ and a small $SELR^L$ (Type 4). Their difference is that the type 1 driver prefers to give the priority to vehicle S during a lane change, leading to a higher lane change rate from a macroscopic view. While the type 4 driver prefers to give priority to vehicle L, leading to a lower lane change rate from a macroscopic view. With a small $SELR^S$ and a large $SELR^L$, the type 3 driver is a kind of egoistic driver because he/she, as a subject vehicle, always believes that vehicle L is supposed to accept the lane change request; while as a lag vehicle, he/she always rejects other vehicle's lane change request. In contrast to an egoistic driver, the type 4 driver with a larger $SELR^S$ and a small $SELR^L$ is considered as an extremely cautious driver.

Table 0-1 Driver's characteristics based on $SELR^S$ and $SELR^L$

	Large $SELR^S$	Small $SELR^S$
Large $SELR^L$	Type 1: Rational driver and bias to decide priority to S driver	Type 2: Egoistic driver
Small $SELR^L$	Type 3: Extremely serious driver	Type 4: Rational driver and bias to decide priority to L driver

Vehicle corresponding actions based on priority decision

After the priority decisions are determined, vehicle S and vehicle L will take corresponding actions based on their decisions. In this section, the behaviors of vehicle S and vehicle L will be introduced respectively. At the second part, a interpretation of mandatory lane change (MLC) and discretionary lane change (DLC) will be discussed.

Actions of vehicle S and vehicle L based on priority decision

After a priority decision is made by vehicle S, two different behaviors might exist based on its priority decisions, which are illustrated in Fig. 0-5. The dotted lines indicate vehicle S's considered leading vehicles, and the solid arrow presents vehicle S's moving direction. As shown in Fig. 0-5, when vehicle S has priority, vehicle S will consider Lc & Lt as its leading vehicles, and move toward to the target lane. If vehicle S doesn't has priority, it will give up the current lane change plan, and consider Lc as leading vehicle. If vehicle S wants to make a DLC, it will go back

A driver decision-based lane change execution model

to the center of current lane. However, if vehicle S wants to make a MLC, vehicle S will still stay at the current lateral position, and wait for the next chance to finish the MLC.

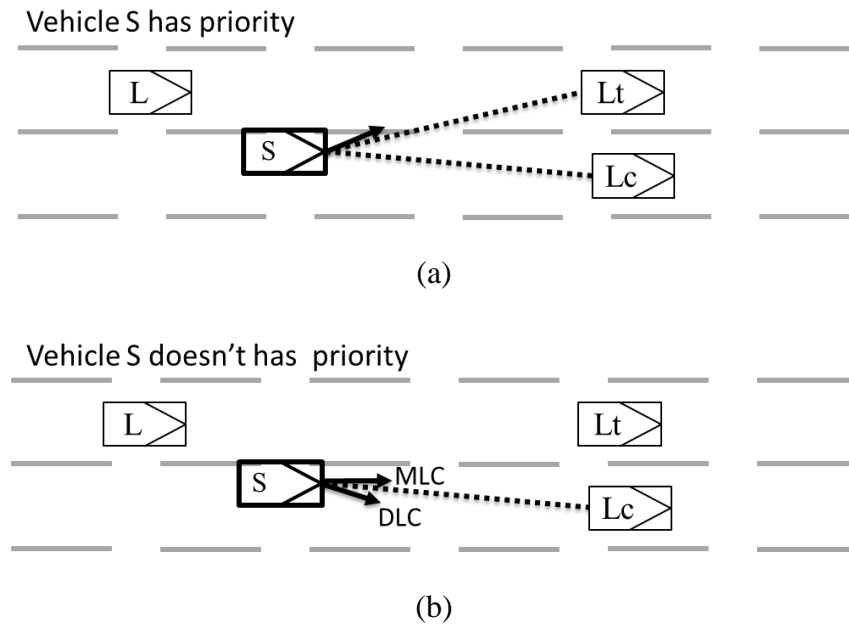


Fig. 0-5 vehicle S's corresponding behaviors. (a) Vehicle S has priority. (b) Vehicle S doesn't have priority

After a priority decision is made by vehicle L, two different behaviors might exist based on its priority decisions, which are shown in Fig. 0-6. When vehicle L has the priority, it will consider Lt as its leading vehicle, and ignore vehicle S's lane change request. In such situation, vehicle L usually increases its speed to reduce the gap to Lt. While, if vehicle L doesn't have the priority, it will accept vehicle S's lane change request and consider vehicle S as leading vehicle. To keep a proper gap for the new entering vehicle S, vehicle L will slow down to extend the gap between vehicle L and Lt.

A driver decision-based lane change execution model

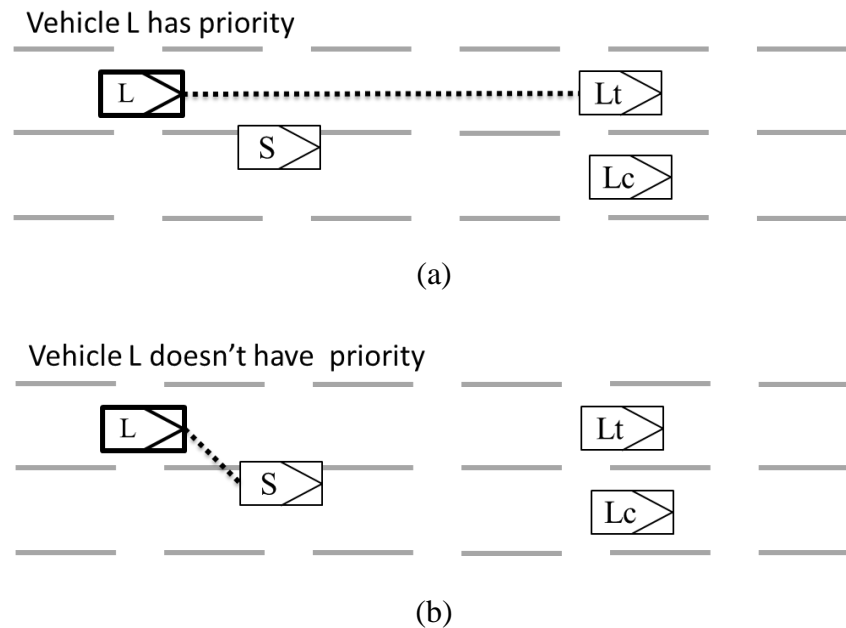


Fig. 0-6 vehicle L's corresponding behaviors. (a) Vehicle L has priority. (b) Vehicle L doesn't has priority

The interpretation of MLC and DLC

Generally, a lane change is often classified as either MLC or DLC [85]. MLC is performed when a driver must leave the current lane, such as getting to an exit. DLC is performed in order to improve driving conditions, such as entering a high-speed lane. To guarantee the MLC lane change successful rate, most exiting lane change execution model set more “aggressive” criteria for MLC. For example, In gap acceptance model the length of the critical gap for MLC[9-10,19-20] is shorter than DLC. It means that a driver needs to take more risks to perform a MLC. Although such assumptions can obtain a reasonable successful rate of MLC in simulation, it is not that reasonable to represent a real lane change maneuver.

In this model, no matter vehicle S makes a MLC or DLC, it will follow the same criteria in the steps of desire point setting and priority decision making. The only difference is that the corresponding actions after vehicle S doesn't have priority (Fig. 0-5(b)): If vehicle S makes a DLC, it will go back to its original road center, and if vehicle S wants to make a MLC, it will not go back to the original lane center but rather stay in the current lateral position. In general, when vehicle S doesn't have priority in a MLC, it will have more advantages to finish the MLC lane change in the

A driver decision-based lane change execution model

next chance. According to the priority decision criterion (Eq.(0.7)), a shorter lateral distance w to the target lane will have more chances to gain a priority at next chance and finish the MLC.

Achievement of consensus

Because a lane change requires a cooperation between vehicle S and vehicle L, one vehicle's decision cannot determine the result of a lane change. For example, even vehicle S believes that vehicle S has the priority, it does not mean that vehicle L will have the same priority decision and make a cooperation for vehicle S. To simulate such phenomena, the achievement of consensus is introduced.

If the two vehicles arrive at the achievement of consensus, the lane change will be confirmed. If vehicle S and L have a conflicting priority decisions, the lane change will not be confirmed, and the two vehicles have to repeat the three steps: desire point setting, priority decision-making and corresponding actions in the next time interval. The consensus and conflicts based on vehicle S and vehicle L's priority decisions are listed in Table 0-2.

Table 0-2 Consensus and conflicts based on priority decision of vehicle S and L

	Driver S: Vehicle S has priority	Driver S: Vehicle L has priority
Driver L: Vehicle L has priority	Vehicle S and vehicle L have conflicts: they will repeat the procedures, including desire point setting, priority decision and corresponding action in the next time interval.	Vehicle S and vehicle L achieved consensus: Vehicle S gives up the lane change request. The lane change is confirmed.
Driver L: Vehicle S has priority	Vehicle S and vehicle L achieved consensus: Vehicle S successfully obtains the right to complete the lane change request. The lane change is confirmed	Vehicle S and vehicle L achieved consensus: Vehicle S give up the lane change request. The lane change is confirmed.

In this present lane change execution model, "the lane change is confirmed" means that vehicle S and L have arrived at a consensus on a lane change, and the competition between vehicle S and L is finished. After that, vehicle L and S will complete the rest lane change process.

A driver decision-based lane change execution model

If vehicle L and vehicle S in the conflicting situation in Table 0-2, they have to repeat the procedures, including desire point setting, priority decision and corresponding action in the next time interval. Generally, after several tries, one of the vehicles will change its priority decision. In this sense, the present lane change execution model is able to describe the dynamical interaction and competition process between vehicle S and L in a lane change process.

Parameter determinations

In the driver decision-based lane change model, the parameter $SELR$ is introduced to describe the different “feeling distance” between lateral and longitudinal distances in a priority decision process. The value of $SELR^*$ will be discussed in the first part. Considering lane change is a complex procedure, it is impossible to cover all driver’s details and all situations on the road. A rational lane change execution model can keep a balance between the realistic and a programmable consideration. The rational approximate approaches applied in the simulation are introduced in the second part.

Determination of $SELR$

Considering that the gap acceptance model has been widely used in the real traffic situations, and that the parameters have been calibrated in different field tests, the value of $SELR^*$ will be selected based on the data of gap acceptance model. Although $SELR^*$ includes $SELR^S$ and $SELR^L$, considering the difference between them is small for a normal driver (type 1 and type 3 in Table 0-1), the difference can be neglected.

Generally, the gap acceptance model is developed to evaluate the gap in a lane change execution process: if the adjacent gap is longer than a critical gap, the lane change execution is acceptable; otherwise, it is unacceptable. In most gap acceptance models[80], an adjacent gap is further separated into the lag and lead gap (Fig. 0-7). To merge into an adjacent lane, a gap is acceptable only when both the lead and lag gaps are larger than the minimum acceptable ones, which are termed as the lead and lag critical gaps respectively [77].

A driver decision-based lane change execution model

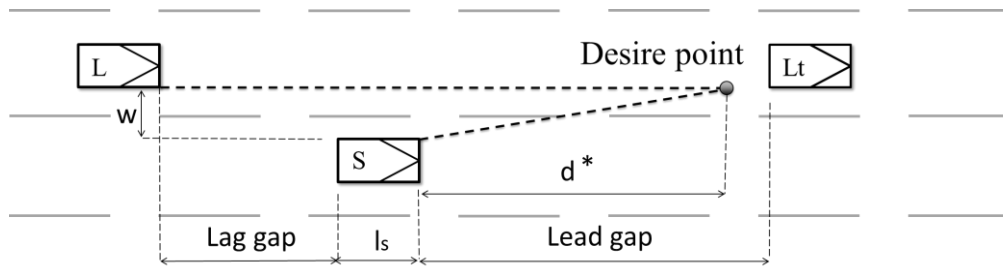


Fig. 0-7 The lag gap and lead gap in a lane change scenario

Based on the gap acceptance model, the critical gaps for a driver at time t are assumed to have the following general expression:

$$G^{cr,g}(t) = \exp(X^g(t)\beta'^g + \alpha'^g\xi + \epsilon^g(t)) \quad (0.8)$$

where $g \in \{lead, lag\}$, ξ is a specific random term which is constant for a given driver, $\epsilon^g(t)$ is a generic random term. $X^g(t)$ is a set of parameters of gap in the adjacent lane, α'^g and β'^g are contents. In the gap acceptance models [6,7,11], X^g is considered as a function of the relative speed $\Delta v^g(t)$ of the vehicle S with respect to the vehicle L in the target lane, which can be expressed in Eq. (0.9):

$$X^g(t)\beta'^g = \gamma'^g + \delta'^g\Delta v^g(t) \quad (0.9)$$

where γ'^g and δ'^g are constants which are determined by field test, whose values applied in different studies are summarized in Table 3.

Table 0-3 Parameters of gap acceptance models

Study	γ'^{lead}	δ'^{lead}		γ'^{lag}	δ'^{lag}		Average speed v_a (m/s)
		If leading vehicle faster	If leading vehicle slower		If lag vehicle faster	If lag vehicle slower	
Interstate 93 at the Central Artery, Bistin [80]	0.665	-0.412		1.69	0.172	0.177	16.9
I-395 Southbound in Arlington, VA [7]	1.353	-2.700	-0.231	1.429	0.471		15.6

A driver decision-based lane change execution model

Interstate 395 (I-395)						
Southbound in Arlington, Virginia [194]	1.54	-6.21	-0.130	1.43	0.640	15.75
Lankershim Boulevard [195]	2.38	-0.0221		1.44	0.263	12.4
Lankershim Boulevard [196]	2.31	-0.0482		1.51	0.0314	10.32

The random terms $\epsilon^g(t)$ and $\alpha'^g \xi$ are used to describe each driver's behavior in the observation. Considering in this study, only the average relationship between critical gap and relative speed is required, then from a statistical point of view, the random terms $\epsilon^g(t)$ and $\alpha'^g \xi$ can be neglected. Thus, the critical gap can be simplified as:

$$G^{cr,g}(t) = \exp(\gamma'^g + \delta'^g \Delta v^g(t)) \quad (0.10)$$

According to the definition of critical gap, it is assumed that when the lag-gap equals to the critical one (Fig. 0-7), vehicles L and S will have the same priority to reach their own desire points. In such a case, vehicles L and S will satisfy the following relationship based on Eq. (0.7):

$$\frac{ELRS^* * w + d^*}{v_{lon_S}} = \frac{d^* + G^{cr,g} + l_S}{v_{lon_L}} \quad (0.11)$$

Generally, $SELR^*$ is related to vehicle S's speed, it is assumed in this study as a quadratic function of the longitudinal speed of vehicle S, i.e., $SELR^* = a(v_{lon_S})^2 + bv_{lon_S} + c$, where a, b and c are the constants to be calibrated by comparing with existing gap acceptance models. Since the lateral distance w, vehicle S's lateral speed $v_{lat_S}^*$ and vehicle L's longitudinal speed v_{lon_L} are not included in the gap acceptance models, they are selected as $w = 1.8m$ [197], $v_{lat_S}^* = 0.5 m/s$ for general cases [198,199], while v_{lon_L} is considered as an average speed v_a taken from the gap acceptance models listed in Table 0-3. To conduct the regression analysis, the value of v_{lon_S} is selected in the range of $[0.7v_a, 2v_a]$. The position of desire point is based on vehicle S's lateral speed limitation, thus d^* can be determined as $\frac{w}{v_{lat_S}^*} v_{lon_S}$. Therefore, the regression analysis

A driver decision-based lane change execution model

equation to determine $SELR^*$ can be shown in Eq. (0.12), and the regression results are provided in Table 4.

$$\left[wv_{lon_L}a + \frac{w}{v_{lat_S}^*} (v_{lon_L} - 1) \right] v_{lon_S} + cwv_{lon_L} \frac{1}{v_{lon_S}} + (bwv_{lon_L} - l_s) = G^{cr,lag} \quad (0.12)$$

Table 0-4 Parameters selection based on the gap acceptance

Study	Fitting parameter			sum of the squared errors	R-square	Root mean square deviation
	a	b	c			
Interstate 93 at the Central Artery, Bistin[80]	0.126 4	-1.442	11.2	0.02196	0.9999	0.01784
I-395 Southbound in Arlington,VA[7]	0.153 7	-2.224	21.44	3.29	0.9931	0.1912
Interstate 395 (I-395) Southbound in Arlington, Virginia[194]	0.147 0	-1.933	18.09	2.52	0.9943	0.1712
Lankershim Boulevard[195]	0.178 4	-1.396	8.557	0.568	0.9991	0.0761
Lankershim Boulevard [196]	0.195	-0.536	0.448 6	0.0018	0.9996	0.0043

As shown in Table 5-4, the large values of R-square and the small values of the sum of the squared errors and root square deviation demonstrate that the assumption of $SELR^*$ is acceptable, with which the simulation results based on the present decision-based lane change execution model agree well with those provided by the gap acceptance models.

Approximation of other factors

A lane changing in reality is a complex process. It will be very hard to cover a driver's performance and traffic situations. Considering this, a rational lane change execution model shall

A driver decision-based lane change execution model

keep a balance between the realistic and a programmable consideration. Fig. 0-8 (a) and (b) illustrate a typical lane change procedures in a real situation and a simplified case, respectively. In order to better reflect the real situation while keeping the simulation in a rational realm, three assumptions are made in this lane change execution model:

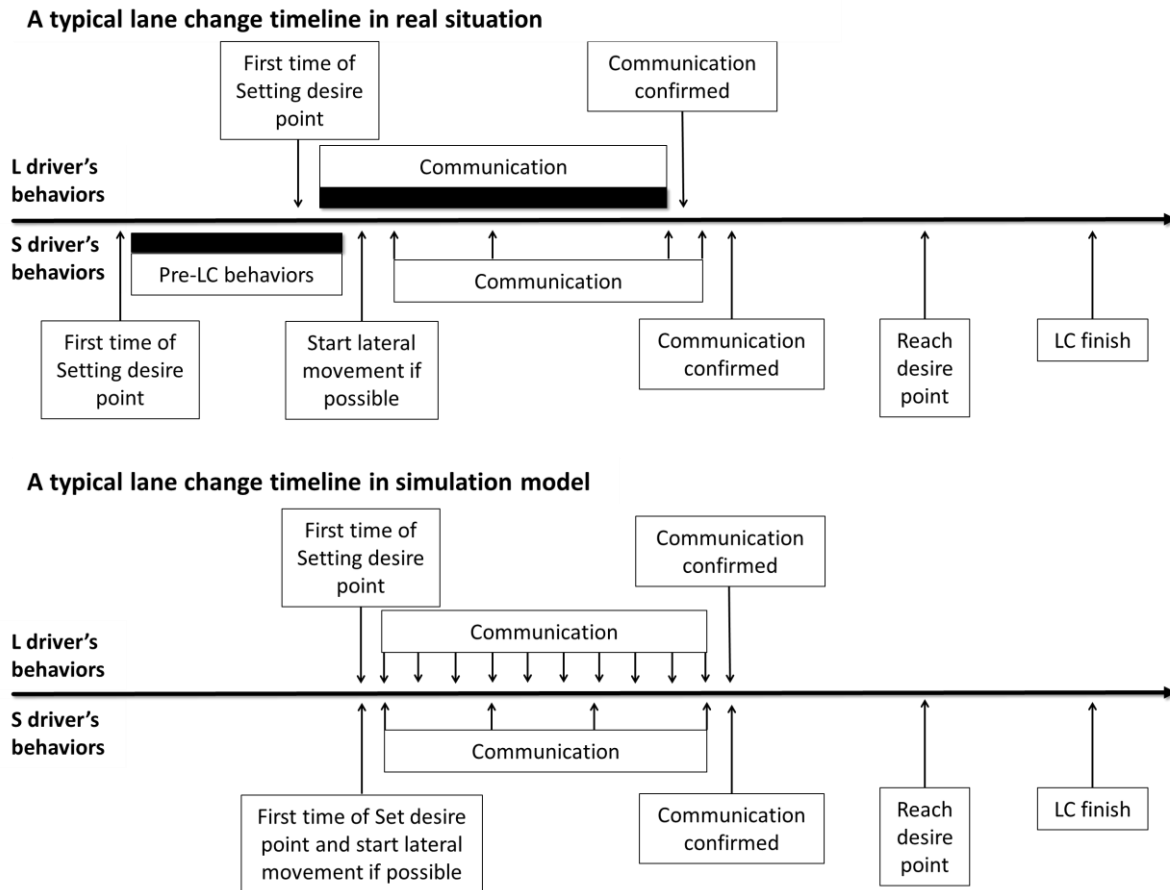


Fig. 0-8 Timelines at real situation and simulation model

- The first one is the exclusion of the pre-Lane-Change (pre-LC) behaviors. In a real lane change scenario, vehicle S will take some actions before lane change, such as turning on the signal light, or making a slight lateral movement toward the lane mark, etc., which can be considered as the pre-LC behaviors and be a part of a lane change process. However, considering that the factors influencing the pre-LC behaviors are hard to be quantified, they are ignored in this LC execution model as most gap acceptance model did [7,76,200].

A driver decision-based lane change execution model

- The second one is that the process of setting desire point for both drivers S and L are at the same time. Theoretically, driver L is passive in a lane change process, and not able to realize the lane change until vehicle S has started lateral movement. As a result, driver L usually starts to set the desire point and makes priority decision a little later than driver S does. However, considering that such a time period is very short and unstable, this time difference is neglected. As a result, vehicle S and vehicle L will start to set desire point at the same time in this model.
- The third assumption is that the observation frequencies for drivers L and S are constants. Theoretically, whenever driver S observes vehicle L through the side mirror, it can be considered as a priority decision-making. In this sense, the decision-making frequency for driver S is the frequency to view side mirror. However, driver L's observation is continuous through the front view. Thus, vehicle L is able to update its priority decision simultaneously. To unify the drivers' observation frequency, the decision-making frequencies in this model are considered as 1 Hz and 3 Hz for vehicles L and S, respectively.

Simulation

A microscopic simulation program has been developed in MATLAB to fulfill the present lane change execution model. The structure of the simulation system is introduced in Section 5.1. The simulation results of different scenario will be illustrated in Section 5.2.

Simulation structure

The structure of the simulation program is shown in Fig. 0-9, where the traffic rule, road data and vehicle generation are the three main inputs of the simulation system. Each vehicle will be calculated in the following steps, vehicle logical position updating, lane change request analysis, desire point setting, priority decision making, vehicle lateral and longitudinal behaviors updating, etc. In each simulation step, each vehicle obtains its surrounding traffic information through the observation module, which is constrained by the vehicle's view scope and frequency. The simulation results in each step are stored in the vehicle lane change statistics module, which consists of static data and time series data in order to increase the simulation speed and reduce its storage space requirement.

A driver decision-based lane change execution model

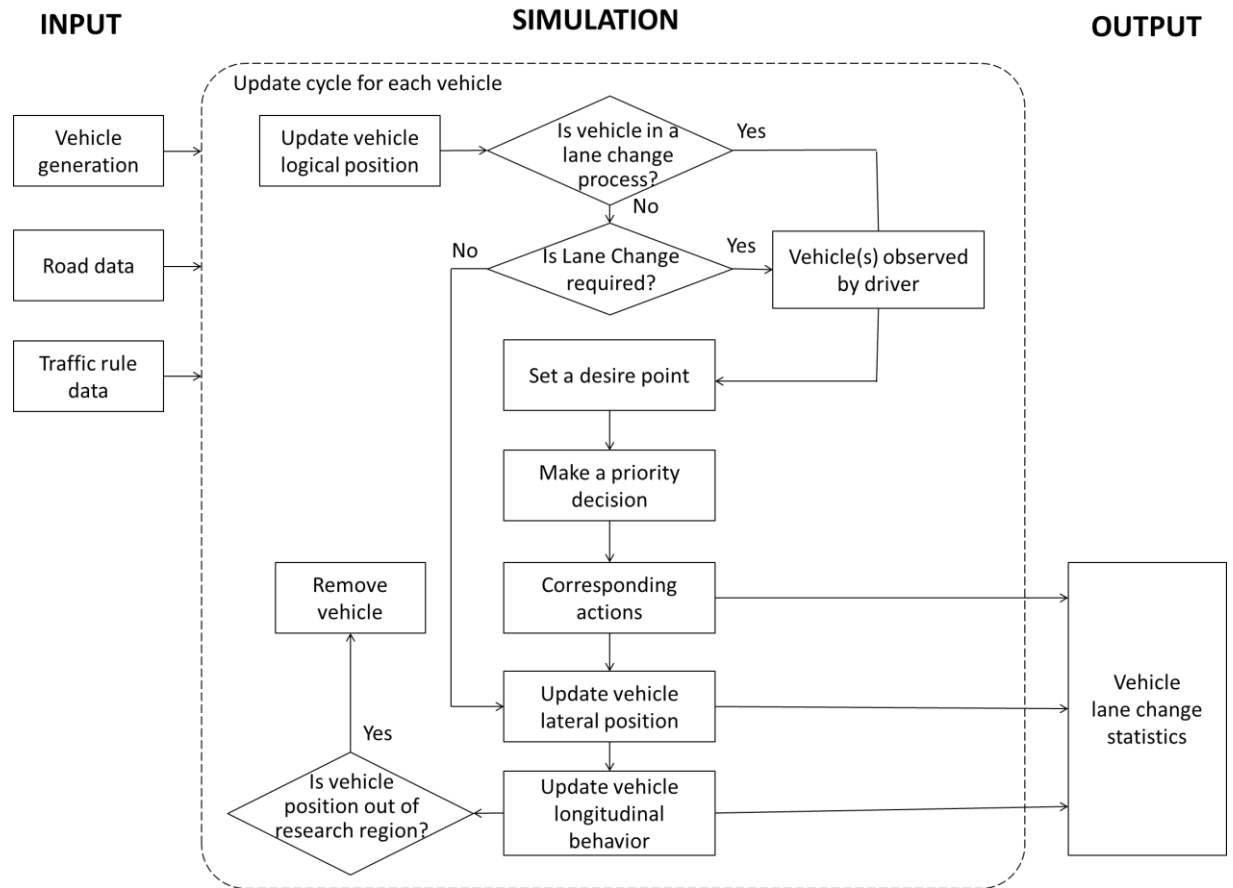


Fig. 0-9 Lane change model structure

In this simulation, a set of parameters is assigned to each vehicle to represent different features of different vehicles and different drivers. The vehicle's parameters and corresponding descriptions are listed in Table 0-5, which are classified into three categories, including vehicle size, lane change parameters and acceleration behavior's parameters. The lane selection process is the decision to consider a lane change and the lane choice for a driver [6]. In this model, the lane selection process based on Simulation of Intelligent Transport Systems (SITRAS) [81,93] is applied. If a vehicle perceives that the driving conditions in a target lane are better than its current lane over a critical value CV , a lane change request is triggered. The critical value CV can be a speed advantage or travel time advantage [81]. In this model, the travel time advantage is selected.

Table 0-5 Each vehicle's static parameters

A driver decision-based lane change execution model

Category	Parameter	Description	Value in experiment
Vehicle size	s	Vehicle length	N(6.5,0.3)
	ss	Vehicle width	2
Lane change parameters	v_{lat}^S	Driver's lateral speed	N(0.5,0.05)
	$d_{max_L}^L$	The estimated maximum deceleration for vehicle L in vehicle L's view	N(-3.5,0.1)
	$d_{max_L}^S$	The estimated maximum deceleration for vehicle L in vehicle S's view	N(-3,0.1)
	$a_{max_S}^L$	The estimated maximum acceleration for vehicle S in vehicle L's view	N(3,0.1)
	$a_{max_S}^S$	The estimated maximum acceleration for vehicle S in vehicle S's view	N(3,0.1)
	a	Parameter of ELRS*	0.1264
	b	Parameter of ELRS*	-1.442
	c	Parameter of ELRS*	11.2
	k1	$SELR^S = k1(a(v_{lonS})^2 + bv_{lonS} + c)$	N(1,0.2)
	k2	$SELR^L = k2(a(v_{lonS})^2 + bv_{lonS} + c)$	N(1,0.2)
CV	Critical value for triggering a lane change (second)	N(15,3)	
Acceleration behavior parameters	v_0	Optimal longitudinal speed	N(30,2)
	α	Subject vehicle's speed parameter	N(0.25,0.02)
	β	Acceleration sensitivity parameter	N(1.25,0.1)
	γ	Gap-reducing desire parameter	N(0.1,0.01)
	δ	Safety-consideration parameter	N(60,5)
	ϵ	Relative speed sensitivity parameter	N(0.2,0.01)
	ζ	equivalent longitudinal rate	N(4,1.5)

A screenshot of the simulation platform is shown in Fig. 0-10. In this study, a four-lane road with traffic direction from left to right is considered. To enlarge the simulation length, the road is separated into several 500-meter sections for better illustration. The basic road information, such as lane number and lane width, can be adjusted for specific applications. The road at the left side with blue vertical lines is the buffering zone, where vehicles are not allowed to make lane changes. The buffering zone is designed to minimize the effects of initial parameter setting, such as vehicle initial speed. The green vehicles represent those who have a left lane change intention, and blue

A driver decision-based lane change execution model

ones represent those with right lane change wish. The red slope line is the link between vehicle S and its desire point.

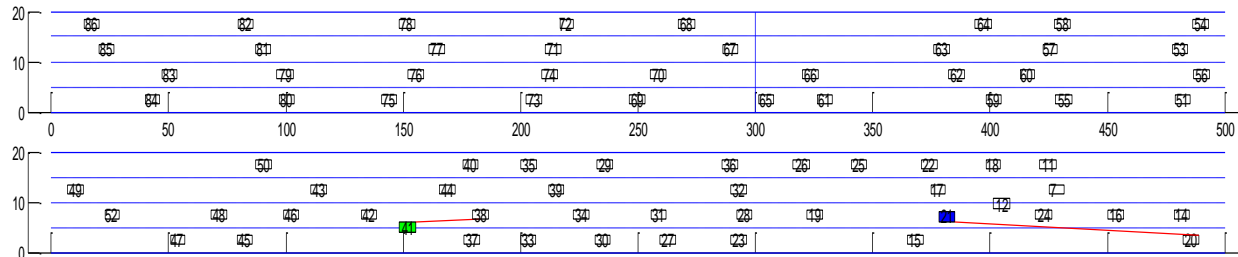


Fig. 0-10 A screen shot of simulation result

To facilitate the developed lane change execution model for engineers to operate, a graphic user interface (GUI) has been further developed as shown in Fig. 0-11. There are four main modules, in this GUI, including simulation control, lane change analysis, vehicle data and illustration modules. Through this interface, users can read, analysis and edit each vehicle's parameters during the simulation.

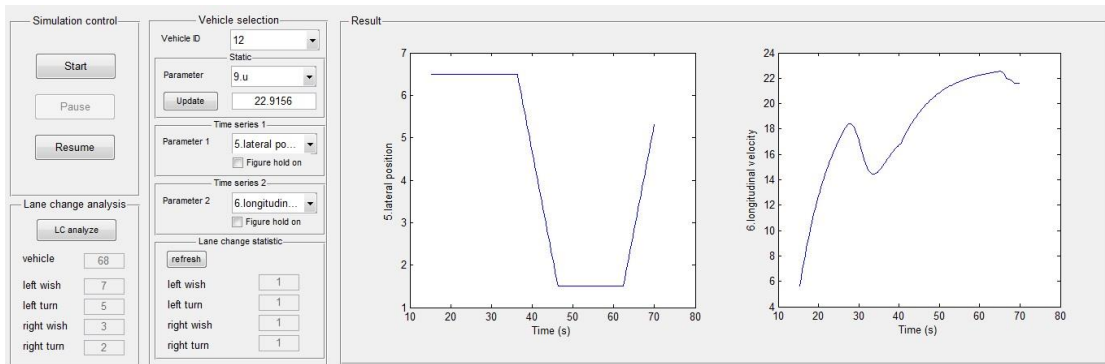


Fig. 0-11 The screen shot of user control interface

Simulation results

In order to present the feasibilities and advantages of the driver decision-based lane change execution model, a series of traffic cases are simulated.

Lane change simulation at different traffic situations

In this study, a 1000-meter four-lane road is considered. The first 300 meters are considered as a buffer zone. The simulation time is 20 minutes for each case, and the data starts to be recorded at the 5th minute. The generation gap is used to simulate different traffic situations. In this

A driver decision-based lane change execution model

simulation, if the gap is longer than the predefined generation gap at each lane, a new vehicle is generated. To simulate the speed differences among different lanes, a 25% larger gap is generated at the third and fourth lanes, which are considered as fast speed lanes. The simulation results are summarized in Table 0-6, where the first generation gap is for the first two lanes (slow lanes) while the second value is for the third and fourth lanes (fast lanes); vehicle number denotes the generated vehicles in whole simulation (15 minutes).

Table 0-6 Lane change simulation results at different generation gaps

Generation gap (m)	105/ 140	90/ 120	75/ 100	60/ 80	45/ 60	30/ 40	15/ 20
vehicle number	249	282	327	387	481	649	930
Average speed (m/s)	28.3	27.8	25.2	24.7	23.1	19.0	12.8
left LC	3	5	7	11	21	57	68
right LC	3	2	5	12	21	28	28
LC requests per vehicle in 1 km	0.034	0.036	0.066	0.122	0.220	0.381	2.120
LC per vehicle in 1 km	0.034	0.036	0.052	0.085	0.125	0.187	0.148

The simulation results show reasonable values at different traffic situations, which is shown in Fig. 0-12. When the generation gap decrease, the LC requests increase, since vehicles cannot reach their expected speed and will try to improve traffic environment by lane change. When the generation gap ranges from 140 m to 40 m, the lane change rate increases as traffic density increases. However, when the generation gap further reduces from 40 to 20 m, the lane change rate becomes decreasing as majority of lane changes requests is rejected.

A driver decision-based lane change execution model

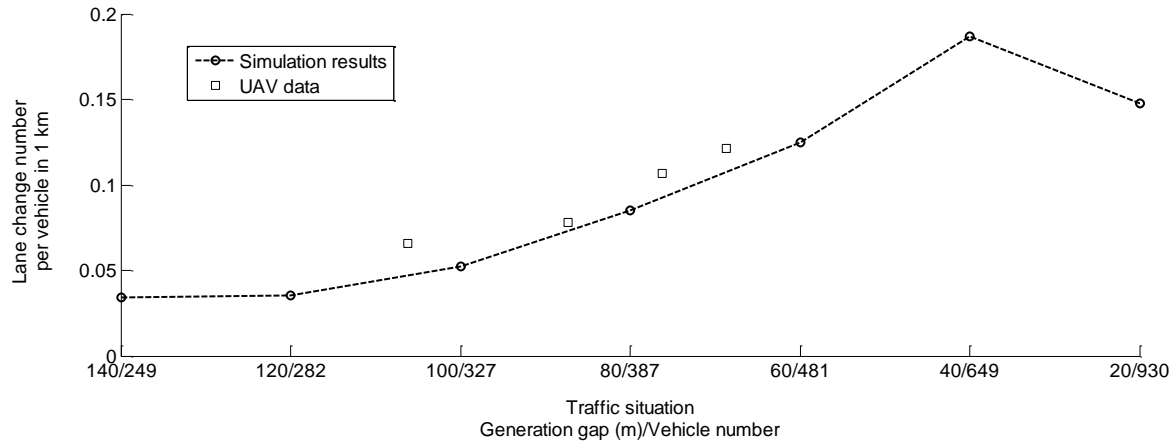


Fig. 0-12 Lane change number per vehicle simulation and field test results at different traffic situation

To verify the present lane change model, the simulation results are compared with the vehicle's lane change data obtained in a field test. Unmanned Aerial Vehicle (UAV) was applied to capture the lane change data in the field test. The details of the UAV experiment can be found in the authors' recent study [124], which is briefly summarized in Section 6. The image of the experiment road is shown in Fig. 0-13. The test field was selected is the Derenwu No.1 Bridge on the S12 highway in China. The UAV altitude is 150 m and the road section length in the video is about 300 m. The traffic flow at the bottom four lanes was selected. Because of the UAV's battery limitation, the duration of the experiment video is about 9 minutes. The field test results are summarized in Table0-7, which is also compared with the simulation results as shown in Fig. 0-12.



Fig. 0-13 The experiment location (altitude is 150 m)

A driver decision-based lane change execution model

Table0-7 Lane change data from UAV

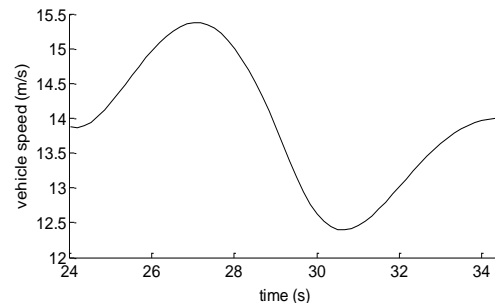
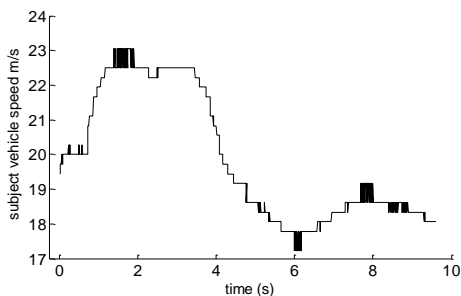
	Test1	Test2	Test3	Test4
Road section length (m)	300	300	300	300
Time (min)	9	9	9	9
Vehicle	313	365	405	440
LC number	6	9	13	16
LC number per vehicle in 1 km	0.044	0.055	0.068	0.076

In general, the simulation results based on the present model are reasonable and agree well with the real traffic situations at different traffic densities. For the higher traffic flow density, no field test result is available, as UAV is not allowed to operate in the center city by local law.

Dynamical lane change execution process

According to the present lane change model, the lane change execution between vehicle S and L is a dynamical process. Currently, none of existing gap acceptance model is able to capture such a dynamic process. However, the present model can simulate it. In this section, such a process is investigated by the present model by considering two typical scenarios.

In the first scenarios, vehicle S wants to make a lane change. However, both vehicle S and L believe that they have the priority at the beginning. After a while, vehicle L changes its mind and slow down to cooperate vehicle S's lane change request. In this scenario, vehicle L's longitudinal speed data in the real traffic is collected, which is shown in Fig. 0-1(a). At the first 3 seconds, vehicle L has the priority and increases its speed to reduce the gap to its leading vehicle. After that, vehicle L realizes that it might not have the priority, and then slows down to maintain a longer gap to vehicle S. Such a lane change dynamical process has been successfully captured by the present lane change model, which is shown in Fig. 0-14(b).



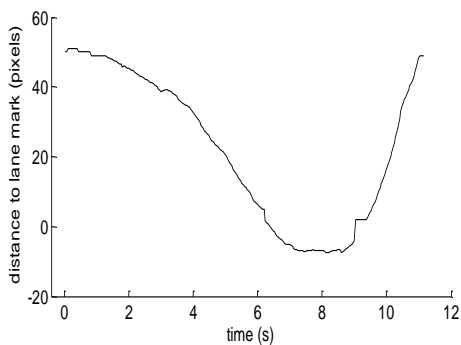
A driver decision-based lane change execution model

(a)

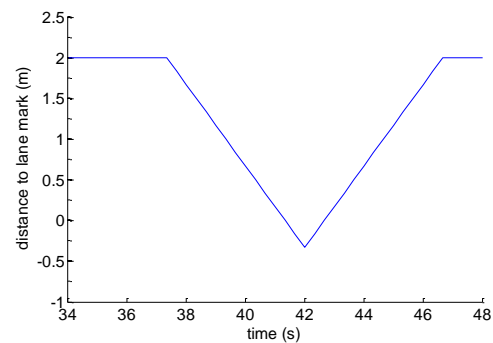
(b)

Fig. 0-14 Vehicle L longitudinal speed changes in a dynamical lane change process. (a) field test data, (b) simulation data

In the second scenario, Vehicle S wants to make a lane change. However, both vehicle S and L believe that they have priority at the beginning, but after a while, vehicle S changes its minds and turns back to its original lane at the lateral direction. In such scenario, vehicle S's lateral movement is collected, which is shown in Fig. 0-15(a). At the first 8 secs, vehicle S has priority and moves toward to the target lane. After that, vehicle S doesn't have priority, and moves back to its original lane. Such a lane change dynamical process has been successfully captured by the present lane change model, which is shown in Fig. 0-15(b). Because the lateral speed is considered as constant speed in the calculation, the lateral position curve is composed with straight lines.



(a)



(b)

Fig. 0-15 Vehicle S lateral position changes in a dynamical lane change process. (a) field test data, (b) simulation data

In this study, two typical dynamical lane change scenarios are presented to support that the lane change decision is a dynamical process. In addition, such dynamical lane change process can be simulated in the present model.

Simulation of MLC and DLC

Generally, a lane changes is often classified as either MLC or DLC. MLC is performed when a driver must leave the current lane, while DLC is performed to improve the driving conditions. In gap acceptance models, the critical gap in MLC [9-10,19-20] is smaller than that in DLC, which indicates that a driver needs to take more risks to perform a MLC.

A driver decision-based lane change execution model

However, in this model, the MLC and DLC follow the same criteria in a lane change execution process. The only difference between MLC and DLC is the following actions of vehicle S when it doesn't have the priority. If vehicle S makes a DLC to the target lane, it will go back to its original road center. However, if vehicle S wants to make a MLC to the target lane, it will try to maintain its lateral position.

To directly observe vehicle's lateral behaviors during MLCs, a lane mark recognition experiment has been conducted, which is a component of the individual vehicle data collection system. As shown in Fig. 0-16(a), the camera marked in the red circle was placed at the rare-side part of the vehicle body. The camera is able to capture the lane mark and the tires at the same time (Fig. 0-16 (b)). In Fig. 0-16 (b), the red dotted line is the recognized lane mark at the current frame, the two green dotted lines in Fig. 0-16 (b) are the distance between the front tire and lane mark and the distance between rear tire and lane mark, respectively. The number shows the measured distances in the unit of pixels. For example, in Fig. 0-16 (b), the distance from the lane mark to the front and rear tires are 62 pixels and 216 pixels, respectively.

In this experiment, the testing vehicle was required to make MLCs. Two records of the MLCs trajectory data are shown in Fig. 0-16. In the first one, the target lane was free, and thus the vehicle was able to successfully move to the target lane. However, in the second MLC test, there was a truck in the target lane (Fig. 0-16 (b)). The testing driver had to slow down and enter the gap behind the truck. Fig. 0-17 shows the collected data of distances from the vehicle tires to the lane mark during the two MLCs. It shows that the second lane change has a pause at the lateral distance within the period from 4 sec to 8 sec, in which the testing vehicle was maintained at its lateral position (about 60 pixels in Fig. 0-17 (a), and about 18 pixels in Fig. 0-17 (b)).

A driver decision-based lane change execution model

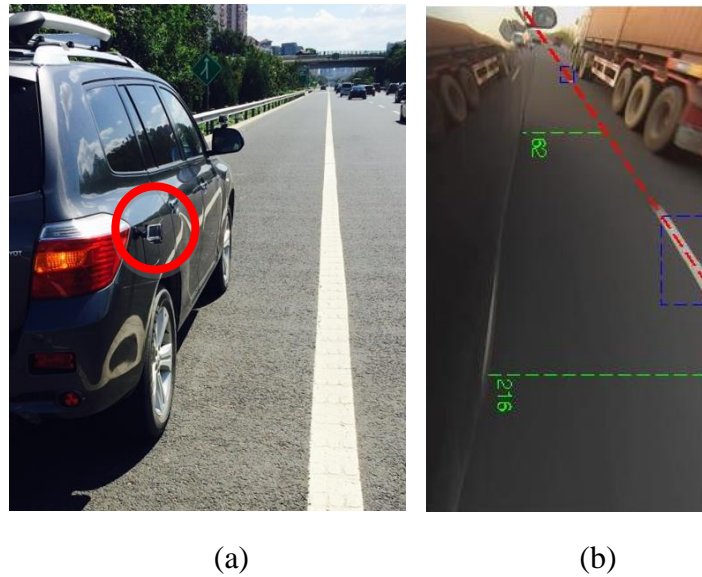


Fig. 0-16 Lane mark recognition experiment. (a) The camera position on the test vehicle, and (b) the results of lane mark recognition of a frame

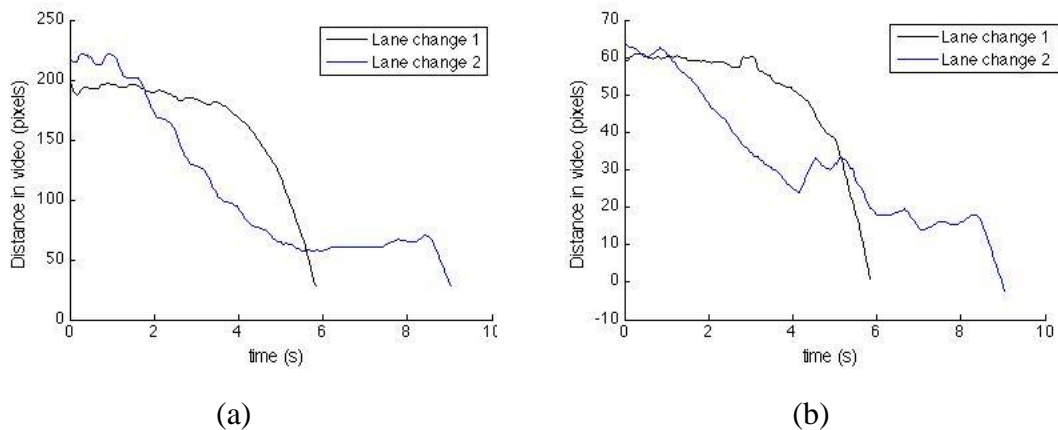


Fig. 0-17 Lane mark recognition results. (a) Distance between lane mark and front tire, and (b) distance between lane mark and rear tire

The field test result shown in Fig. 0-17 is a typical example to illuminate the applied assumption, i.e., when a lane change fails, the vehicle in the MLC will stay at its current lateral position and wait for a next opportunity.

To prove the present simulation method can get a reasonable MLCs success rate, a simplified contrast test for the MLC and DLC was designed. The first group consider that all lane change are MLC, the other group consider that all lane change are DLC. The simulation duration is 20 minutes.

A driver decision-based lane change execution model

Generation gap is 75/100. The experiment results are shown in Table 0-8. The results show that at the first attempt, MLCs and MLCs have almost same lane change success rate. However, in the second attempt, almost all MLCs can obtain the opportunity to finish lane change. Therefore, the present simulation of MLC and DLC is able to get a reasonable MLC success rate in simulation. Therefore, the proposed interpretation of MLC and DLC is rational.

Table 0-8 Lane change success rate on MLC and DLC

Group number	MLC (success times/all requests)			DLC (success times / all requests)
	Attempt 1	Attempt 2	Attempt 3	
	1	110/154	43/44	
2	114/142	28/28	-	111/130
3	103/134	31/31	-	94/120

Observation limitation simulation

In a complex traffic situation a driver will possibly overlook some vehicles around due to the blind spot and human errors. For example, during a lane change process, vehicle S needs to observe multiple vehicles simultaneously. As illustrated in Fig. 0-18, during a lane change, execution, vehicle S is considering vehicles Lt, Lc, L, and vehicles S1 and S2 simultaneously. As previously stated, each vehicle obtains its surrounding traffic information through the observation module, which is limited by the vehicle's view scope and frequency. Thus, it is possible that vehicle S might miss some vehicles during this process in a real situation. By adjusting the setting of observation module, the present model is able to simulate such observation limitations. To this end, a blind spot assistant system (BSAS) experiment is designed in this simulation.

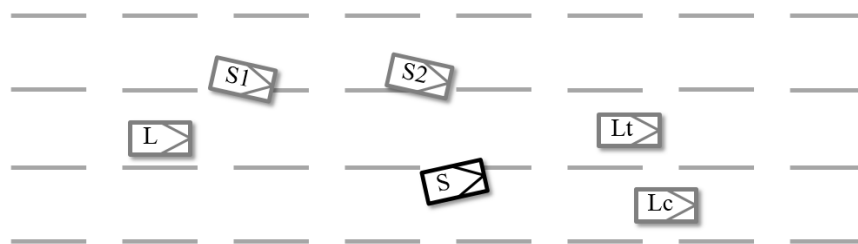


Fig. 0-18 The vehicles required to be observed by driver S

Theoretically, the BSAS can reduce human errors in the blind spot observation during a lane change. To quantify the influence of BSAS, two simulations are designed. In the first one, each

A driver decision-based lane change execution model

driver is able to perfectly observe nearby traffic situations with the help of BSAS. In the second case, it is assumed that 5% vehicles are not able to fully observe the lane change vehicles targeting the same gap (assume vehicle S will overlook vehicle S1 and S2 in Fig. 0-18). In this simulation, the simulation duration time is about 2 hours, and the generation gap is set as 75/100. The simulation results are listed in Table 0-9. Based on the two simulations, the BSAS can improve the driving safety by about 0.063% to 0.16% per vehicle per Km. Notes that such a BSAS simulation is only an example to exhibit the ability of the model in quantitative evaluating the effects of safety improving devices.

Table 0-9 Traffic crash rate with and without BSAS

Group number	With BSA (Accident per vehicle)	Without BSA (Accident per vehicle)
1	0/3954	2/3200 (0.063%)
2	0/3304	6/3694 (0.16%)
3	0/2966	3/3612(0.083%)

Conclusions

A proposed lane change execution model has been developed in this chapter to describe the leading and subject vehicle's behaviors in a lane change process. A lane change execution can be considered as a driver's decision making process, which contains four main steps, including desire point setting, priority decision-making, corresponding actions and achievement of consensus analysis. The simulation results agree well with the field test results at different traffic scenarios. Compared with traditional lane change simulations, the present model has the following four significant characteristics:

- The proposed lane change execution model is based on driver's decision. Each Driver's lane change execution process is based on driver's personal criteria and judgments.
- In addition to the longitudinal dimension, one more dimension, the lateral dimension, has been accounted for by introducing the concept of a feeling distance.
- This model is able to describe dynamical lane change execution process.
- A more reasonable simulation and interpretation of the MLC and DLC is fulfilled.

Reverse lane change simulation

Although the simulation results demonstrate the high potential of the present model in the driver behavior analysis and microscopic traffic analysis, the following factors may need to be considered in our future work to further improve the model:

- Driver decisions in a lane change are very complex. Besides the lateral and longitudinal distances, many factors may influence a driver's feeling distance, such as lane mark, vehicle size and view scope etc. To better reflect the driver decisions in a real lane change process, those factors might need to be considered.
- To accurately calibrate the parameters used in the model, more tests need to be conducted for different traffic situations, geographic regions, and cultures.

Reverse lane change simulation

The information on incident-induced traffic flow, such as reduced road capability, waiting time, and queue length estimation etc., is important for accurate traffic simulation and prediction in OMITS, as it will provide the OMITS with optimized routing and navigating services for users. However, very few efforts have been found in the literature to obtain such information by microscopic traffic simulations. This chapter proposes a reverse lane change model to simulate driver behaviors during a reverse lane change process at a two-way-two-lane road section where

Reverse lane change simulation

one lane is blocked by a traffic incident. In this model, the road nearby the incident location is divided into different regions for subject and lag vehicles' prospective to fulfill their lane change requirements. By introducing the concept of passing section's direction, the present reverse lane change model is classified into two scenarios: (1) the passing section's direction is the same as target lane, and (2) the passing section's direction is inverse to the target lane. Correspondingly, two passing section's impact factors are introduced to describe a driver's different decision making criteria for the two situations. Finally, a microscopic simulation program is developed with the MATLAB, to demonstrate and validate the present model. Three different groups of passing section's impact factors are simulated.

Introduction

Traffic congestion can be broadly classified as recurrent or non-recurrent based on its relation with daily variation of traffic demand [25]. The recurrent congestion is mainly caused by the unbalance between traffic demand and road network capacity. The non-recurrent traffic congestion mainly results from traffic incidents such as accidents, vehicle breakdowns or any other scenarios that impedes the normal traffic flow. According to Federal Highway Administration (FHWA), approximately 60% of the delays are caused by non-recurrent incidents, such as stalled vehicle, highway debris, and collisions [201,202]. Comparing with the recurrent traffic congestion, the non-recurrent traffic congestion has more effects on the short time traffic prediction and also residents' daily lives as well. As an important component of traffic flow, the incident-induced traffic greatly affects travel time prediction and incident management [203,204]. Therefore, it is necessary and important to quantify incident negative effects, such as road capability reducing and travel time delaying.

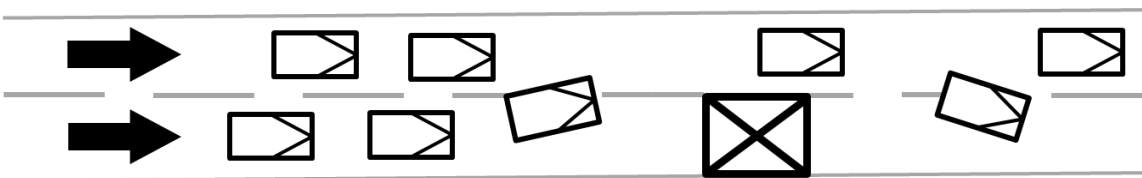
Currently, modeling incident-induced lane traffic maneuvers remains challenging in the field of traffic flow theory [204]. Various issues caused by lane-blocking incidents have resulted in many difficulties in traffic control and management [205–207]. Compared with incident-free situation, the traffic flow blocked by an incident decreases the road capacity and thus generates unusual queue lengths and delays in the upstream of the incident location. From driver behavior's point of view, the effects of rubbernecking and driving pressure in trying to pass an incident site will also increase the complexity in incident traffic analysis [208,209]. In addition, subsequent

Reverse lane change simulation

lane changes may further generate other traffic phenomena, such as secondary accidents and spillback events [210]. Therefore, understanding a driver's behavior in an incident-induced traffic scenario and further modeling such phenomenon have significant meaning in advancing traffic control and management.

Microscopic traffic behavior modeling has gained increasing recognition for its ability to accurately reproduce incident-induced lane traffic dynamics, particularly in simulating the lane changing behavior during incident-induced lane traffic jams [211,212]. Janowsky and Lebowitz [213] applied the asymmetrical simple exclusion process by using a unique transition probability to characterize incident-induced traffic jams on a one-dimensional lattice. Nagatani [214] extended this asymmetrical simple exclusion model for two-lane highway incident cases. Kurata and Nagatani [215] employed an optimal velocity model to generate a two-lane traffic model in which the symmetrical lane-changing rules were adopted to investigate incident-induced traffic congestion. Kerner et al. [216] proposed parameter-rich microscopic models to investigate spatial-temporal traffic congestion patterns of highway bottlenecks, and discussed the effects of lane changes on the structure of highway bottlenecks and moving traffic jams. This was followed by the development of a cellular automation (CA)-based traffic model by Zhu et al. [217], in which the symmetrical and asymmetrical lane-changing rules proposed by Chowdhury et al. [218] were utilized to improve the model's ability to characterize incident-affected lane changing. Sheu [204] modeled inter-lane and intra-lane traffic maneuvers in lanes arterial lane blocking incidents, where the effects of lane blocking incidents on lane traffic behavior, including car-following and lane change behaviors were investigated. Some driver behavior studies, which did not focus on incident cases, are able to simulate simple incident-induced traffic scenarios [79,82,85].

When an incident happens on a multiple-lane road, the traffic flow has to make a lane change to pass the incident position (Fig. 0-1 (a)). In such a scenario, a driver will make a lane change at the upstream of the incident position and may make DLC after passing the incident. Such a traffic incident passing has been modeled in the literature [104,219,220].



Reverse lane change simulation

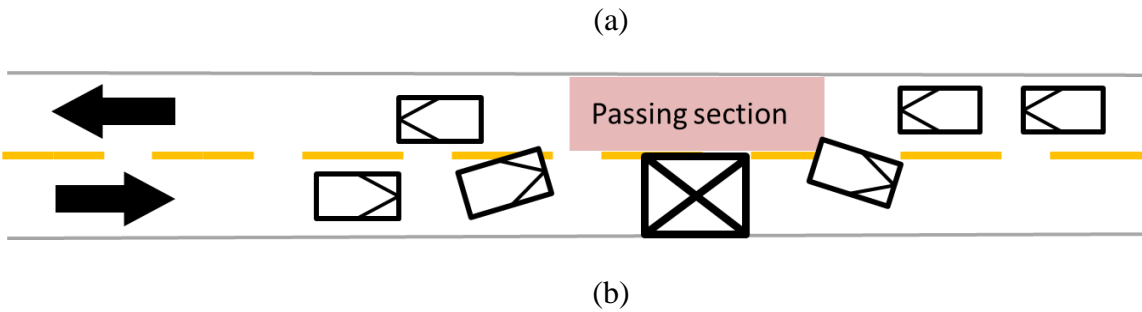


Fig. 0-1 Two types of traffic incident scenarios; (a) an incident happened on a multiple-lanes road, and (b) an incident happened on a two-lane-two-way road

When an incident happens on a two-lane-two-way road and blocks one of the lanes, vehicles have to temporarily use the reverse lane to pass the incident, which is a very common phenomenon in the distribution roads as shown in Fig. 0-1 (b). Such type of incident is not limited to an accident, any objects that block the road, such as a temporarily stopped vehicle, can be considered as an incident. Differently from the incident in a multiple-lane-flow as shown in Fig. 0-1 (a), to pass an incident in a two-lane-two-way traffic flow, vehicles have to share a lane section as highlighted in Fig. 0-1 (b), which is defined as a “passing section” in this study. A vehicle in the incident lane has to make two consecutive lane changes to pass the incident. This two consecutive lane changes are named as reverse lane change. Since a driver has to make more interactions with other vehicles in the reverse lane to obtain the priority to use the passing section, the reverse lane change shown in Fig. 0-1 (b) is different with a conventional lane change or the one shown in Fig. 0-1 (a). To the authors’ knowledge, no relevant driver behavior analysis or microscopic simulation method has been developed yet to simulate such a reverse lane change. In this chapter, based on the analysis on driver behavior [148], and the basic concept of driver decision-based lane execution change model [181], a proposed reverse lane change model is introduced.

The remainder of this chapter is organized as follows. Section 6.2 will clarify the research scope of the reverse lane change model. In Section 6.3, the road around the incident location will be classified into different regions to better understand a vehicle’s behavior in a reverse lane change. Section 6.4 will introduce the driver-decision making model designed for the reverse lane change process. Parameter selections and data collections will be discussed in Section 6.5. Based on the present reverse lane change model, a microscopic simulation program will be developed

Reverse lane change simulation

with MATLAB. Several cases will be simulated and discussed in Section 6.6. Finally, conclusions will be provided in Section 6.7.

System specification

Similarly to a conventional multiple-lane change scenario, four vehicles will be involved in a reverse lane change process as illustrated in Fig. 0-2. A reverse lane change subject vehicle (S) plans to make a lane change to the passing section. The lag vehicle (L) in the opposite lane has to share the passing section with vehicle S. To be consistent with a conventional lane change scenario, the lane with incident is named as the current lane and the opposite is named as target lane; the leading vehicles of S and L are Lc and Lt, respectively.

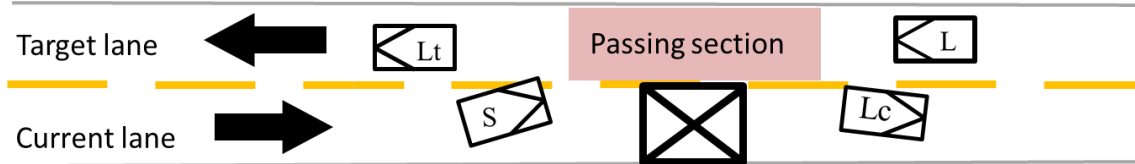


Fig. 0-2 Notations of the vehicles during a reverse lane change

By following the driver decision-based lane change model, the concept of “competition” between vehicle S and L is applied in this reverse lane change scenario to obtain the priority to pass the passing section. The status of leading vehicles Lc and Lt are considered as parameters affecting the interactions between vehicle S and L. In addition, three basic assumptions are proposed to facilitate the reverse lane change process:

- There is no traffic management or instruction nearby the incident position, which means that the behavior of vehicles L and S will be based on their own decisions. The clearance of this traffic regulation is trying to understand and simulate driver’s behavior at the incident location.
- Only one vehicle queue in one direction is allowed to occupy the passing section at a time. The scenario of two vehicles with direct direction drive on the passing section at the same time shown in Fig. 0-3 (a) will not be considered in this study. In Fig. 0-3, the black boxes denote the incident position; the white boxes represent moving vehicles; arrows indicate a vehicle’s driving directions.
- Each vehicle will follow their original order in a reverse lane change, which means that the vehicles’ order in a lane (S following Lc and L follow Lt) will not change. The cases shown in

Reverse lane change simulation

Fig. 0-3 (b) that vehicle A passes its original leading vehicle B during a reverse lane change will not be considered in this simulation.

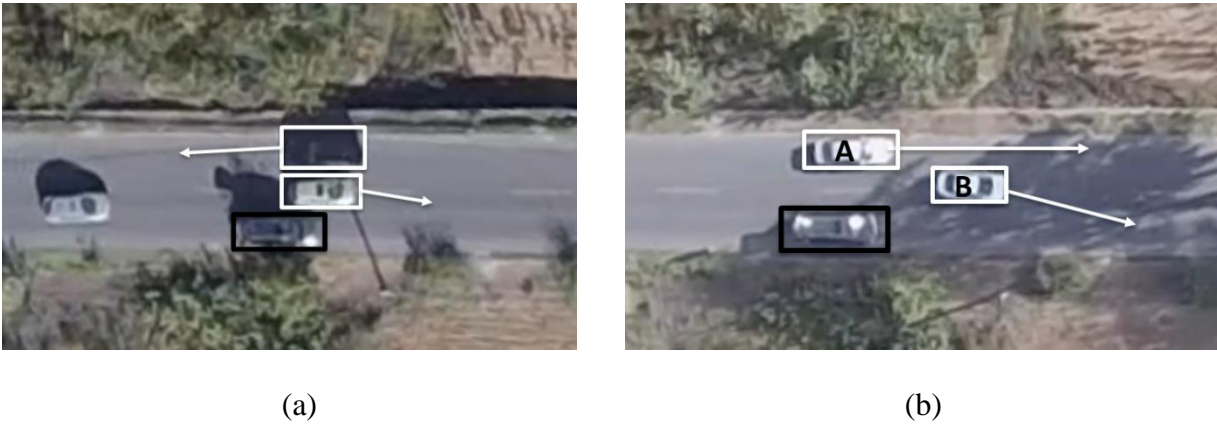


Fig. 0-3 Excluded scenarios in this study. (a) Two vehicles at the “passing section”; and (b) Vehicle order change during a reverse lane change.

Region analysis for Vehicle S and L

In a reverse lane change, the road nearby the incident location can be separated into different regions to fulfill the lane change of vehicle S. In this section, different road regions for vehicle S and L are introduced respectively.

Regions for vehicle S

From the vehicle S’s perspective, the road section near an incident location can be classified into six different regions, including irrelevant region, competition region, wide-view region, dilemma region, passing section and Minimum turning back region. Where vehicle S will perform differently. Fig. 0-4 illustrates such six different regions for vehicle S.

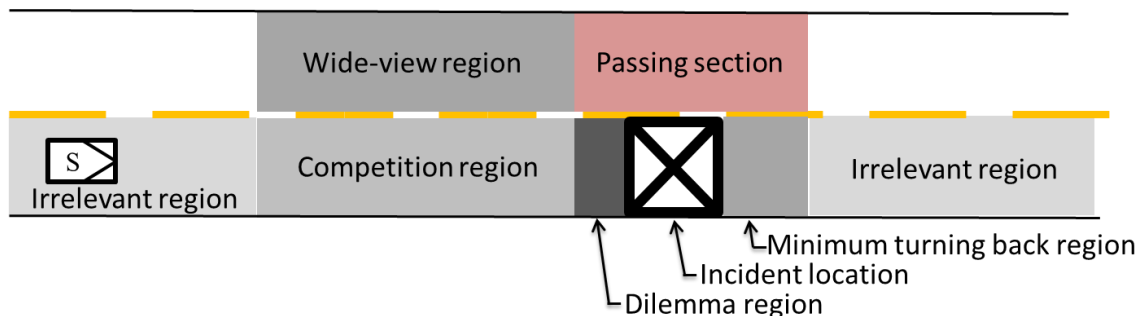


Fig. 0-4 Region analysis for vehicle S

Reverse lane change simulation

Irrelevant region

As shown in Fig. 0-4, there are two irrelevant regions for vehicle S. The first one is located at the upstream of incident location and the second one is at the downstream. Vehicle S will not take any specific actions in these two irrelevant regions. In the upstream irrelevant region, since there is a large gap between vehicle S and the incident location, vehicle S needs a closer distance to confirm the incident location and obtain more detailed information before taking subsequent actions. While in the downstream irrelevant region, after vehicle S passed the incident location and turned back to the current lane, vehicle S completes its lane change process and will not take further actions related to the incident.

Competition region

In the competition region, vehicle S will set the desire points, make priority decisions, take corresponding actions, and judge consensus with vehicle L. The details will be described in Section 6.4.

Wide-view region

As shown in Fig. 0-4, the wide-view region is located in the target lane and next to the competition region. There are two reasons that motivate vehicle S shifting from the competition region to the wide-view region: (1) to obtain a larger view scope. Since only the target lane can be used to pass the incident, vehicle S will try to obtain more traffic information in the target lane. As the driving direction of vehicle S is different from those in the target lane, a much wider view scope will be required for vehicle S than that in a conventional lane change. As shown in Fig. 0-5,, vehicle S will possess a wider view scope on the target lane in the wide-view region than it will have in the competition region; and (2) vehicle S will have more advantage in the priority decision-making. From vehicle S's point of view, shifting from the competition region to the wide-view region is an initial step to obtain the priority to enter the passing section. More detailed descriptions of the corresponding actions in this region will be discussed in Section 6.4.

Reverse lane change simulation

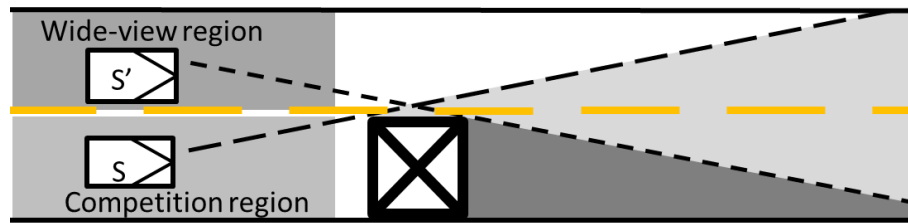


Fig. 0-5 View scope difference between wide-view and competition regions

Dilemma region

As shown in Fig. 0-4, the dilemma region is located between the incident location and the competition region. Generally, vehicle S will not enter into such a region in a reverse lane change for two considerations. Firstly, it will be hard for vehicle S to make a lane change to the passing section if it hits into the dilemma region. Usually, a minimum distance is required for vehicle S to make a smooth lane change. Thus if vehicle S is not able to obtain the priority to enter the passing section, it will stop at the right end of competition region rather than hit into the dilemma region. Secondly, vehicle S will try to maintain a proper distance to the incident location for safety considerations as an incident may involve unexpected dangers.

Passing section

As shown in Fig. 0-4, the passing section is located beside the incident location. In this section, only vehicles in one direction can occupy the passing section at one time, which also means that when one side of vehicle has entered the region, the opposite vehicles have to wait outside of the passing section. The left and right sides of the passing section are determined by the length of dilemma region and the minimum turning back region, respectively.

Minimum turning back region

As shown in Fig. 0-4, the minimum turning back region is located next to the incident location. When vehicle S passed the incident location, it will turn back to the current lane to avoid any collision from the target lane traffic flow. The length of the minimum turning back region depends on the size and its steering system of vehicle S.

Reverse lane change simulation

Regions for vehicle L

Since vehicle L in the target lane has to share the passing section with the vehicles in the current lane, it will consider the interruption from vehicles in the current lane. Based on vehicle L's actions in a reverse lane change process, the road in the target lane can also be separated into different regions corresponding to those in the current lane for vehicle S. According to this definition, vehicle L will continuously pass the irrelevant region, competition region, passing section and irrelevant region in a reverse lane change, which is shown in Fig. 0-6,

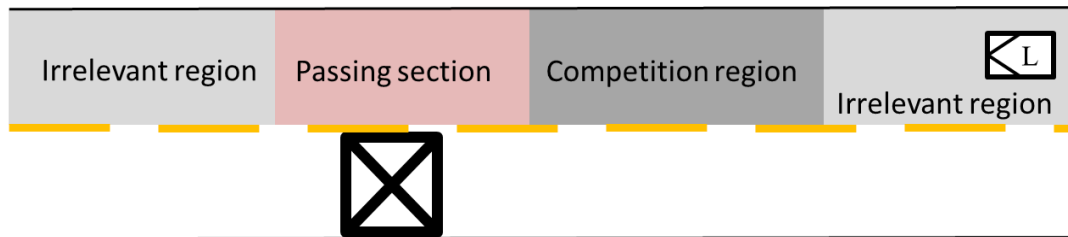


Fig. 0-6 Region analysis for vehicle L

Compared with the different regions that vehicle S needs to drive through in order to pass an incident, there is no turning back region and dilemma region for vehicle L, as it does not need to make a lateral movement. Since vehicle L can easily observe the current lane's information, no wide-view region is necessary for vehicle L either. However, because the passing section is the intersection part for both vehicle S and L, the passing section for L and S is located the same position.

Driver decision-based execution model for a reverse lane change

Both vehicle S and L in their competition region will try to obtain the priority to enter the passing section. Based on the driver decision-based lane change execution model [181], vehicle L and S will also follow the four steps: desire point setting, priority decision-making, corresponding actions and achievement of consensus (Fig. 0-7). Each step has been specifically designed for a reverse lane change scenario.

Reverse lane change simulation

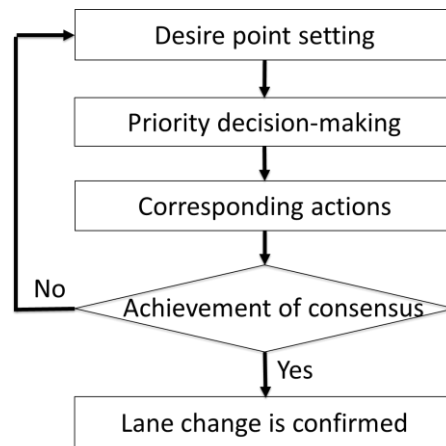


Fig. 0-7 Structure of driver decision-based lane change execution model

Desire point setting

Similar to a desire point in a conventional lane change, the Desire Point (DP) in the reverse lane change is an estimated intersection point that vehicle S and L will drive through to pass the incident. Before arriving at their individual DPs, there is no overlap between vehicles L and S's trajectories. When they arrive at their DPs (may not at the same time), vehicle L and S have to decide that who has the priority to use the overlapped road section. As previously stated, the passing section belongs to an overlapped region. Fig. 0-8 shows that vehicle S and L's DPs are located at the left and right sides of the passing section. To simplify the analysis, it is assumed that vehicle L will not take any lateral movement during a lane change. Thus, the desire point of vehicle L is located in its extend line side boundary. It is assumed that the lateral distance between vehicle S and the desire point is w (Fig. 0-8).

In a reverse lane change process, the positions of DP are affected by vehicle S's speed. At a higher longitudinal speed, vehicle S needs a longer longitudinal distance to finish the two consecutive lane changes. In other words, the distance between vehicle S's DP and the passing section's left edge needs to be longer as vehicle S's speed increases. Similarly, the distance between vehicle L's DP and the passing section's right edge needs to be longer as vehicle S's speed increases (Fig. 0-8).

Reverse lane change simulation

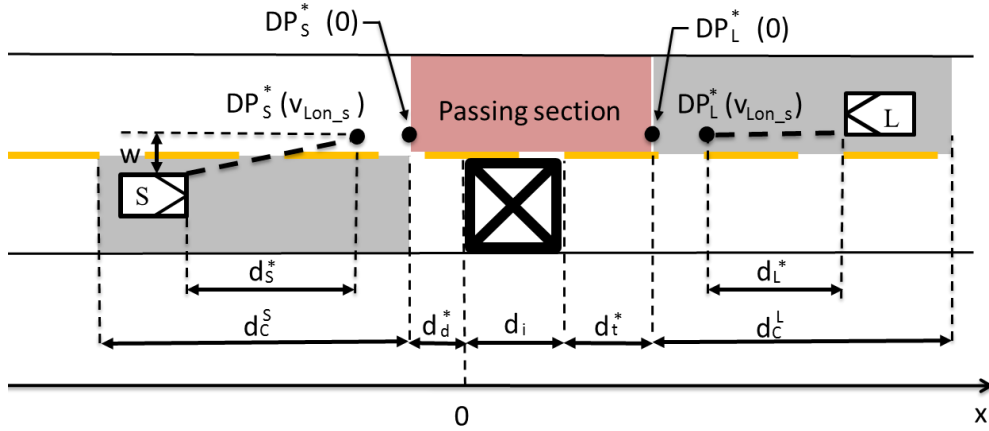


Fig. 0-8 Desire points in a reverse lane change scenario

It is worth noting that DP_S^* is the desire point from vehicle S; $* \in \{L, S\}$ reflects different point of views from different vehicles, i.e., DP_S^L represents the desire point of vehicle S based on vehicle L's decision while DP_S^S represents the desire point of vehicle S based on vehicle S's decision. In the following, all the terms with the superscript $*$ are defined in this way.

Since the passing section is the shortest overlapped region of the routes of vehicle S and L, assuming that when vehicle S's speed is zero, the longitudinal position of the DP_L^* for a vehicle L is located at the right side of the passing section, and the longitudinal position of DP_S^* for vehicle S is located at the left side of the passing section. Thus the longitudinal distance d_S^* between DP_S^* and vehicle S is expressed in Eq. (6.1), and the longitudinal distance d_L^* between DP_L^* and vehicle L is expressed in Eq. (6.2).

$$d_S^* = -x_S - \left(\frac{w}{v_{lat_S}^*} \cdot v_{lon_S} + d_d^* \right) \quad (0.1)$$

$$d_L^* = x_L - \left(\frac{w}{v_{lat_S}^*} \cdot v_{lon_S} + d_t^* \right) - d_i \quad (0.2)$$

where, d_S^* is the longitudinal distance between vehicle S and its DP. x_S is the longitudinal position of vehicle S, w is the lateral distance between vehicle S and its desire point. $v_{lat_S}^*$ is the expected lateral speed of vehicle S. v_{lon_S} is the longitudinal speed of vehicle S, d_d^* is the expected length

Reverse lane change simulation

of dilemma region, d_L^* is the longitudinal distance between vehicle L and its DP. x_L is the longitudinal position of vehicle L, d_t^* is the length of minimum turning back region.

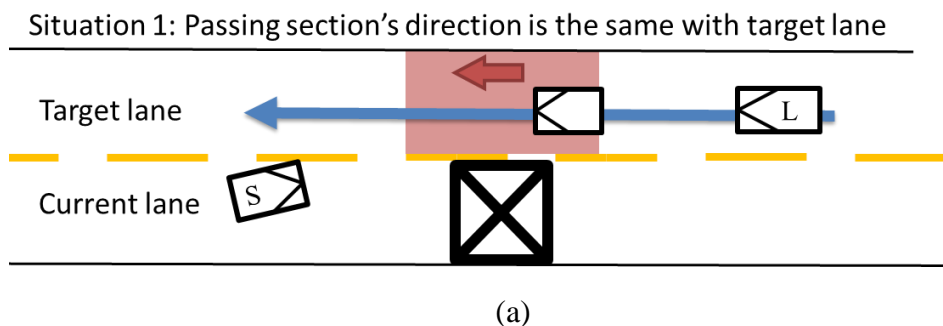
To describe the relationship between vehicle S and DP at the lateral direction, w is defined as negative when vehicle S passed the DP's lateral position; while before vehicle S reaches its DP's lateral position, w is defined as positive.

Priority decision with different passing section directions

After their desire points are determined, both vehicle S and vehicle L need to decide that who will have the priority to firstly arrive at their own desire points and pass the passing section. By introducing the concept of passing section's direction, the reverse lane change is classified into two situations. Correspondingly, two priority decision rules are presented for different directions of the passing section. A special interaction between vehicle S and L is discussed.

Direction of passing section

As only one direction traffic flow is allowed to pass the passing section at one time, the passing section's direction is thus defined as vehicles driving directions, which is illustrated in Fig. 0-9. If the passing section's direction is the same as target lane (Fig. 0-9(a)), vehicle S has to break the current traffic flow before entering the passing section. When the passing section's direction is same with current lane's direction, vehicle L has to break current traffic flow before entering the passing section, but vehicle S just follows its leading vehicle to enter the passing section.



Reverse lane change simulation

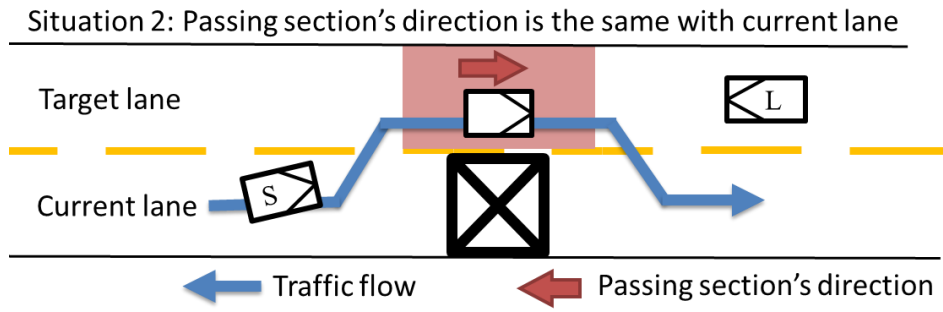


Fig. 0-9 Two situations based on the passing section's direction.

Priority decision criteria

Compared with the conventional lane change, there are two criteria for priority decision. One is designed for the situation that the passing section's direction is the same to the target lane's direction, and the other one is applied for the situation that the passing section's direction is the same with the current lane's direction.

In the first situation (shown in the Fig. 0-9 (a)), the traffic flow in the passing section is from the right to the left in the target lane. In such a case, since vehicle S has to break the original traffic flow in the target lane before entering the passing section, while vehicle L only needs to maintain the original traffic flow and follow its leading vehicle to entering passing section, vehicle L has more advantages than vehicle S in the priority decision. To describe such advantage for vehicle L, a parameter $r1$ is introduced. Accordingly, the priority decision making criterion can be mathematically expressed in Eq. (6.3), where priority decision is 1 means that vehicle L has priority and verse vise.

$$Priority\ decision = \begin{cases} 1 & \frac{r1 \cdot (SELR^* \cdot w + d_S^*)}{v_{lon_S}} \geq \frac{d_L^*}{v_{lon_L}} \\ 0 & otherwise \end{cases} \quad (0.3)$$

where $SELR^*$ is Equivalent Lateral Rate of vehicle S. $r1$ is a parameter representing that the passing section's direction is the same as that in the target lane. w is the lateral distance between vehicle S and its desire point. d_S^* is the longitudinal distance between vehicle S and its desire point.

Reverse lane change simulation

d_L^* is the longitudinal distance between vehicle L and its desire point. v_{lon_S} and v_{lon_L} are longitudinal speed of vehicle S and L respectively.

Similarly, when the direction of pass section is the same as current lane (shown in Fig. 0-9 (b)), the priority decision making criterion can be expressed in Eq. (6.4).

$$Priority\ decision = \begin{cases} 1 & \frac{r2 \cdot (SELR^* \cdot w + d_S^*)}{v_{lon_S}} \geq \frac{d_L^*}{v_{lon_L}} \\ 0 & otherwise \end{cases} \quad (0.4)$$

where $r2$ is a parameter representing that the passing section's direction is the same as that in the current lane.

Notes that $r1$ and $r2$ are two parameters affecting the priority decision during a reverse lane change. From driver S's perspective, a larger value of $r1$ reflects two disadvantages of vehicle S in the priority decision. The first one is that vehicle S does not have the road right on the target lane, and the second one is that vehicle S has to break the original traffic flow. Therefore, when $r1$ is large, vehicle has less chance to obtain the priority to enter the passing section. Similarly, while the parameter $r2$ includes one advantage and one disadvantage in the priority decision. The advantage is that vehicle S only follows its leading vehicle to pass the incident, and doesn't need to break the original traffic flow. The disadvantage is that vehicle S doesn't have the road right on the target lane. When $r2$ is large, vehicle has less chance to obtain the priority to enter the passing section.

Different combination of $r1$ and $r2$ can describe different situations in a reverse lane change process. If a vehicle is sensitive with the passing section's direction, $r1$ will be large and $r2$ will be small, which means that the vehicle has strong wish to keep the original traffic flow and try to avoid to break it, and vise verse.

Corresponding actions

After the priority decisions are determined, vehicle S and vehicle L will take corresponding actions based on their decisions. In this section, the behaviors of vehicle S and vehicle L will be introduced respectively.

Reverse lane change simulation

After a priority decision is made by vehicle S, two different behaviors might exist based on its priority decisions, which are illustrated in Fig. 0-10. The dotted lines indicate vehicle S's considered leading vehicles, and red line indicate a stop sign for vehicle S. As shown in Fig. 0-10, when vehicle S has the priority, it will consider Lc as its leading vehicle, and has the priority to enter the passing section. If vehicle S doesn't have the priority, it will give up the current lane change plan and stop before the red line.

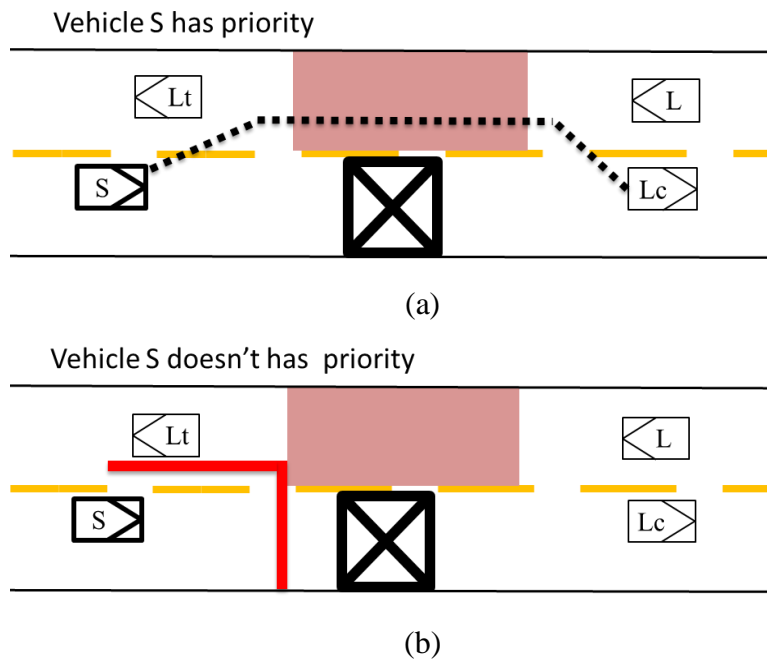
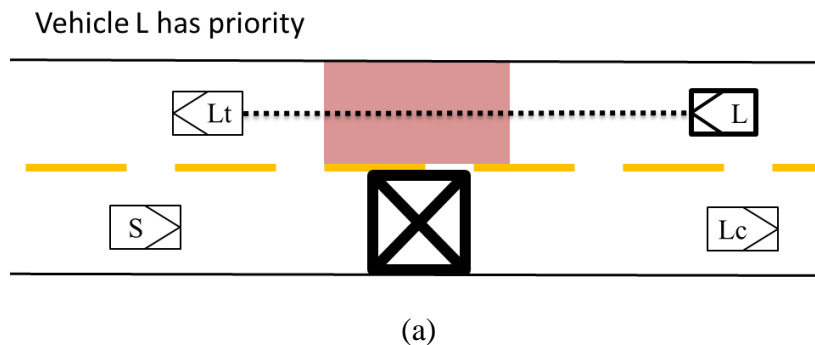


Fig. 0-10 Vehicle S's corresponding behaviors.(a) Vehicle S has priority, (b) Vehicle S doesn't has priority



Reverse lane change simulation

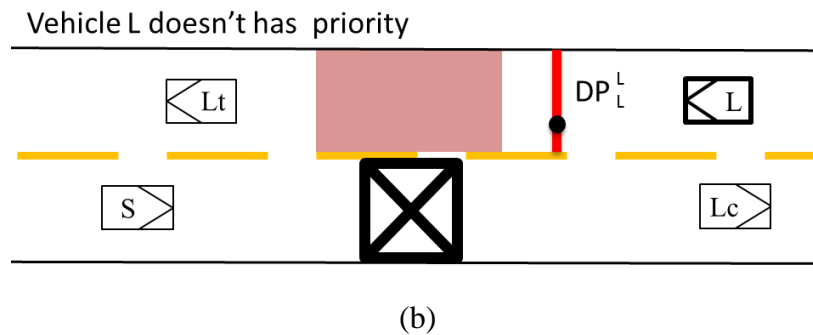


Fig. 0-11 Vehicle L's corresponding behaviors. (a) Vehicle L has priority, (b) Vehicle L doesn't has priority

After a priority decision is made by vehicle L, two different behaviors might exist based on its priority decisions, which are shown in Fig. 0-11. When vehicle L has priority, it will consider Lt as its leading vehicle. While, if vehicle L doesn't have priority, it will plan to stop before the DP_L^L point and wait for another opportunity to enter the passing section.

Achievement of consensus

If two vehicles arrive at certain achievement of consensus, the lane change will be confirmed. If vehicle S and L have a conflicting priority decisions, the lane change will not be confirmed, and the two vehicle have to repeat the previous steps: desire point setting, priority decision-making and corresponding actions subsequently. The consensus and conflicts based on vehicle S and vehicle L's priority decisions are listed in Table 0-1.

Table 0-1 Consentaneous and conflicting situations based on priority decision of vehicle S and L

	Driver S: Vehicle S has priority	Driver S: Vehicle L has priority
Driver L: Vehicle L has priority	Vehicle S and vehicle L have conflicts: they will repeat the procedures, including desire point setting, priority decision and corresponding action in the next time interval.	Vehicle S and vehicle L achieved consensus: Vehicle L will firstly enter the passing section. The lane change is confirmed.

Reverse lane change simulation

Driver L:
Vehicle S
has
priority

Vehicle S and vehicle L achieved consensus: Vehicle S will firstly enter the passing section. The lane change is confirmed

Vehicle S and vehicle L achieved consensus: Vehicle S gives up the lane change. They will repeat the procedures, including desire point setting, priority decision and corresponding action in the next time interval.

Parameter selection and data collection

To describe a driver's behavior in a reverse lane change process, the concepts of competition region, passing section, dilemma region and minimum turning back region have been introduced. A vehicle in different regions might have different behaviors during a reverse lane change process. The critical lengths, including d_c^S , d_d^* , d_t^* and d_c^L (Fig. 0-12), are important in the simulation. If the distance between vehicle S and the incident location is smaller than d_c^S , vehicle S will start to consider the competition with vehicle in the target lane. If the distance between vehicle L and incident location is smaller than d_c^L , vehicle L may start to consider the competition with the current lane vehicle. The values of d_t^* and d_d^* determine the length of passing section, where vehicle S and L will not enter it until a priority is obtained.

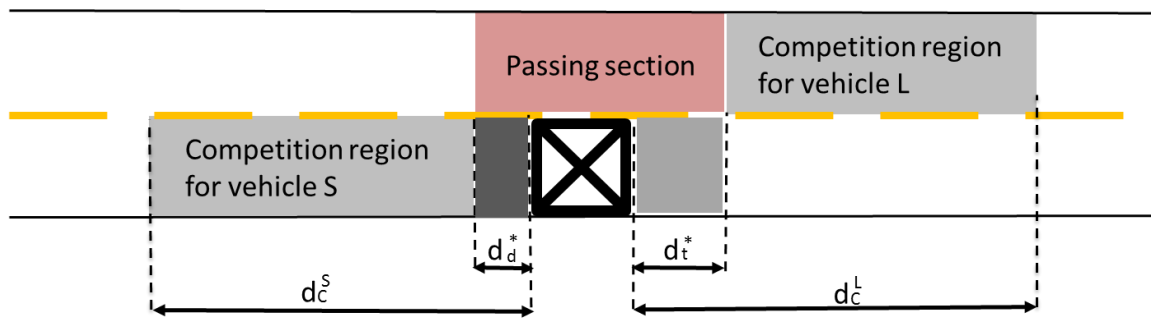


Fig. 0-12 Important parameter in reverse lane change

Parameter selection and approximate approach

It is hard to directly obtain the four critical lengths as they describe a driver's thoughts during a reverse lane change. An approximation of each parameter will be discussed in this section. Firstly, d_c^S is defined as the distance between vehicle S and the incident location that vehicle S firstly notices and starts to compete with vehicle L. Thus, the position that vehicle S makes an observable lateral movement toward target lane is considered as the start point of the competition region (Fig.

Reverse lane change simulation

0-12). To make sure vehicle S obtains the priority, a measurement of d_c^S will be recorded only when there is no vehicle in the target lane.

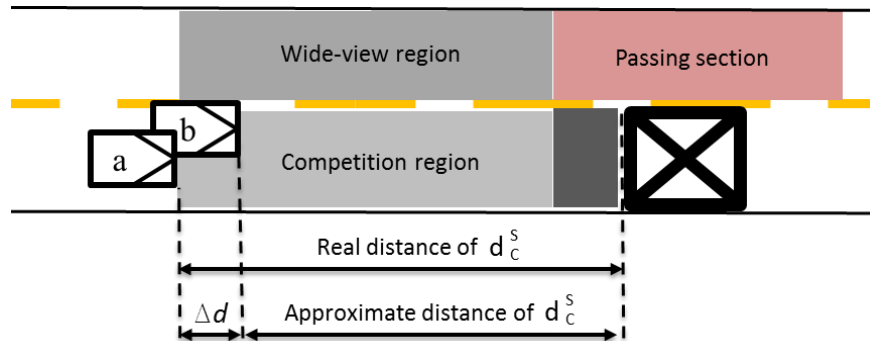


Fig. 0-13. The difference between real position and observable position of d_c^S

The relationship between the real distance and observable approximated distance of d_c^S are shown in Fig. 0-13. Vehicle S arrives at position a at the moment when the driver notices the incident position, it will start to set a desire point and make a priority decision (vehicle S has priority as there is no vehicle on target lane) and move toward the wide-view region. The distance from position a to the incident location is the real distance of d_c^S , however, it is impossible to identify this position in a real traffic. After vehicle S moves to position b , there will be an observable lateral movement of vehicle S. The distance between vehicle S and the incident position is the approximated distance of d_c^S . The gap between the real distance and approximated distance is Δd . Considering that the time from position a to b is short, the distance of Δd can be negligible.

The length of d_c^L is defined as the distance between vehicle L and the incident location that vehicle L firstly notices the incident and starts to compete with a potential vehicle S. Because vehicle L does not make any special observable movement in such process, it is impossible to obtain the length of d_c^L in a field test. The length of d_c^L is assumed to equal to d_c^S . Considering that the value of d_c^S and d_c^L have the same meanings for vehicle S and L, it is reasonable to assume that driver S and L will have similar observation abilities.

The value of d_t^* is the minimum distance with the incident location that vehicle S will not turn back to the current lane, after it passed the incident. In the field test, when vehicle S stopped and waited nearby the incident location for more than 5 seconds, the distance between vehicle S and

Reverse lane change simulation

the incident location is considered as d_t^* . It is reasonable to assume that vehicle S has reached the edge of the dilemma region (it is also the left-edge of the passing section) in such situation.

The value of d_d^* is the smallest gap that vehicle S would turn back to the current lane. In the field test, it was observed that when vehicle S stopped in front of the incident position, and there were waiting vehicles in the target lane, vehicle S were tried to turn back to the current lane as soon as possible. In this case, the distance of turning back position to incident location is considered as d_d^* .

Data collection method

To obtain the approximated values of four parameters, three data collection methods has been designed, including cameras on the top of a vehicle, camera on the top of a building and camera on UAV.

Cameras on the top of a vehicle

Two cameras were fixed on the top of a testing vehicle (Fig. 0-14 (a)), one is to capture vehicle's front image (Fig. 0-14 (b)), and the other is to obtain vehicle's backward images (Fig. 0-14 (c)). During experiments, the testing vehicle stopped on a lane as an incident.

The testing location is Claremont Ave between 116th Street and 119th street, New York City, NY. Test time was 2014-8-8 from 11:00 a. m to 3:00 p.m. The measuring range was 3 m - 45 m in the forward camera and 3 m - 60 m in the backward camera.



Fig. 0-14 Cameras on a top of a vehicle. (a) Testing vehicle, (b) Forward camera image, and

Reverse lane change simulation

(c) Backward camera image

As shown in Fig. 0-14 (b) - (c), the scale is not uniform in the forward and backward camera images. Camera's pitch angle, yaw angle and height will significantly affect the accuracy of measurement. To bridge the point's position in the image and its real position in the road coordination, the inverse perspective mapping (IPM) method is applied.

The IPM method consists of mapping images to a new coordinate system where perspective effects are removed [221,222]. The removal of perspective associated effects facilitates road and obstacle detection and also assists in free space estimation. Such method has been successfully applied to several problems in the field of Intelligent Transportation Systems. The IPM is often used in vision-based road estimation algorithms as a pre-processing component. IPM uses information from the camera's position and orientation towards the road to produce a bird's eye view image where perspective effects are removed. The correction of perspective allows much more efficient and robust road detection, lane marker tracking, or pattern recognition algorithms to be implemented. In reality, IPM has been employed not only with the purpose of detecting the vehicle's position with respect to the road, but also in many other related applications, e.g., obstacle detection [223,224], free space estimation [225], pedestrian detection [226] or ego motion estimation [227].

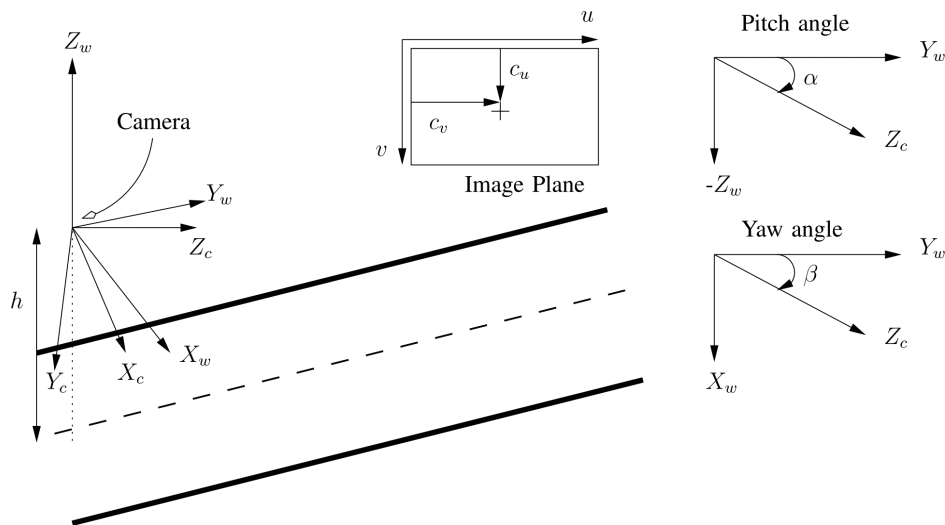


Fig. 0-15 IPM coordinates, Left: the coordinate axes (world, camera, and image frames) right: definition of pitch α and yaw β angles. [228]

Reverse lane change simulation

To get the IPM of the input image, a world frame $\{F_w\} = \{X_w, Y_w, Z_w\}$ centered at the camera optical center, a camera frame $\{F_c\} = \{X_c, Y_c, Z_c\}$ and an image frame $\{F_i\} = \{u, v\}$ are defined, which are shown in Fig. 0-15. The pitch angle and yaw angle between world frame and camera frame are defined as angle α and β respectively. The height of the camera frame above the ground plane is defined as h . Assume point P^w in the world frame and point $P^i = \{u, v, 1, 1\}$ in the image plane describe the same physical point on the road. Based on the homogeneous transformation T , the point P^i in the image frame's corresponding position in the world frame can be obtained by Eq. (0.5) [221,228]

$$p^w = T p^i \quad (0.5)$$

where T is the homogeneous transformation matrix, which can be expressed in Eq. (0.5) [228]

$$T = h \begin{bmatrix} -\frac{1}{f_u} c_2 & \frac{1}{f_v} s_1 s_2 & \frac{1}{f_u} c_u c_2 - \frac{1}{f_v} c_v s_1 s_2 - c_1 s_2 & 0 \\ \frac{1}{f_u} s_2 & \frac{1}{f_v} s_1 c_1 & -\frac{1}{f_u} c_u s_2 - \frac{1}{f_v} c_v s_1 c_2 - c_1 c_2 & 0 \\ 0 & \frac{1}{f_v} c_1 & -\frac{1}{f_v} c_v c_1 + s_1 & 0 \\ 0 & -\frac{1}{h f_v} c_1 & \frac{1}{h f_v} c_v c_1 - \frac{1}{h} s_1 & 0 \end{bmatrix} \quad (0.6)$$

where f_u, f_v are the horizontal and vertical focal length, respectively, c_u, c_v are the coordinates of the optical center in image frame. c_1, c_2, s_1, s_2 are parameters describe the pitch and yaw angles, which are defined as $c_1 = \cos\alpha$, $c_2 = \cos\beta$, $s_1 = \sin\alpha$ and $s_2 = \sin\beta$.

Camera on the top of a building

To get a more uniform scale in measurement, the testing camera was fixed on the 9th floor of a building. To reduce the sample size, the video's frequency is limited to 2 Hz. Each frame is required to be defished (Fig. 0-16(b)) and cropped to a proper region for measurement (Fig. 0-16(c)). During the testing, a vehicle stopped on a lane as an incident (black box in Fig. 0-16(c)). The black horizontal lines are calibrated scalers for measurement

Reverse lane change simulation

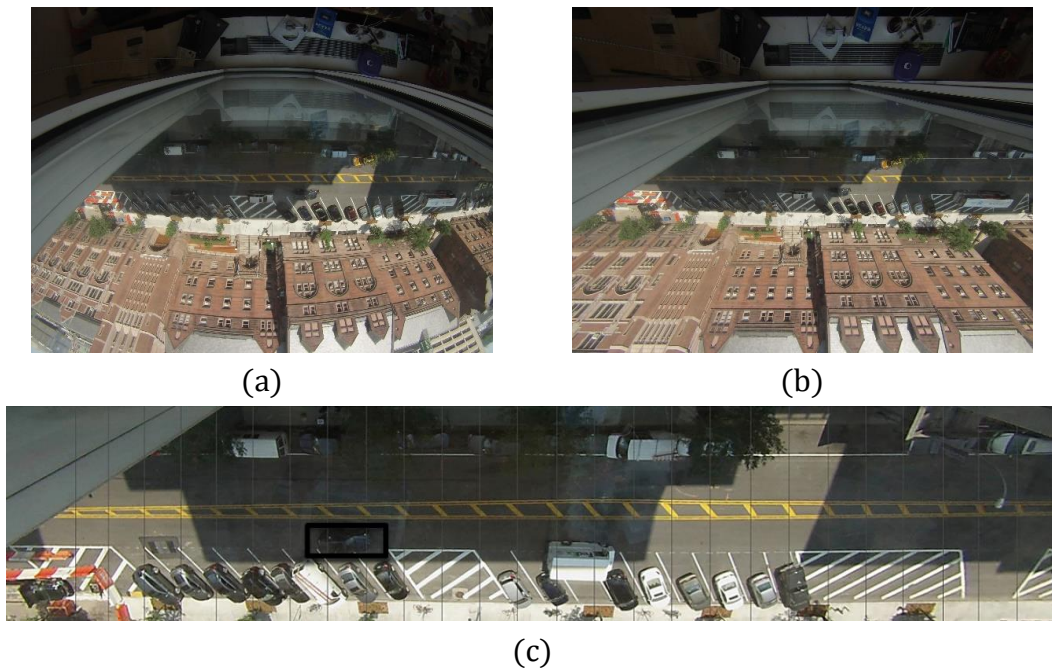


Fig. 0-16 A frame in camera on the top of a building

The testing location is 120th street between Amsterdam and Broadway, New York. The camera is fixed on the 9th floor of Schapiro building. Test time is 2014-7-26 from 11:00 a. m to 3:00 p.m. the measuring range is 85.5 m.

Camera on UAV

To get a larger view scope, a camera was fixed on UAV (Fig. 0-17 (a)). During the test, a vehicle stopped on a lane as an incident (the black box in Fig. 0-17 (c)). For safety considerations, one person was standing at the back of the vehicle during experiment (Fig. 0-17 (b)). To minimize the experimenter's influence in traffic flow, the experimenter is not allowed to make any instruction or communication to the coming vehicles. The detail testing procedures and data analysis can be found in Chapter 4.

Reverse lane change simulation

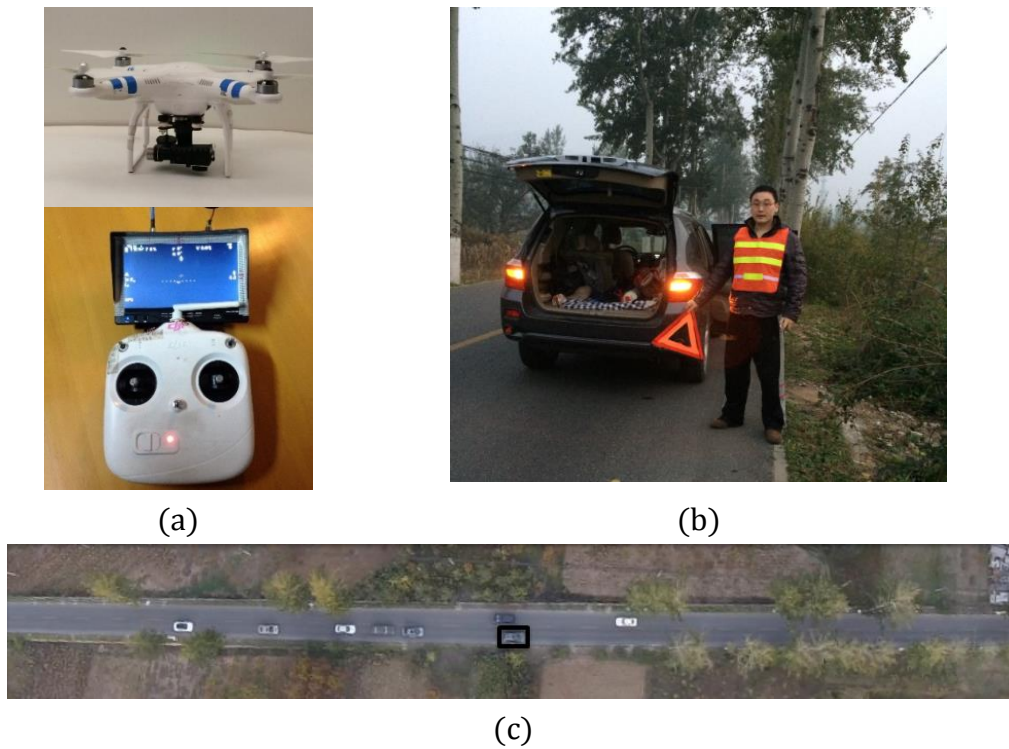


Fig. 0-17 Camera on UAV

The testing location is Ansi road, Jiuduhezhen, Huairou, Beijing. The UAV's altitude was about 300 m. Test time was 2014-10-25 from 11:00 a. m to 5:00 p.m., and 2014-10-26 from 11:00 a. m to 5:00 p.m. The measuring range was about 520 m.

In conclusion, the advantages and disadvantage are shown in Table 0-2. Because the measurement ranges of cameras on the top of the vehicle and that on the top of the building are short, the collected data by these two cameras are mainly applied to determine the value of d_t^* and d_d^* . The test data from UAV can be used in all four parameters' setting. The results of parameters d_c^S , d_d^* , d_t^* and d_c^L are listed in Table 0-3.

Table 0-2 Pros and Cons of the three data collection methods

	PROS	CONS
Cameras on the top of a vehicle	Easy to deploy, high mobility.	This method can't obtain accurate data at far distance with testing vehicle. If the distance is longer than 50 m the error is large.
Camera on the	Uniform scale	The view scope is short, and the

Reverse lane change simulation

top of a building		testing result is limited by the building's position and height.
Camera on UAV	Easy to deploy, high mobility, large view scope, uniform scale	The testing field is limited by the rules and regulations of UAV.

Table 0-3 Parameters based on field tests

	d_c^L and d_c^S	d_a^*	d_t^*
Mean (m)	86.1	5.1	10.6
Variance (m)	15.9	0.5	1.6
Sample size	62	17	27

Simulation results

Based on the reverse lane change model, a microscopic simulation program has been developed with the MATLAB. The structure of the simulation program is shown in Fig. 0-18. This reverse lane change are developed from the driver decision based lane change execution model presented in Chapter 5. To simulate such reverse lane change process, each module has been accordingly modified. The open mechanics-based acceleration model is applied to simulate a vehicle's longitudinal behaviors.

Reverse lane change simulation

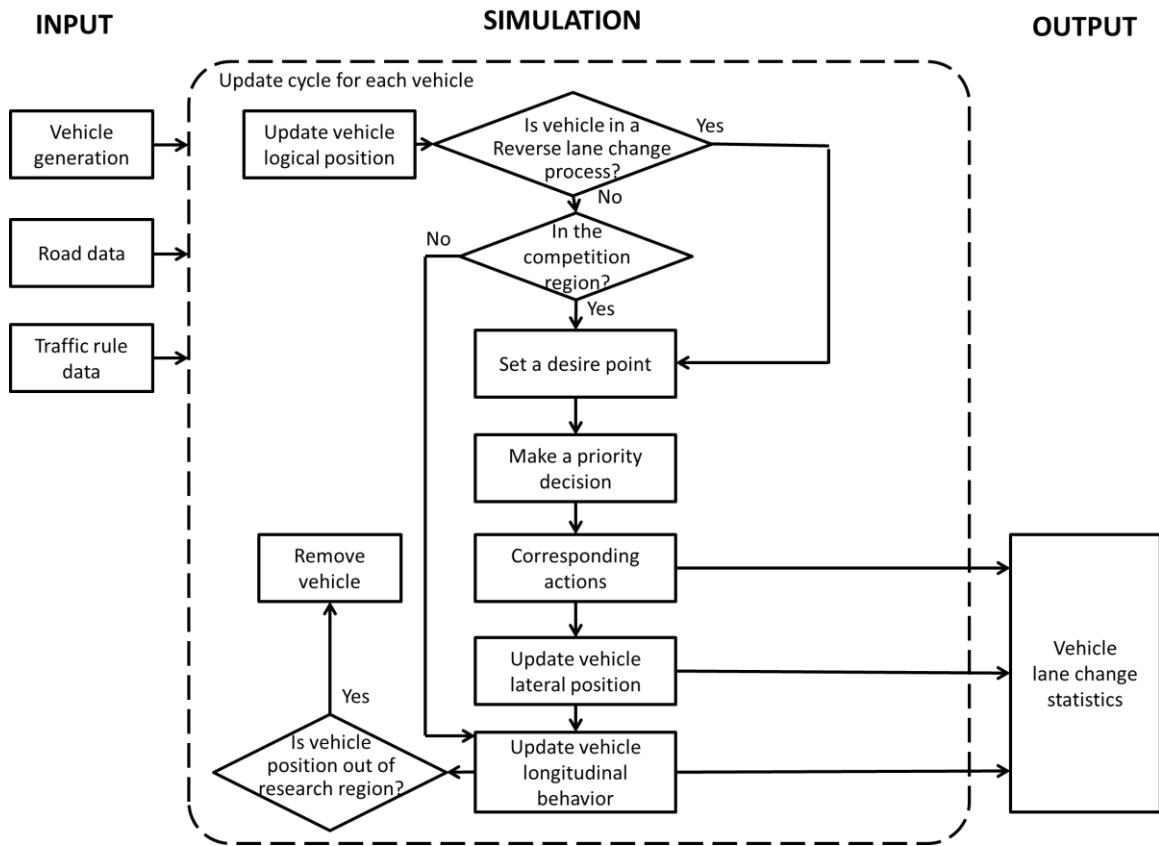


Fig. 0-18 Reverse lane change model structure

The reverse lane change case was designed as: the road section length was 800 m with two-lane-two-way traffic flow and the incident was located at 400 m – 410 m at the bottom lane. A screen shot of the simulation are shown in Fig. 0-19. The red arrow in the middle of the road indicates the passing section's direction. The initial passing section's direction was set as left (the same as target lane's direction). The black box indicates the incident location. The green boxes are vehicles traveling from left to right, and the yellow boxes are vehicle traveling from right to left. Each vehicle's basic parameters are listed in Table 0-4.



Fig. 0-19 A screen shot of simulation

Reverse lane change simulation

Table 0-4 Each vehicle's static parameters

Category	Parameter	Description	Value in experiment
Vehicle size	s	Vehicle length	N(6.5,0.3)
	ss	Vehicle width	2
Driver's lane change parameters	v_{lat}^S	Driver's lateral speed	N(1.5,0.1)
	d_{lon}	The estimated maximum deceleration for other vehicle	N(-1.5,0.1)
	SELR	Equivalent lateral rate for vehicle S	N(3,0.1)
Driver's longitudinal behavior's parameters	v_0	Optimal speed	N(10,1)
	α	Subject vehicle's speed	N(0.20,0.01)
	β	Acceleration sensitivity	N(1.25,0.1)
	γ	Gap reduce desire	N(0.1,0.01)
	δ	Safety consideration	N(60,5)
Reverse lane change parameters	ε	Relative speed sensitivity	N(0.3,0.03)
	d_c^S	Shown in Fig. 0-12	86.1
	d_d^*	Shown in Fig. 0-12	5.1
	d_t^*	Shown in Fig. 0-12	10.6
	d_c^L	Shown in Fig. 0-12	86.1

Simulation result with different r1 and r2

As previously stated, two proposed parameters $r1$ and $r2$ are introduced in the driver's priority decision to describe the scenarios of different passing section's directions. Different combinations of $r1$ and $r2$ can describe different effects of the passing section's directions, such as strong effect ($r1=5, r2=0.2$), weak effect ($r1=2, r2=1$), and non-effect ($r1=1, r2=1$). Based on the different effects of the passing section's direction, three groups of $r1$ and $r2$ are simulated respectively. The generation gap for current lane and target lane are 100 m, simulation time is 600 seconds. The simulation results are listed in Table 0-5, where the notation "CL/TL" means that the first number is the current lane's simulation result, and the second number is the target lane's simulation result; "TCT" means the total direction change number of the passing section.

Reverse lane change simulation

Table 0-5 Simulation result for different r1 and r2

	Traffic flow *CL/TL (vehicle / 10 mins)	Passing section's direction distribution rate *CL/TL/TCT	Average traveling time *CL/TL (second)
Strong effect (r1=5,r2=0.2)	44/46	0.48/0.52/12	118/110
Week effect (r1=2,r2=1)	39/38	0.52/0.48/24	115/105
Non-effect (r1=1,r2=1)	28/31	0.46/0.54/51	159/157

*CL: Current lane; TL: Target lane; TCT: Total number of passing section's direction change

As shown in Table 0-5, the strong effect result has the highest traffic flow 44/46 and the passing section's direction change number is only 12, which means that more vehicles are able to pass the passing section at one time as a queue. While the non-effect result has the lowest traffic flow 28/31 and the passing section's direction change number is 51, as a result less vehicles can pass the incident at one time as a queue.

Since the non-effect simulation has a long waiting queue at each lane, the average traveling time is much longer than that in the other two simulations. In the strong effect simulation, vehicles have to wait for a long queue to pass the incident location, therefore, the average traveling time is a little more than that in the week effect simulation result.

In conclusion, the strong effect simulation reflects the scenario that traffic flow under traffic instruction. Normally, reducing the frequency of the passing section's direction changing is an effective way to increase the traffic flow on an incident location [229–231]. The simulation of week effect is close to a normal unmanaged traffic situation in a reverse lane change situation.

Simulation result with different generation gaps

To investigate the influence of traffic situations on the target and current lanes in a reverse lane change scenario without instructions, different traffic situation at the current and target lanes are simulated. The generation gap is used to simulate different traffic situations. If the gap is larger than the predefined generation gap at each lane, a new vehicle will be generated. By adjusting the values of generation gap, different traffic conditions can be simulated. Parameters r1 and r2 are

Reverse lane change simulation

selected as week effect (r1=2, r2=1) and the simulation results are summarized in Table 6-6, 6-7 and 6-8.

Table 0-6 Traffic flow at different traffic situation

Traffic flow CL/TL (vehicle / 10 mins)		Generation gap at the target lane (m)			
		50	100	150	200
Generation gap at the current lane (m)	50	24/47	39/41	51/26	57/22
	100	21/59	39/38	42/39	42/23
	150	21/57	28/42	28/29	29/23
	200	15/65	23/42	22/30	23/23

Table 0-7 Passing section's direction at different traffic situation

Passing section's direction distribution rate CL/TL/TCT		Generation gap at the target lane (m)			
		50	100	150	200
Generation gap at the current lane (m)	50	0.39/0.61/45	0.55/0.45/33	0.65/0.34/17	0.70/0.30/16
	100	0.36/0.64/33	0.52/0.47/24	0.58/0.42/27	0.63/0.37/28
	150	0.38/0.62/35	0.47/0.53/27	0.50/0.50/31	0.54/0.45/35
	200	0.29/0.71/19	0.42/0.58/25	0.44/0.56/28	0.55/0.45/33

Table 0-8 Average traveling time at different traffic situation

Average traveling time CL/TL (second)		Generation gap at the target lane (m)			
		50	100	150	200
Generation gap at the current lane (m)	50	243/177	207/112	164/113	146/118
	100	201/146	118/110	112/99	98/96
	150	168/145	128/96	123/93	93/89
	200	134/107	102/92	100/89	95/88

The simulation results shown in Tables 6-6 to 6-8 indicate that 1) traffic flow generally increases as the traffic increase. The maximum traffic flow at the current lane is 57 (vehicle/10

Reverse lane change simulation

mins), which happens at the group of generation gap is 50 m at the current lane and 200 m at the target lane (noted as 50/200). The maximum traffic flow at the target lane is 65 (vehicle/10 mins) at 200/50. The maximum traffic flow for both sides is 81(vehicle/10 mins) at 100/150; and 2) the average traveling time increases, when the number of vehicles increase on the other lane. It is worth noting that the current lane's average traveling time is more sensitive with the traffic situation changes the traffic flow on the target lane. Because the vehicles in the current lane need to make a reverse lane change to pass the incident location, they should take more responsibilities and consider more about the traffic situation. In that sense, such phenomenon is reasonable in real traffic situation.

Conclusions

Based on the presented open mechanics-based acceleration model and the driver decision-based lane change execution model, a reverse lane change model has been developed in this chapter to simulate some complex traffic situations such as reverse lane change process at a two-way-two-lane road section where one lane is blocked by a traffic incident. In this model, the road around the incident location is divided into different regions for vehicle S and L respectively, and each vehicle will take different behaviors in the different regions. By introducing the passing section's direction, the reverse lane change model is classified into two scenarios. By introducing the parameters r_1 and r_2 , two priority decision-making criteria are correspondingly offered. Different values of r_1 and r_2 are able to describe driver's different feeling to the passing section's directions. To calibrate the model parameters, three data collection methods and approximate approaches are designed. Subsequently, a microscopic simulation program has been developed to demonstrate and validate the present model. Driver's different effects on the passing section's directions are simulated. In addition, different traffic situations have also been considered, the simulation results show that the present model is able to reflect the real driver behaviors and corresponding traffic phenomenon during a reverse lane change process.

Conclusions and Future Work

This chapter summarizes the main research activities and contributions from the present dissertation and envisions the future research direction based on our current research works as well.

Research summary

The structure and main features of the Open-Mode Integrated Transportation System (OMITS) are presented, which aims to improve the traffic condition of roadways by increasing the ridership of vehicles and optimizing transportation modes through smart services that integrate emerging information communication technologies, big data management, social networking, and transportation management. A carpooling based OMITS prototype has been developed and tested in New York City. It can provide optimized ridesharing and transit services based on spontaneous transportation demands and service availabilities. To form friendly and trustable ridesharing groups, a social network is designed for the OMITS.

In the subject of microscopic traffic simulation researches, four main areas have been discussed. The presented UAV-based vehicle trajectory data collection and vehicle detection algorithm is an application of computer vision in the transportation field. Inspired by the similarity between vehicle interactions and particle interactions, the open mechanics-based acceleration model is developed. The proposed driver decision-based lane change execution model is based on the psychology and decision-making behavior of each driver during the lane change process. Also the reverse lane change model is an application of the developed acceleration and lane change execution models. It demonstrates a unique capability that is currently lacking in the literature, specifically its ability to simulate certain complex traffic situations such as the reverse lane change

Conclusions and Future Work

process at a two-way-two-lane road section where one lane is blocked by a traffic incident. The discussed four parts of the work constitute a representative microscopic simulation research scope.

Conclusions

The main structure of the Open-Mode Integrated Transportation System is presented. This work provides a proposed method to improve the traffic condition of roadways and to optimize transportation modes. The main contributions include:

- The vehicles, riders, and roadways are connected through GPS, mobile communication, Internet, and social networking as a next-generation information infrastructure.
- A carpooling based OMITS application has been developed, which can provide an optimized ridesharing and transit service based on spontaneous transportation demands and service availabilities.
- In order to construct a friendly and trustable ridesharing environment, a social network is designed and integrated into the OMITS.

An accurate and robust vehicle trajectory data collection method based on UAV's image data has been presented, which advances microscopic simulation models by overcoming the obstacle of the availability of trajectory data. Compared with traditional methods, the contributions of the presented UAV-based vehicle trajectory data collection method include:

- Three image features, including edge, optical flow and local feature point, work jointly in this method to detect and track vehicles in a UAV's video. Compared with traditional single image feature methods, the presented method considerably improves the recognition accuracy and the system robustness.
- This method is specifically designed for vehicle detection and tracking. Based on the analysis of road, traffic flow and driver behavior characteristics, some adjustments, such as transforming the image's color form into HSV to obtain road features, extracting longitudinal direction feature of optical flow for vehicle detection, vehicle shape detection region and checking vehicle speed based on the Gipps acceleration model have been introduced in the model to further improve efficiency and accuracy.
- The collection of vehicle trajectory data based on the present method shows that a considerable

Conclusions and Future Work

improvement in the detecting accuracy has been reached. Three road section lengths 190 m, 228 m and 285 m, are studied. All the test results are reliable, with the vehicle detection error lower than 3.9% and vehicle tracking error lower than 2.1%.

A novel open mechanics-based acceleration model has been presented to simulate longitudinal motion. Compared with traditional acceleration methods, the contributions of the present open mechanics-based acceleration model include:

- A mechanical system with force elements is introduced to quantify the vehicle's motion. Based on Newton's second law of motion, the subject vehicle's governing equation of longitudinal behavior is derived in this open mechanics-based acceleration model.
- Five general factors are taken into account, including the subject vehicle's speed, acceleration sensitivity, safety consideration, relative speed sensitivity, and gap reducing desire. These factors can describe the driver's preferences and interactions between vehicles, and each of them can function as a trigger to change vehicle's behaviors.
- The open mechanics-based acceleration modeling method is general and is open to any new factors, which can be added into the model as a force element.
- The presented model is adapted with both single lane and multilane car following scenarios.
- Model parameters can be calibrated based on a special designed individual vehicle data collection system, including LIDAR rangefinder, video camera and ECU data collection.
- The parameter calibration of the presented model is based on the vehicle's dynamical behaviors, as a result, the model can accurately capture a driver's dynamical driving behavior in car following scenarios.

A driver decision-based lane change execution model has been developed to describe a vehicle's lane change execution process, which fills the gap of lane change execution behavior analysis in microscopic traffic simulation. The main contributions of the model include:

- The proposed lane change execution model is based on the driver's decision. Each driver's lane change execution process is based on the driver's personal criteria and judgments. The decision-making process is refined as four main steps: setting desire point, priority decision-making, corresponding actions and achievement of consensus.

Conclusions and Future Work

- The lateral dimension is considered in the proposed lane change execution model. By introducing the concept of “feeling distance”, vehicle’s lateral and longitudinal positions are both considered into the presented lane change execution model.
- The present lane change execution model can simulate the dynamical lane change execution process in real situations.
- A more reasonable simulation and interpretation of the MLC and DLC are fulfilled.

Based on the presented open mechanics-based acceleration model and the driver decision-based lane change execution model, a reverse lane change model has been developed to study a reverse lane change process at a two-way-two-lane road section where one lane is blocked by a traffic incident. The main contributions of the model include:

- The reverse lane change situation has been, for the first time in the literature, simulated at microscopic level.
- Drivers’ decision making and corresponding vehicles’ behaviors in a reverse lane change process have been analyzed.
- Two passing section’s impact factors have been introduced to describe driver’s different decision making criteria for different situations in a reverse lane change.

Future work

After the OMITS system was proposed in 2009, we have conducted tremendous research to form the simulation, operation, and data management framework. This dissertation has documented the early stage research of this project. However, it is far from the intended end-results of our OMITS system to be used in metropolitan areas. Certainly, more exciting studies could be further explored beyond the scope of this dissertation in the near future as follows:

- Multiple-UAVs system will enhance advance the accuracy and efficiency of data collection and vehicle detection and tracking. In macroscopic transportation analysis, longer road sections, say 5 km, are required. However it is hard to extend the observation scope by increasing a UAV’s altitude while keeping enough resolution for each vehicle. In order to extend the observation scope, multiple-UAVs systems could be applied.
- Infrared wave band cameras can be considered in the UAV-based data collection. The infrared waveband camera might be an alternative way to address the shadow problem, where each

Conclusions and Future Work

vehicle can be detected and tracked by extracting the engine's heat.

- The existing acceleration models can be expanded to a multi-following model. Driver's acceleration behavior is not only affected by its directly leading vehicle, but also influenced by its multi-following vehicles ahead. In this sense, more factors such as interactions between the subject vehicle and multiple leading vehicles shall be considered.
- Vehicle acceleration behavior is a very complex analysis, more impact factors need to be considered. Much research has been conducted in psychology to analyze a driver's behaviors in his/her personal character, for example driver's age, genders, states, temper and perception. Such research results can be integrated in the acceleration model, to accurately reflect the real traffic situations.
- Besides the lateral and longitudinal distances, many factors may influence a driver's feeling of distance, such as lane markings, vehicle size and view scope, etc. which can be analyzed in the future. To better simulate the lane change process, more impact factors need to be considered in the feeling distance.
- The proposed microscopic traffic simulation models have the potential to be extended to driverless technologies and autonomous vehicles. Since driver behavior models are able to capture most details of human driving at the microscopic level, they may also give reasonable human-like instructions based on the road information observed by the sensors. However, to fulfill the function of driverless technologies and autonomous vehicles, extensive relevant research and technologies such as road sensors and vehicle control system are required.

Bibliography

- [1] Kumar, P., Singh, V., and Reddy, D., 2005, “Advanced traveler information system for Hyderabad City,” *Intelligent Transportation Systems, IEEE Transactions on*, **6**(1), pp. 26–37.
- [2] Si, B., Yan, X., Sun, H., Yang, X., and Gao, Z., 2012, “Travel Demand-Based Assignment Model for Multimodal and Multiuser Transportation System,” *J. Appl. Math.*, p. 592104.
- [3] Bielli, M., Boulmakoul, A., and Mouncif, H., 2006, “Object modeling and path computation for multimodal travel systems,” *European Journal of Operational Research*, **175**(3), pp. 1705–1730.
- [4] Mahmassani, H. S., and Liu, Y. H., 1999, “Dynamics of commuting decision behaviour under advanced traveller information systems,” *Transp. Res. Pt. C-Emerg. Technol.*, **7**(2-3), pp. 91–107.
- [5] Engelbrecht, J., Booysen, M. J., van Rooyen, G.-J., and Bruwer, F. J., 2015, “Survey of smartphone-based sensing in vehicles for intelligent transportation system applications,” *IET Intell. Transp. Syst.*, **9**(10), pp. 924–935.
- [6] Toledo, T., 2007, “Driving Behaviour: Models and Challenges,” *Transport Reviews*, **27**(1), pp. 65–84.
- [7] Toledo, T., Koutsopoulos, H. N., and Ben-Akiva, M. E., 2003, “Modeling integrated lane-changing behavior,” *Transportation Network Modeling 2003: Planning and Administration*, Transportation Research Board Natl Research Council, Washington, pp. 30–38.
- [8] Ben-Akiva, M., Bierlaire, M., Koutsopoulos, H., and Mishalani, R., 1998, “DynaMIT: a simulation-based system for traffic prediction,” Citeseer.
- [9] Hounsell, N., Shrestha, B., Piao, J., and McDonald, M., 2009, “Review of urban traffic management and the impacts of new vehicle technologies,” *Intelligent Transport Systems, IET*, **3**(4), pp. 419–428.

Bibliography

- [10] Rahman, M., Chowdhury, M., Xie, Y., and He, Y., 2013, "Review of Microscopic Lane-Changing Models and Future Research Opportunities," *IEEE Transactions on Intelligent Transportation Systems*, **14**(4), pp. 1942–1956.
- [11] Moridpour, S., Sarvi, M., and Rose, G., 2010, "Lane changing models: a critical review," *Transp. Lett.*, **2**(3), pp. 157–173.
- [12] Zarco-Tejada, P. J., González-Dugo, V., and Berni, J. A. J., 2012, "Fluorescence, temperature and narrow-band indices acquired from a UAV platform for water stress detection using a micro-hyperspectral imager and a thermal camera," *Remote Sensing of Environment*, **117**, pp. 322–337.
- [13] Watts, A. C., Ambrosia, V. G., and Hinkley, E. A., 2012, "Unmanned Aircraft Systems in Remote Sensing and Scientific Research: Classification and Considerations of Use," *Remote Sensing*, **4**(6), pp. 1671–1692.
- [14] Herwitz, S. R., Johnson, L. F., Dunagan, S. E., Higgins, R. G., Sullivan, D. V., Zheng, J., Lobitz, B. M., Leung, J. G., Gallmeyer, B. A., Aoyagi, M., Slye, R. E., and Brass, J. A., 2004, "Imaging from an unmanned aerial vehicle: agricultural surveillance and decision support," *Computers and Electronics in Agriculture*, **44**(1), pp. 49–61.
- [15] Merino, L., Caballero, F., Martínez-de Dios, J. r., Ferruz, J., and Ollero, A., 2006, "A cooperative perception system for multiple UAVs: Application to automatic detection of forest fires," *J. Field Robotics*, **23**(3-4), pp. 165–184.
- [16] Rodriguez-Canosa, G. R., Thomas, S., del Cerro, J., Barrientos, A., and MacDonald, B., 2012, "A Real-Time Method to Detect and Track Moving Objects (DATMO) from Unmanned Aerial Vehicles (UAVs) Using a Single Camera," *Remote Sens.*, **4**(4), pp. 1090–1111.
- [17] Peng, K., Cai, G., Chen, B. M., Dong, M., Lum, K. Y., and Lee, T. H., 2009, "Design and implementation of an autonomous flight control law for a UAV helicopter," *Automatica*, **45**(10), pp. 2333–2338.

Bibliography

- [18] Du, R., Peng, Z., and Lu, Q., 2012, “Comparison of SMS Calculation Methods Based on NGSIM data for UAV Detection,” 2012 4th International Conference on Intelligent Human-Machine Systems and Cybernetics (ihmsc), Vol 2, IEEE, New York, pp. 112–115.
- [19] Toledo, T., Koutsopoulos, H. N., and Ben-Akiva, M., 2009, “Estimation of an integrated driving behavior model,” *Transportation Research Part C: Emerging Technologies*, **17**(4), pp. 365–380.
- [20] Tang, T.-Q., He, J., Yang, S.-C., and Shang, H.-Y., 2014, “A car-following model accounting for the driver’s attribution,” *Physica A*, **413**, pp. 583–591.
- [21] Hamdar, D. S., 2012, “Driver Behavior Modeling,” *Handbook of Intelligent Vehicles*, A. Eskandarian, ed., Springer London, pp. 537–558.
- [22] Toledo, T., 2007, “Driving Behaviour: Models and Challenges,” *Transport Reviews*, **27**(1), pp. 65–84.
- [23] Adler, J. L., and Blue, V. J., 1998, “Toward the design of intelligent traveler information systems,” *Transportation Research Part C: Emerging Technologies*, **6**(3), pp. 157–172.
- [24] Shekhar, S., Kohli, A., and Coyle, M., 1993, “Path computation algorithms for advanced traveller information system (ATIS),” *IEEE*, pp. 31–39.
- [25] Kramers, A., 2014, “Designing next generation multimodal traveler information systems to support sustainability-oriented decisions,” *Environmental Modelling & Software*, **56**, pp. 83–93.
- [26] Rilett, L., Blumentritt, C., and Fu, L., 1994, “Minimum path algorithms for in-vehicle route guidance systems.”
- [27] Scott, K., Pabón-Jiménez, G., and Bernstein, D., 1997, “Finding alternatives to the best path.”

Bibliography

- [28] Rehl, K., Bruntsch, S., and Mentz, H.-J., 2007, "Assisting Multimodal Travelers: Design and Prototypical Implementation of a Personal Travel Companion," *IEEE Transactions on Intelligent Transportation Systems*, **8**(1), pp. 31–42.
- [29] Kanistras, K., Martins, G., Rutherford, M. J., and Valavanis, K. P., 2013, "A survey of unmanned aerial vehicles (UAVs) for traffic monitoring," *2013 International Conference on Unmanned Aircraft Systems (ICUAS)*, pp. 221–234.
- [30] Xu, J., Wang, G., and Sun, F., 2013, "A novel method for detecting and tracking vehicles in traffic-image sequence," p. 88782P–88782P–4.
- [31] Farnebäck, G., and Nordberg, K., 2002, "Motion Detection in the WITAS Project," pp. 99–102.
- [32] Lingua, A., Marenchino, D., and Nex, F., 2009, "Performance Analysis of the SIFT Operator for Automatic Feature Extraction and Matching in Photogrammetric Applications," *Sensors* (14248220), **9**(5), pp. 3745–3766.
- [33] Zhao, T., and Nevatia, R., 2003, "Car detection in low resolution aerial images," *Image and Vision Computing*, **21**(8), pp. 693–703.
- [34] Kaaniche, K., Champion, B., Pegard, C., and Vasseur, P., 2005, "A Vision Algorithm for Dynamic Detection of Moving Vehicles with a UAV," *Proceedings of the 2005 IEEE International Conference on Robotics and Automation, 2005. ICRA 2005*, pp. 1878–1883.
- [35] Kim, Z., and Malik, J., 2003, "Fast vehicle detection with probabilistic feature grouping and its application to vehicle tracking," *Ninth IEEE International Conference on Computer Vision, 2003. Proceedings*, pp. 524–531 vol.1.
- [36] Gleason, J., Nefian, A. V., Bouysounousse, X., Fong, T., and Bebis, G., 2011, "Vehicle Detection from Aerial Imagery," *2011 IEEE International Conference on Robotics and Automation (icra)*, pp. 2065–2070.

Bibliography

- [37] Leitloff, J., Hinz, S., and Stilla, U., 2010, "Vehicle Detection in Very High Resolution Satellite Images of City Areas," *IEEE Transactions on Geoscience and Remote Sensing*, **48**(7), pp. 2795–2806.
- [38] Tuermer, S., Kurz, F., Reinartz, P., and Stilla, U., 2013, "Airborne Vehicle Detection in Dense Urban Areas Using HoG Features and Disparity Maps," *IEEE Journal of Selected Topics in Applied Earth Observations and Remote Sensing*, **6**(6), pp. 2327–2337.
- [39] Leitloff, J., Rosenbaum, D., Kurz, F., Meynberg, O., and Reinartz, P., 2014, "An Operational System for Estimating Road Traffic Information from Aerial Images," *Remote Sensing*, **6**(11), pp. 11315–11341.
- [40] Cao, X., Lan, J., Yan, P., and Li, X., 2011, "Vehicle detection and tracking in airborne videos by multi-motion layer analysis," *Machine Vision and Applications*, **23**(5), pp. 921–935.
- [41] Cao, X., Wu, C., Yan, P., and Li, X., 2011, "Linear SVM classification using boosting HOG features for vehicle detection in low-altitude airborne videos," 2011 18th IEEE International Conference on Image Processing (ICIP), pp. 2421–2424.
- [42] Heintz, F., Rudol, P., and Doherty, P., 2007, *From images to traffic behavior - A UAV tracking and monitoring application*, IEEE, New York.
- [43] Liu, F., Liu, X., Luo, P., Yang, Y., and Shi, D., 2012, "A New Method Used in Moving Vehicle Information Acquisition from Aerial Surveillance with a UAV," *Advances on Digital Television and Wireless Multimedia Communications*, W. Zhang, X. Yang, Z. Xu, P. An, Q. Liu, and Y. Lu, eds., Springer Berlin Heidelberg, pp. 67–72.
- [44] Zhang, L., Wang, H., and Li, L., 2014, "Vehicle Detection and Tracking in Video from Moving Airborne Platform," *Journal of Computational Information Systems*, **10**(12), pp. 4965–4972.
- [45] Ren, W., and Beard, R. W., 2004, "Trajectory tracking for unmanned air vehicles with velocity and heading rate constraints," *IEEE Transactions on Control Systems Technology*, **12**(5), pp. 706–716.

Bibliography

- [46] Rosenbaum, D., Kurz, F., Thomas, U., Suri, S., and Reinartz, P., 2008, "Towards automatic near real-time traffic monitoring with an airborne wide angle camera system," *Eur. Transp. Res. Rev.*, **1**(1), pp. 11–21.
- [47] Coifman, B., McCord, M., Mishalani, R. G., Iswalt, M., and Ji, Y., 2006, "Roadway traffic monitoring from an unmanned aerial vehicle," *Intelligent Transport Systems, IEE Proceedings*, **153**(1), pp. 11–20.
- [48] Donaldormack, M., Edward, and Ted, T., 2008, *The use of small unmanned aircraft by the Washington State Department of Transportation*, Washington State Department of Transportation.
- [49] Nejadasl, F. K., and Lindenbergh, R., 2014, "Sequential and Automatic Image-Sequence Registration of Road Areas Monitored from a Hovering Helicopter," *Sensors*, **14**(9), pp. 16630–16650.
- [50] Saifuzzaman, M., and Zheng, Z., 2014, "Incorporating human-factors in car-following models: A review of recent developments and research needs," *Transportation Research Part C: Emerging Technologies*, **48**, pp. 379–403.
- [51] Brackstone, M., and McDonald, M., 1999, "Car-following: a historical review," *Transportation Research Part F: Traffic Psychology and Behaviour*, **2**(4), pp. 181–196.
- [52] Pipes, L. A., 1953, "An Operational Analysis of Traffic Dynamics," *Journal of Applied Physics*, **24**(3), pp. 274–281.
- [53] Gipps, P. G., 1981, "A behavioural car-following model for computer simulation," *Transportation Research Part B: Methodological*, **15**(2), pp. 105–111.
- [54] Toledo, T., Koutsopoulos, H. N., and Ben-Akiva, M., 2007, "Integrated driving behavior modeling," *Transportation Research Part C: Emerging Technologies*, **15**(2), pp. 96–112.
- [55] Chandler, R. E., Herman, R., and Montroll, E. W., 1958, "Traffic Dynamics: Studies in Car Following," *Operations Research*, **6**(2), pp. 165–184.

Bibliography

- [56] May, J., Adolf, D., Harmut, E., and Keller, M., 1967, "Non-integer car-following models," *Highway Research Record*, (199).
- [57] Gazis, D. C., Herman, R., and Rothery, R. W., 1961, "Nonlinear Follow-the-Leader Models of Traffic Flow," *Operations Research*, **9**(4), pp. 545–567.
- [58] Rockwell, T. H., Ernst, R. L., and Hanken, A., 1968, "A sensitivity analysis of empirically derived car-following models," *Transportation Research*, **2**(4), pp. 363–373.
- [59] Kometani, E., and Sasaki, T., 1961, "Dynamic behaviour of traffic with a non-linear spacing- speed relationship," Amsterdam : Elsevier Publishing Co.
- [60] Newell, G. F., 1961, "Nonlinear Effects in the Dynamics of Car Following," *Operations Research*, **9**(2), pp. 209–229.
- [61] van Winsum, W., 1999, "The human element in car following models," *Transportation Research Part F: Traffic Psychology and Behaviour*, **2**(4), pp. 207–211.
- [62] Helly, W., 1961, "Simulation of bottlenecks in single-lane traffic flow," *Proceedings of the symposium on the theory of traffic flow*, pp. 207–238.
- [63] Treiber, M., Hennecke, A., and Helbing, D., 2000, "Congested traffic states in empirical observations and microscopic simulations," *Phys. Rev. E*, **62**(2), pp. 1805–1824.
- [64] Treiber, M., and Helbing, D., 2003, "Memory effects in microscopic traffic models and wide scattering in flow-density data," *Phys. Rev. E*, **68**(4), p. 046119.
- [65] Lawson, V., King, W. D., Nichols, M., and Monroe, K., 2015, "Teenage Drinking and Driving Behaviors," *J. Invest. Med.*, **63**(2), pp. 461–461.
- [66] Koisaari, T., Michelsson, K., Holopainen, J. M., Maksimainen, R., Paivansalo, J., Rantala, K., and Tervo, T., 2015, "Traffic and Criminal Behavior of Adults with Attention Deficit-Hyperactivity with a Prospective Follow-Up from Birth to the Age of 40 Years," *Traffic Inj. Prev.*, **16**(8), pp. 824–830.

Bibliography

- [67] Simons-Morton, B., Lerner, N., and Singer, J., 2005, "The observed effects of teenage passengers on the risky driving behavior of teenage drivers," *Accid. Anal. Prev.*, **37**(6), pp. 973–982.
- [68] Harre, N., Field, J., and Kirkwood, B., 1996, "Gender differences and areas of common concern in the driving behaviors and attitudes of adolescents," *J. Saf. Res.*, **27**(3), pp. 163–173.
- [69] Li, X., Yan, X., and Wong, S. C., 2015, "Effects of fog, driver experience and gender on driving behavior on S-curved road segments," *Accid. Anal. Prev.*, **77**, pp. 91–104.
- [70] Donovan, D., Marlatt, G., and Salzberg, P., 1983, "Drinking Behavior, Personality-Factors and High-Risk Driving - a Review and Theoretical Formulation," *J. Stud. Alcohol*, **44**(3), pp. 395–428.
- [71] Scheetz, L. J., 2015, "One for the Road: A Comparison of Drinking and Driving Behavior Among Younger and Older Adults Involved in Fatal Crashes," *J. Trauma Nurs.*, **22**(4), pp. 187–193.
- [72] Qu, W., Ge, Y., Xiong, Y., Carciofo, R., Zhao, W., and Zhang, K., 2015, "The relationship between mind wandering and dangerous driving behavior among Chinese drivers," *Saf. Sci.*, **78**, pp. 41–48.
- [73] Sun, D. (Jian), and Elefteriadou, L., 2012, "A Driver Behavior-Based Lane-Changing Model for Urban Arterial Streets," *Transportation Science*, **48**(2), pp. 184–205.
- [74] Ahmed, K. I., 1999, "Modeling drivers' acceleration and lane changing behavior," Thesis, Massachusetts Institute of Technology.
- [75] Muhrer, E., and Vollrath, M., 2011, "The effect of visual and cognitive distraction on driver's anticipation in a simulated car following scenario," *Transportation Research Part F: Traffic Psychology and Behaviour*, **14**(6), pp. 555–566.
- [76] Xiaorui, W., and Hongxu, Y., 2013, "A Lane Change Model with the Consideration of Car Following Behavior," *Procedia - Social and Behavioral Sciences*, **96**, pp. 2354–2361.

Bibliography

- [77] Toledo, T., Koutsopoulos, H. N., and Ben-Akiva, M., 2007, "Integrated driving behavior modeling," *Transportation Research Part C: Emerging Technologies*, **15**(2), pp. 96–112.
- [78] Kim, S., Suh, W., and Kim, J., 2014, "Traffic Simulation Software: Traffic Flow Characteristics in CORSIM," 2014 International Conference on Information Science and Applications (ICISA), pp. 1–3.
- [79] Toledo, T., Koutsopoulos, H., and Ben-Akiva, M., 2003, "Modeling Integrated Lane-Changing Behavior," *Transportation Research Record*, **1857**(1), pp. 30–38.
- [80] Ahmed, K. I., 1999, "Modeling drivers' acceleration and lane changing behavior."
- [81] Hidas, P., 2002, "Modelling lane changing and merging in microscopic traffic simulation," *Transportation Research Part C: Emerging Technologies*, **10**(5–6), pp. 351–371.
- [82] Ahmed, K. I., BenAkiva, M. E., Koutsopoulos, H. N., and Mishalani, R. G., 1996, *Models of freeway lane changing and gap acceptance behavior*, Pergamon Press Ltd, Oxford.
- [83] Herman, R., and Weiss, G., 1961, "Comments on the Highway-Crossing Problem," *Operations Research*, **9**(6), pp. 828–840.
- [84] Miller, A. J., "Nine estimators of gap-acceptance parameters," *Publication of: Traffic Flow and Transportation*, (0).
- [85] Gipps, P. G., 1986, "A model for the structure of lane-changing decisions," *Transportation Research Part B: Methodological*, **20**(5), pp. 403–414.
- [86] Salvucci, D., Boer, E., and Liu, A., 2001, "Toward an Integrated Model of Driver Behavior in Cognitive Architecture," *Transportation Research Record: Journal of the Transportation Research Board*, **1779**, pp. 9–16.
- [87] Kesting, A., Treiber, M., and Helbing, D., 2007, "General Lane-Changing Model MOBIL for Car-Following Models," *Transportation Research Record: Journal of the Transportation Research Board*, **1999**, pp. 86–94.

Bibliography

- [88] Schakel, W., Knoop, V., and van Arem, B., 2012, “Integrated lane change model with relaxation and synchronization,” *Transportation Research Record: Journal of the Transportation Research Board*, (2316), pp. 47–57.
- [89] Hani, M., and Yosef, S., 1981, “Using gap sequences to estimate gap acceptance functions,” *Transportation Research Part B: Methodological*, **15**, pp. 143–148.
- [90] Sayed, T., Brown, G., and Navin, F., 1994, “Simulation of Traffic Conflicts at Unsignalized Intersections with Tsc-Sim,” *Accid. Anal. Prev.*, **26**(5), pp. 593–607.
- [91] Kaysi, I. A., and Abbany, A. S., 2007, “Modeling aggressive driver behavior at unsignalized intersections,” *Accid. Anal. Prev.*, **39**(4), pp. 671–678.
- [92] Hamed, M. M., Easa, S. M., and Batayneh, R. R., 1997, “Disaggregate gap-acceptance model for unsignalized T-intersections,” *J. Transp. Eng.-ASCE*, **123**(1), pp. 36–42.
- [93] Hidas, P., 2005, “Modelling vehicle interactions in microscopic simulation of merging and weaving,” *Transportation Research Part C: Emerging Technologies*, **13**(1), pp. 37–62.
- [94] Kind, M. T., and Kesting, A., 2009, *Modeling Lane-Changing Decisions with MOBIL*, Springer-Verlag Berlin, Berlin.
- [95] Kita, H., 1999, “A merging–giveway interaction model of cars in a merging section: a game theoretic analysis,” *Transportation Research Part A: Policy and Practice*, **33**(3–4), pp. 305–312.
- [96] Kita, H., Tanimoto, K., and Fukuyama, K., 2002, “A game theoretical analysis of merging-giveway interaction: a joint estimation model,” *Transportation and traffic theory*, **15**, pp. 503–518.
- [97] Khatib, O., 1986, “Real-time obstacle avoidance for manipulators and mobile robots,” *The international journal of robotics research*, **5**(1), pp. 90–98.
- [98] Yang, Z.-S., Yu, Y., Yu, D.-X., Zhou, H.-X., and Mo, X.-L., 2013, “APF-Based Car Following Behavior Considering Lateral Distance,” *Adv. Mech. Eng.*, p. 207104.

Bibliography

- [99] Yin, H. M., Wang, L., Maurin, P., and Xu, H., 2013, “Dynamic Transit Service Through Open Mode Integrated Transportation System.”
- [100] Wang, L., and Yin, H., 2014, “Social Network Based Dynamic Transit Service Through the OMITS System,” National Technical Information Service.
- [101] Liu, Z., Jia, X., and Cheng, W., 2012, “Solving the last mile problem: Ensure the success of public bicycle system in beijing,” *Procedia-Social and Behavioral Sciences*, **43**, pp. 73–78.
- [102] Drane, C. R., and Rizos, C., 1998, *Positioning Systems in Intelligent Transportation Systems*, Artech House, Inc., Norwood, MA, USA.
- [103] Min, W., and Wynter, L., 2011, “Real-time road traffic prediction with spatio-temporal correlations,” *Transportation Research Part C: Emerging Technologies*, **19**(4), pp. 606–616.
- [104] Huang, B., and Pan, X., 2007, “GIS coupled with traffic simulation and optimization for incident response,” *Computers, Environment and Urban Systems*, **31**(2), pp. 116–132.
- [105] Baharom, M. N., 2009, “Analysing and presenting road traffic volume using geographical information system (GIS),” Ph.D., The University of Manchester (United Kingdom).
- [106] Sun, W., Liu, C., Lin, H., and Xie, S., 2012, “T-GIS data model for urban complex road network,” *Journal of Tongji University. Natural Science*, **40**(1), pp. 127–132.
- [107] Steg, L., and Vlek, C., 2009, “Encouraging pro-environmental behaviour: An integrative review and research agenda,” *Journal of Environmental Psychology*, **29**(3), pp. 309–317.
- [108] Geller, E. S., 2002, “The challenge of increasing proenvironment behavior,” *Handbook of environmental psychology*, **2**, pp. 525–540.
- [109] Buliung, R. N., Soltys, K., Bui, R., Habel, C., and Lanyon, R., 2010, “Catching a ride on the information super-highway: toward an understanding of internet-based carpool formation and use,” *Transportation*, **37**(6), pp. 849–873.

Bibliography

- [110] Delhomme, P., and Gheorghiu, A., 2016, “Comparing French carpoolers and non-carpoolers: Which factors contribute the most to carpooling?,” *Transportation Research Part D: Transport and Environment*, **42**, pp. 1–15.
- [111] Lau, J., Hung, W., Cheung, C., and Yuen, D., 2008, “Contributions of roadside vehicle emissions to general air quality in Hong Kong,” *Transportation Research Part D: Transport and Environment*, **13**(1), pp. 19–26.
- [112] Stradling, S. G., 2007, “Determinants of car dependence.”
- [113] Kocur, G., and Hendrickson, C., 1983, “A model to assess cost and fuel savings from ride sharing,” *Transportation Research Part B: Methodological*, **17**(4), pp. 305–318.
- [114] Litman, T., 2009, “Transportation cost and benefit analysis,” *Victoria Transport Policy Institute*, **31**.
- [115] Agatz, N., Erera, A., Savelsbergh, M., and Wang, X., 2012, “Optimization for dynamic ride-sharing: A review,” *European Journal of Operational Research*, **223**(2), pp. 295–303.
- [116] Ferguson, E., Hodge, K., and Berkovsky, K., 1994, “Psychological benefits from vanpooling and group composition,” *Transportation*, **21**(1), pp. 47–69.
- [117] Dailey, D., Loseff, D., and Meyers, D., 1999, “Seattle smart traveler: dynamic ridematching on the World Wide Web,” *Transportation Research Part C: Emerging Technologies*, **7**(1), pp. 17–32.
- [118] Bajwa, S. U. I., Chung, E., and Kuwahara, M., 2005, “Performance evaluation of an adaptive travel time prediction model,” *IEEE*, pp. 1000–1005.
- [119] Yin, H., Saleh, A., and Shields, M. D., 2011, “Design and Payoff Prediction for Open Mode Integrated Transit System.”
- [120] Chang, W.-L., 2016, “A two-step model for self-organized social network pre-construction,” *Telematics and Informatics*, **33**(1), pp. 165–175.

Bibliography

- [121] Leskovec, J., Huttenlocher, D., and Kleinberg, J., 2010, “Signed networks in social media,” *ACM*, pp. 1361–1370.
- [122] Wasserman, S., and Faust, K., 1994, *Social network analysis: Methods and applications*, Cambridge university press.
- [123] Dijkstra, E. W., 1959, “A note on two problems in connexion with graphs,” *Numerische mathematik*, **1**(1), pp. 269–271.
- [124] Wang, L., Chen, F., and Yin, H., “Detecting and tracking vehicles in traffic by unmanned aerial vehicles,” *Automation in Construction*, (**Under review**).
- [125] Leitloff, J., Rosenbaum, D., Kurz, F., Meynberg, O., and Reinartz, P., 2014, “An Operational System for Estimating Road Traffic Information from Aerial Images,” *Remote Sensing*, **6**(11), pp. 11315–11341.
- [126] Papageorgiou, M., Diakaki, C., Dinopoulou, V., Kotsialos, A., and Wang, Y., 2003, “Review of road traffic control strategies,” *Proceedings of the IEEE*, **91**(12), pp. 2043–2067.
- [127] Brackstone, M., and McDonald, M., 1999, “Car-following: a historical review,” *Transportation Research Part F: Traffic Psychology and Behaviour*, **2**(4), pp. 181–196.
- [128] Hamdar, D. S., 2012, “Driver Behavior Modeling,” *Handbook of Intelligent Vehicles*, A. Eskandarian, ed., Springer London, pp. 537–558.
- [129] Vincent, E., and Laganier, R., 2001, “Detecting planar homographies in an image pair,” *Univ. Zagreb*, pp. 182–187.
- [130] Umbaugh, S. E., 2010, *Digital Image Processing and Analysis: Human and Computer Vision Applications with CVIPtools*, Second Edition, CRC Press, Inc., Boca Raton, FL, USA.
- [131] Shapiro, L., 1992, *Computer Vision and Image Processing*, Academic Press.

Bibliography

- [132] Torr, P. H. S., Fitzgibbon, A. W., and Zisserman, A., 1999, “The Problem of Degeneracy in Structure and Motion Recovery from Uncalibrated Image Sequences,” *International Journal of Computer Vision*, **32**(1), pp. 27–44.
- [133] Alex M., A., 2001, “Multiple View Geometry in Computer Vision,” *Kybernetes*, **30**(9/10), pp. 1333–1341.
- [134] Lowe, D. G., 2004, “Distinctive Image Features from Scale-Invariant Keypoints,” *International Journal of Computer Vision*, **60**(2), pp. 91–110.
- [135] Lucas, B. D., and Kanade, T., 1981, “An Iterative Image Registration Technique with an Application to Stereo Vision,” *Proceedings of the 7th International Joint Conference on Artificial Intelligence - Volume 2*, Morgan Kaufmann Publishers Inc., San Francisco, CA, USA, pp. 674–679.
- [136] Lindeberg, T., 1998, “Edge Detection and Ridge Detection with Automatic Scale Selection,” *International Journal of Computer Vision*, **30**(2), pp. 117–156.
- [137] Royden, C. S., and Moore, K. D., 2012, “Use of speed cues in the detection of moving objects by moving observers,” *Vision Research*, **59**, pp. 17–24.
- [138] Karimi Nejadasl, F., Gorte, B. G. H., and Hoogendoorn, S. P., 2006, “Optical flow based vehicle tracking strengthened by statistical decisions,” *ISPRS Journal of Photogrammetry and Remote Sensing*, **61**(3–4), pp. 159–169.
- [139] Lowe, D. G., 1999, “Object recognition from local scale-invariant features,” *The Proceedings of the Seventh IEEE International Conference on Computer Vision*, 1999, pp. 1150–1157 vol.2.
- [140] Lowe, D. G., 1999, “Object recognition from local scale-invariant features,” *The Proceedings of the Seventh IEEE International Conference on Computer Vision*, 1999, pp. 1150–1157 vol.2.

Bibliography

- [141] Se, S., Lowe, D., and Little, J., 2001, "Vision-based mobile robot localization and mapping using scale-invariant features," IEEE International Conference on Robotics and Automation, 2001. Proceedings 2001 ICRA, pp. 2051–2058 vol.2.
- [142] Gipps, P. G., 1981, "A behavioural car-following model for computer simulation," *Transportation Research Part B: Methodological*, **15**(2), pp. 105–111.
- [143] Vedaldi, A., and Fulkerson, B., 2010, "Vlfeat: An Open and Portable Library of Computer Vision Algorithms," Proceedings of the International Conference on Multimedia, ACM, New York, NY, USA, pp. 1469–1472.
- [144] Yang, Q., and Koutsopoulos, H. N., 1996, "A Microscopic Traffic Simulator for evaluation of dynamic traffic management systems," *Transportation Research Part C: Emerging Technologies*, **4**(3), pp. 113–129.
- [145] Punzo, V., Borzacchiello, M. T., and Ciuffo, B., 2011, "On the assessment of vehicle trajectory data accuracy and application to the Next Generation SIMulation (NGSIM) program data," *Transportation Research Part C: Emerging Technologies*, **19**(6), pp. 1243–1262.
- [146] Sun, Z., Bebis, G., and Miller, R., 2006, "On-road vehicle detection: a review," *IEEE Transactions on Pattern Analysis and Machine Intelligence*, **28**(5), pp. 694–711.
- [147] Cao, J., Hadiuzzaman, M., Qiu, T. Z., and Hu, D., 2015, "Real-time queue estimation model development for uninterrupted freeway flow based on shockwave analysis," *Can. J. Civ. Eng.*, **42**(3), pp. 153–163.
- [148] Wang, L., Chen, F., and Yin, H., "A open mechanics-based acceleration model considering vehicle interactions," **in submitting**.
- [149] Olstam, J. J., and Tapani, A., 2004, "COMPARISON OF CAR-FOLLOWING MODELS," Publication of: Swedish National Road and Transport Research Institute.
- [150] Bando, M., Hasebe, K., Nakanishi, K., Nakayama, A., Shibata, A., and Sugiyama, Y., 1995, "Phenomenological Study of Dynamical Model of Traffic Flow," *J. Phys. I*, **5**(11), pp. 1389–1399.

Bibliography

- [151] Yu, S., Liu, Q., and Li, X., 2013, “Full velocity difference and acceleration model for a car-following theory,” *Commun. Nonlinear Sci. Numer. Simul.*, **18**(5), pp. 1229–1234.
- [152] Helbing, D., and Tilch, B., 1998, “Generalized force model of traffic dynamics,” *Phys. Rev. E*, **58**(1), pp. 133–138.
- [153] Jiang, R., Wu, Q. S., and Zhu, Z. J., 2001, “Full velocity difference model for a car-following theory,” *Phys. Rev. E*, **64**(1), p. 017101.
- [154] Wang, J., Ding, J.-X., Shi, Q., and Kühne, R. D., 2015, “Lane-changing behavior and its effect on energy dissipation using full velocity difference model,” *Int. J. Mod. Phys. C*, **27**(02), p. 1650013.
- [155] Nagel, K., Wolf, D. E., Wagner, P., and Simon, P., 1998, “Two-lane traffic rules for cellular automata: A systematic approach,” *Phys. Rev. E*, **58**(2), pp. 1425–1437.
- [156] Jia, B., Jiang, R., Wu, Q. S., and Hu, M. B., 2005, “Honk effect in the two-lane cellular automaton model for traffic flow,” *Physica A*, **348**, pp. 544–552.
- [157] Li, X. G., Jia, B., Gao, Z. Y., and Jiang, R., 2006, “A realistic two-lane cellular automata traffic model considering aggressive lane-changing behavior of fast vehicle,” *Physica A*, **367**, pp. 479–486.
- [158] Tang, T., Wang, Y., Yang, X., and Wu, Y., 2012, “A new car-following model accounting for varying road condition,” *Nonlinear Dyn.*, **70**(2), pp. 1397–1405.
- [159] Tang, T.-Q., Huang, H.-J., and Shang, H.-Y., 2010, “A Dynamic Model for the Heterogeneous Traffic Flow Consisting of Car, Bicycle and Pedestrian,” *Int. J. Mod. Phys. C*, **21**(2), pp. 159–176.
- [160] Peng, G. H., and Sun, D. H., 2010, “A dynamical model of car-following with the consideration of the multiple information of preceding cars,” *Physics Letters A*, **374**(15–16), pp. 1694–1698.

Bibliography

- [161] Punzo, V., and Tripodi, A., 2007, “Steady-state solutions and multiclass calibration of Gipps microscopic traffic flow model,” *Transp. Res. Record*, (1999), pp. 104–114.
- [162] Siuhi, S., and Kaseko, M. S., 2010, “Parametric Study of Stimulus-Response Behavior for Car-Following Models.”
- [163] Koutsopoulos, H. N., and Farah, H., 2012, “Latent class model for car following behavior,” *Transportation Research Part B: Methodological*, **46**(5), pp. 563–578.
- [164] Gazis, D. C., Herman, R., and Potts, R. B., 1959, “Car-Following Theory of Steady-State Traffic Flow,” *Operations Research*, **7**(4), pp. 499–505.
- [165] Broughton, K. L. M., Switzer, F., and Scott, D., 2007, “Car following decisions under three visibility conditions and two speeds tested with a driving simulator,” *Accident Analysis & Prevention*, **39**(1), pp. 106–116.
- [166] Sun, D., Kang, Y., and Yang, S., 2015, “A novel car following model considering average speed of preceding vehicles group,” *Physica A*, **436**, pp. 103–109.
- [167] Warner, H. W., and Aberg, L., 2006, “Drivers’ decision to speed: A study inspired by the theory of planned behavior,” *Transp. Res. Pt. F-Traffic Psychol. Behav.*, **9**(6), pp. 427–433.
- [168] Addison, P. S., and Low, D. J., 1998, “A novel nonlinear car-following model,” *Chaos*, **8**(4), pp. 791–799.
- [169] Jones, J. E., 1924, “On the Determination of Molecular Fields. II. From the Equation of State of a Gas,” *Proceedings of the Royal Society of London Series A*, **106**, pp. 463–477.
- [170] Hamdar, S. H., Talebpour, A., and Dong, J., 2015, “Travel Time Reliability Versus Safety: A Stochastic Hazard-Based Modeling Approach,” *IEEE Trans. Intell. Transp. Syst.*, **16**(1), pp. 264–273.
- [171] Knoop, V. L., and Buisson, C., 2015, “Calibration and Validation of Probabilistic Discretionary Lane-Change Models,” *IEEE Transactions on Intelligent Transportation Systems*, **16**(2), pp. 834–843.

Bibliography

- [172] Zheng, Z., 2014, “Recent developments and research needs in modeling lane changing,” *Transportation Research Part B: Methodological*, **60**, pp. 16–32.
- [173] Cho, H.-J., Tseng, M.-T., and Hwang, M.-C., 2014, “Using detection of vehicular presence to estimate shockwave speed and upstream traffics for a signalized intersection,” *Appl. Math. Comput.*, **232**, pp. 1151–1165.
- [174] Cao, J., Hu, D., Hadiuzzaman, M., Wang, X., and Qiu, T. Z., 2014, “Comparison of Queue Estimation Accuracy by Shockwave-Based and Input-Output-Based Models,” 2014 Ieee 17th International Conference on Intelligent Transportation Systems (itsc), pp. 2687–2692.
- [175] Liu, H. X., Wu, X., Ma, W., and Hu, H., 2009, “Real-time queue length estimation for congested signalized intersections,” *Transp. Res. Pt. C-Emerg. Technol.*, **17**(4), pp. 412–427.
- [176] Logghe, S., and Immers, L. H., 2008, “Multi-class kinematic wave theory of traffic flow,” *Transp. Res. Pt. B-Methodol.*, **42**(6), pp. 523–541.
- [177] Xiao-Yan, S., and Jun-Fang, Z., 2015, “Study of the shock wave induced by closing partial road in traffic flow,” *Acta Phys. Sin.*, **64**(11), p. 114502.
- [178] Yang, D., Chen, Y., Xin, L., and Zhang, Y., 2014, “Real-time detecting and tracking of traffic shockwaves based on weighted consensus information fusion in distributed video network,” *IET Intell. Transp. Syst.*, **8**(4), pp. 377–387.
- [179] Chuang, Y.-T., Yi, C.-W., Tseng, Y.-C., Nian, C.-S., and Ching, C.-H., 2015, “Discovering Phase Timing Information of Traffic Light Systems by Stop-Go Shockwaves,” *IEEE. Trans. Mob. Comput.*, **14**(1), pp. 58–71.
- [180] Yang, D., Chen, Y., Xin, L., and Zhang, Y., 2014, “Real-time detecting and tracking of traffic shockwaves based on weighted consensus information fusion in distributed video network,” *IET Intell. Transp. Syst.*, **8**(4), pp. 377–387.
- [181] Wang, L., Chen, F., and Yin, H., “A driver decision-based lane change execution model,” **in submitting**.

Bibliography

- [182] Pei, Y., and Xu, H., 2006, “The Control Mechanism of Lane changing in Jam Condition,” The Sixth World Congress on Intelligent Control and Automation, 2006. WCICA 2006, pp. 8655–8658.
- [183] Tzeng, G. H., and Huang, J. J., 2011, *Multiple Attribute Decision Making: Methods and Applications*, Crc Press-Taylor & Francis Group, Boca Raton.
- [184] Edwards, W., 1954, “The theory of decision making,” *Psychological bulletin*, **51**(4), p. 380.
- [185] Fishburn, P. C., 1970, *Utility theory for decision making*, DTIC Document.
- [186] Lo, C.-W., Chiu, L.-C., and Li, C.-N., 2014, “Using Fuzzy Delphi Method to Indicate the Green Transport & Recreation Routes,” 2014 2nd International Conference on Social Sciences Research (ssr 2014), Pt 1, L. Lee, ed., pp. 220–226.
- [187] Okoli, C., and Pawlowski, S. D., 2004, “The Delphi method as a research tool: an example, design considerations and applications,” *Inf. Manage.*, **42**(1), pp. 15–29.
- [188] Shiftan, Y., Kaplan, S., and Hakkert, S., 2004, *Scenario building for the future of the Tel Aviv metropolitan area and its transportation system using the Delphi method*.
- [189] Lee, T., Kim, B., Yi, K., and Jeong, C., 2011, “Development of lane change driver model for closed-loop simulation of the active safety system,” 2011 14th International IEEE Conference on Intelligent Transportation Systems (ITSC), pp. 56–61.
- [190] Salvucci, D. D., and Gray, R., 2004, “A two-point visual control model of steering,” *Perception*, **33**(10), pp. 1233–1248.
- [191] Ba, Y., Zhang, W., Salvendy, G., Cheng, A. S. K., and Ventsislavova, P., 2016, “Assessments of risky driving: A Go/No-Go simulator driving task to evaluate risky decision-making and associated behavioral patterns,” *Applied ergonomics*, **52**, pp. 265–74.

Bibliography

- [192] Lv, W., Song, W., Liu, X., and Ma, J., 2013, “A microscopic lane changing process model for multilane traffic,” *Physica A: Statistical Mechanics and its Applications*, **392**(5), pp. 1142–1152.
- [193] Schlenoff, C., Madhavan, R., and Kootbally, Z., 2006, “PRIDE: a hierarchical, integrated prediction framework for autonomous on-road driving,” *Proceedings 2006 IEEE International Conference on Robotics and Automation, 2006. ICRA 2006*, pp. 2348–2353.
- [194] Choudhury, C. F., 2007, “Modeling driving decisions with latent plans,” Ph.D., Massachusetts Institute of Technology.
- [195] Choudhury C.F., Ben-Akiva M.E., Ramanujam V., Toledo T., and Rathi V., 2007, “NGSIM Arterial Lane Selection Model – Final Report,” Federal Highway Administration.
- [196] Ramanujam, V., 2007, “Lane changing models for arterial traffic,” Thesis, Massachusetts Institute of Technology.
- [197] Hanson, S., and Giuliano, G., 2004, *The Geography of Urban Transportation*, Guilford Press.
- [198] Toledo, T., and Zohar, D., 2007, “Modeling Duration of Lane Changes,” *Transportation Research Record: Journal of the Transportation Research Board*, **1999**, pp. 71–78.
- [199] Finnegan, P., and Green, P., 1990, *TIME TO CHANGE LANES: A LITERATURE REVIEW*.
- [200] Xu, G., Liu, L., Ou, Y., and Song, Z., 2012, “Dynamic Modeling of Driver Control Strategy of Lane-Change Behavior and Trajectory Planning for Collision Prediction,” *IEEE Transactions on Intelligent Transportation Systems*, **13**(3), pp. 1138–1155.
- [201] Chin, E., Franzese, O., Greene, D., Hwang, H., and Gibson, R., 2002, *Temporary losses of highway capacity and impacts on performance*, Oak Ridge National Laboratory Oak Ridge, TN.

Bibliography

- [202] Chung, Y.-S., Chiou, Y.-C., and Lin, C.-H., 2015, “Simultaneous equation modeling of freeway accident duration and lanes blocked,” *Analytic Methods in Accident Research*, **7**, pp. 16–28.
- [203] Hawas, Y. E., 2007, “A microscopic simulation model for incident modeling in urban networks,” *Transp. Plan. Technol.*, **30**(2-3), pp. 289–309.
- [204] Sheu, J.-B., 2013, “Microscopic traffic behaviour modelling and simulation for lane-blocking arterial incidents,” *Transportmetrica A: Transport Science*, **9**(4), pp. 335–357.
- [205] Jagannathan, K., and Modiano, E., 2013, “The Impact of Queue Length Information on Buffer Overflow in Parallel Queues,” *IEEE Trans. Inf. Theory*, **59**(10), pp. 6393–6404.
- [206] Sheu, J.-B., 2003, “A Stochastic Modeling Approach to Real-Time Prediction of Queue Overflows,” *Transportation Science*, **37**(2), pp. 230–252.
- [207] (Grace) Qi, Y., and Martinelli, D. R., 2009, “An Investigation of Incident Frequency, Duration and Lanes Blockage for Determining Traffic Delay,” *J. Adv. Transp.*, **43**(3), pp. 275–299.
- [208] Holland, E. N., 1998, “A generalised stability criterion for motorway traffic,” *Transp. Res. Pt. B-Methodol.*, **32**(2), pp. 141–154.
- [209] Hamdar, S. H., and Mahmassani, H. S., 2008, “From Existing Accident-Free Car-Following Models to Colliding Vehicles,” *Transp. Res. Record*, (2088), pp. 45–56.
- [210] Conrad, M., Dion, F., and Yagar, S., 1998, “Real-Time Traffic Signal Optimization with Transit Priority: Recent Advances in the Signal Priority Procedure for Optimization in Real-Time Model,” *Transportation Research Record: Journal of the Transportation Research Board*, **1634**, pp. 100–109.
- [211] Choudhury, C. F., 2005, “Modeling lane-changing behavior in presence of exclusive lanes,” Thesis, Massachusetts Institute of Technology.

Bibliography

- [212] Chowdhury, D., Santen, L., and Schadschneider, A., 2000, “Statistical physics of vehicular traffic and some related systems,” *Physics Reports*, **329**(4), pp. 199–329.
- [213] Janowsky, S. A., and Lebowitz, J. L., 1992, “Finite-size effects and shock fluctuations in the asymmetric simple-exclusion process,” *Physical Review A*, **45**(2), p. 618.
- [214] Nagatani, T., 1994, “Effect of Jam-Avoiding Turn on Jamming Transition in Two-Dimensional Traffic Flow Model,” *J. Phys. Soc. Jpn.*, **63**(4), pp. 1228–1231.
- [215] Kurata, S., and Nagatani, T., 2003, “Spatio-temporal dynamics of jams in two-lane traffic flow with a blockage,” *Physica A: Statistical Mechanics and its Applications*, **318**(3), pp. 537–550.
- [216] Kerner, B. S., Klenov, S. L., Hiller, A., and Rehborn, H., 2005, “Microscopic features of moving traffic jams,” arXiv preprint physics/0510167.
- [217] Zhu, H., Lei, L., and Dai, S., 2009, “Two-lane traffic simulations with a blockage induced by an accident car,” *Physica A: Statistical Mechanics and its Applications*, **388**(14), pp. 2903–2910.
- [218] Chowdhury, D., Wolf, D. E., and Schreckenberg, M., 1997, “Particle hopping models for two-lane traffic with two kinds of vehicles: Effects of lane-changing rules,” *Physica A: Statistical Mechanics and its Applications*, **235**(3–4), pp. 417–439.
- [219] Abuelela, M., 2011, “A framework for incident detection and notification in vehicular ad-hoc networks,” Ph.D.
- [220] Baykal-Gürsoy, M., Xiao, W., and Ozbay, K., 2009, “Modeling traffic flow interrupted by incidents,” *European Journal of Operational Research*, **195**(1), pp. 127–138.
- [221] Oliveira, M., Santos, V., and Sappa, A. D., 2015, “Multimodal inverse perspective mapping,” *Information Fusion*, **24**, pp. 108–121.
- [222] Stiller, C., Leòn, F. P., and Kruse, M., 2011, “Information fusion for automotive applications—An overview,” *Information fusion*, **12**(4), pp. 244–252.

Bibliography

- [223] Kastrinaki, V., Zervakis, M., and Kalaitzakis, K., 2003, “A survey of video processing techniques for traffic applications,” *Image and vision computing*, **21**(4), pp. 359–381.
- [224] Simond, N., and Parent, M., 2007, “Obstacle detection from ipm and super-homography,” *IEEE*, pp. 4283–4288.
- [225] Cerri, P., and Grisleri, P., 2005, “Free space detection on highways using time correlation between stabilized sub-pixel precision IPM images,” *IEEE*, pp. 2223–2228.
- [226] Ma, G., Park, S.-B., Müller-Schneiders, S., Ioffe, A., and Kummert, A., 2007, “Vision-based pedestrian detection-reliable pedestrian candidate detection by combining ipm and a 1d profile,” *IEEE*, pp. 137–142.
- [227] Lundquist, C., and Schön, T. B., 2011, “Joint ego-motion and road geometry estimation,” *Information Fusion*, **12**(4), pp. 253–263.
- [228] Aly, M., 2008, “Real time detection of lane markers in urban streets,” *IEEE*, pp. 7–12.
- [229] Pandian, S., Gokhale, S., and Ghoshal, A. K., 2009, “Evaluating effects of traffic and vehicle characteristics on vehicular emissions near traffic intersections,” *Transportation Research Part D-Transport and Environment*, **14**(3), pp. 180–196.
- [230] Gates, T. J., Noyce, D. A., Laracuente, L., and Nordheim, E. V., 2007, “Analysis of driver behavior in dilemma zones at signalized intersections,” *Transp. Res. Record*, (2030), pp. 29–39.
- [231] Yan, X. D., Radwan, E., and Abdel-Aty, M., 2005, “Characteristics of rear-end accidents at signalized intersections using multiple logistic regression model,” *Accident Analysis and Prevention*, **37**(6), pp. 983–995.

Publications during Ph.D. study

- Yin H M, **Wang L**, Maurin P, et al. Dynamic Transit Service Through Open Mode Integrated Transportation System[C]//Transportation Research Board 92nd Annual Meeting. 2013 (13-4385).
- **Wang, L.**, and Yin, H., 2014, “Social Network Based Dynamic Transit Service Through the OMITS System,” Natl. Tech. Inf. Serv.
- **Wang, L.**, Chen, F., and Yin, H., “Detecting and tracking vehicles in traffic by unmanned aerial vehicles,” Autom. Constr., (Under review).
- Song, G., **Wang, L.**, Deng, L., and Yin, H., 2015, “Mechanical characterization and inclusion based boundary element modeling of lightweight concrete containing foam particles,” Mech. Mater., **91**, pp. 208–225.
- **Wang, L.**, Chen, F., and Yin, H., “An open mechanics-based acceleration model.” (in submitting)
- **Wang, L.**, Chen, F., and Yin, H., “A driver decision-based lane change execution model.” (in submitting)
- Chen, F., He, X., **Wang, L.**, and Yin, H., “Consistency of Nuclear Density Measurement with Hydrogen Effects,” Transp. Infrastruct. Geotechnol. (Under review)